A locking-free mixed-primal formulation for the Biot–Brinkman–Forchheimer model *

JESSIKA CAMAÑO† SERGIO CAUCAO‡ CRISTIAN INZUNZA§

Abstract

We analyze a locking-free mixed-primal formulation of the stationary Biot–Brinkman–Forchheimer model. This problem describes the interaction between the deformation of a porous skeleton and a viscous fluid subject to nonlinear inertial resistance. By introducing the total pressure as an additional unknown, the formulation involves the solid displacement, fluid velocity, total pressure, and pore pressure. The well-posedness of the continuous problem is established by means of monotone operator arguments. We then introduce conforming Galerkin discretizations based on Stokes-stable finite element pairs and prove their unique solvability. A priori error estimates are derived with constants independent of the first Lamé parameter, thereby showing that the method is locking-free in the nearly incompressible limit. In addition, we develop a residual-based a posteriori error estimator and establish its reliability and efficiency up to higher-order terms. Several two- and three-dimensional numerical experiments confirm the theoretical convergence rates, the robustness of the method for large values of the first Lamé parameter, and the ability of the estimator to guide the refinement towards localized regions of large pressure gradient. Further experiments involving a strongly heterogeneous porous medium and a brain-shaped domain illustrate the computational performance of the proposed approach in heterogeneous and geometrically complex configurations.

Key words: Biot model, Brinkman–Forchheimer equations, finite element methods, locking-free

Mathematics Subject Classification (2020): 65N30, 65N12, 65N15, 65N50, 76S05, 74F10.

1 Introduction

The interaction between fluid flow and the deformation of a porous solid arises in a wide range of applications in science and engineering. Representative examples include soil consolidation, groundwater flow, subsidence and compaction of hydrocarbon reservoirs, hydraulic stimulation of geological formations, filtration processes, and the mechanical response of fluid-saturated biological tissues. In these applications, variations in the pore pressure induce deformation of the solid skeleton, while changes

*This research was partially supported by ANID-Chile through CENTRO DE MODELAMIENTO MATEMÁTICO (FB210005), and Fondecyt projects 1250937 and 1231336, and Fondecyt Postdoctoral project 3260398; by Grupo de Investigación en Análisis Numérico y Cálculo Científico (GIANuC^2), Universidad Católica de la Santísima Concepción; and by Centro de Investigación en Ingeniería Matemática (CI^{2}MA), Universidad de Concepción.

†GIANuC^2 and Departamento de Matemática y Física Aplicadas, Universidad Católica de la Santísima Concepción, Casilla 297, Concepción, Chile, and CI^{2}MA, Universidad de Concepción, Casilla 160-C, Concepción, Chile, email: jecamano@ucsc.cl

‡GIANuC^2 and Departamento de Matemática y Física Aplicadas, Universidad Católica de la Santísima Concepción, Casilla 297, Concepción, Chile, email: scaucao@ucsc.cl

§GIANuC^2 and Departamento de Matemática y Física Aplicadas, Universidad Católica de la Santísima Concepción, Casilla 297, Concepción, Chile, email: crinzunza@ucsc.cl

in the porous structure affect the transport of fluid through the medium. The classical mathematical description of this coupled behavior is provided by Biot's theory of poroelasticity [5]; see also [39] for further discussion of its physical foundations and applications.

In its standard form, the Biot model combines linear elasticity for the porous skeleton with Darcy's law for the filtration velocity. Although Darcy's law is appropriate in flow regimes dominated by linear drag, it does not account for the internal viscous diffusion of the fluid. This limitation becomes relevant in highly permeable materials and in media containing channels, fractures, vugs, or transition regions where Darcy- and Stokes-type flow mechanisms may coexist. The Brinkman equation [8] extends Darcy's law by incorporating a viscous diffusion term and thus provides a more general description of flow through heterogeneous porous structures; see, for example, [41, 20]. The linear relation between the pressure gradient and the filtration velocity assumed by the Darcy and Brinkman models may also become inadequate when the fluid velocity is sufficiently large. In such regimes, inertial effects give rise to an additional nonlinear resistance, commonly described by the Forchheimer correction [22]. The resulting Brinkman–Forchheimer model combines viscous diffusion, linear Darcy resistance, and nonlinear inertial drag. It therefore provides a suitable framework for describing non-Darcy flow in highly permeable or strongly heterogeneous porous media, particularly in the presence of preferential flow paths or localized sources; see [20] and the references therein. These considerations motivate the coupling of Biot poroelasticity with the Brinkman–Forchheimer equations. The resulting Biot–Brinkman–Forchheimer model describes the deformation of a fluid-saturated porous skeleton when the pore flow is simultaneously affected by viscous diffusion and nonlinear drag. Such a coupling is relevant in geological and reservoir applications involving heterogeneous permeability fields, as well as in filtration devices, deformable porous structures, and biological tissues where localized forcing may generate large pressure gradients and significant variations in the fluid velocity. From the mathematical viewpoint, the model combines the difficulties associated with nearly incompressible elasticity, mixed velocity–pressure coupling, and a nonlinear monotone flow operator.

The numerical approximation of poroelastic systems has received considerable attention over the last decades. One of the main difficulties is the deterioration of standard displacement-based methods in the nearly incompressible regime, characterized by large values of the first Lamé parameter. Locking-free formulations have therefore been developed by introducing the total pressure, volumetric stress, or related scalar variables as additional unknowns. In particular, a three-field formulation involving the solid displacement, pore pressure, and total pressure was analyzed in [37], yielding stability and finite element error estimates robust with respect to the incompressibility parameter. Related mixed, conservative, discontinuous Galerkin, and virtual element schemes for poroelasticity can be found in [35, 9, 43]. Several recent works have extended this type of analysis to the Biot–Brinkman equations. Robust approximations for generalized Biot–Brinkman systems were introduced in [31]. A vorticity-based formulation, together with robust finite element solvers, was studied in [13], while a virtual element discretization based on Nitsche's technique was proposed in [36]. A fully dynamic five-field mixed formulation for the Biot–Brinkman model was analyzed in [11]. These contributions account for the effect of Brinkman viscous diffusion in deformable porous media, but they do not include the nonlinear Forchheimer resistance considered in the present work. In parallel, a variety of finite element and virtual element methods have been developed for nonlinear Brinkman and Brinkman–Forchheimer equations in rigid porous media. An augmented pseudostress-based mixed formulation for a nonlinear Brinkman model was analyzed in [24], and a corresponding mixed virtual element method was proposed in [27]. A vorticity-based mixed formulation for the unsteady Brinkman–Forchheimer equations was studied in [2], whereas an augmented mixed finite element method, including a priori and residual-based a posteriori error analyses, was developed in [14]. Virtual element discretizations for Brinkman–Forchheimer systems coupled with additional transport equations have also been considered; see, for instance, [1]. Motivated by the previous discussion, the present work combines the nonlinear Brinkman–Forchheimer flow law with a total-pressure formulation of poroelasticity. More precisely, we propose and analyze a mixed-primal formulation of the stationary Biot–Brinkman–Forchheimer model in terms of the solid displacement, the fluid velocity, the pore pressure, and the total pressure.

The main contributions of this work are as follows. At the continuous level, we establish the existence and uniqueness of a solution by exploiting the strong monotonicity and continuity of the Brinkman–Forchheimer operator, together with suitable stability properties of the coupling operators and the Browder–Minty theorem. At the discrete level, we introduce conforming Galerkin approximations based on Stokes-stable finite element pairs and prove the well-posedness of the resulting nonlinear problem. We also derive a priori error estimates with constants independent of the first Lamé parameter, thus showing that the method is locking-free in the nearly incompressible limit. Furthermore, we construct a residual-based a posteriori error estimator and establish its reliability and efficiency up to higher-order terms. The theoretical results are complemented by several two- and three-dimensional numerical experiments that confirm the predicted convergence rates and illustrate the robustness of the scheme, the performance of the adaptive procedure in regions of large pressure gradients, and the applicability of the method to heterogeneous media and complex geometries.

The remainder of the paper is organized as follows. In Section 2, we introduce the stationary Biot–Brinkman–Forchheimer equations, define the total-pressure variable, and derive the associated mixed-primal variational formulation. The well-posedness of the continuous problem is established in Section 3. In Section 4, we introduce the conforming Galerkin scheme and derive its stability and a priori error estimates. Section 5 is devoted to the construction and analysis of the residual-based a posteriori error estimator. The numerical experiments are presented in Section 6, including locking-free convergence tests, a heterogeneous permeability benchmark, adaptive computations on two- and three-dimensional L-shaped domains, and an experiment on a brain-shaped geometry. Section 7 summarizes the main conclusions and discusses possible extensions of the proposed framework. Finally, the auxiliary results are collected in three appendices. Appendix A establishes a discrete approximation property used in the a priori error analysis, Appendix B recalls the interpolation estimates used in the reliability analysis, and Appendix C presents the bubble-function and inverse estimates employed in the efficiency analysis.

We conclude this introductory section by introducing some standard notation and the functional spaces employed throughout the paper. Let $\Omega \subset \mathrm{R}^d$, $d \in \{2,3\}$, denote a domain with Lipschitz boundary Γ. For $\mathrm{s} \geq 0$ and $\mathrm{p} \in [1,+\infty]$, we denote by $\mathrm{L}^{\mathrm{p}}(\Omega)$ and $\mathrm{W}^{\mathrm{s},\mathrm{p}}(\Omega)$ the usual Lebesgue and Sobolev spaces endowed with the norms $\|\cdot\|_{\mathrm{L}^{\mathrm{p}}(\Omega)}$ and $\|\cdot\|_{\mathrm{W}^{\mathrm{s},\mathrm{p}}(\Omega)}$, respectively. Note that $\mathrm{W}^{0,\mathrm{p}}(\Omega) = \mathrm{L}^{\mathrm{p}}(\Omega)$. If $\mathrm{p}=2$, we write $\mathrm{H}^{\mathrm{s}}(\Omega)$ in place of $\mathrm{W}^{\mathrm{s},2}(\Omega)$, and denote the corresponding norm by $\|\cdot\|_{\mathrm{H}^{\mathrm{s}}(\Omega)}$. By $\mathbf{M}$ and $\mathbb{M}$ we will denote the corresponding vectorial and tensorial counterparts of a generic scalar functional space M. The $\mathrm{L}^2(\Omega)$ inner product for scalar, vector, or tensor valued functions is denoted by $(\cdot,\cdot)_\Omega$. The $\mathrm{L}^2(\Gamma)$ inner product or duality pairing is denoted by $\langle\cdot,\cdot\rangle_\Gamma$.

In turn, for any vector field $\mathbf{v} := (v_i)_{i=1}^d$, we define its gradient and divergence by

$$\nabla\mathbf{v} := \left(\frac{\partial v_i}{\partial x_j}\right)_{i,j=1}^d \quad \text{and} \quad \mathrm{div}(\mathbf{v}) := \sum_{j=1}^d \frac{\partial v_j}{\partial x_j}.$$

In addition, for any tensor fields $\boldsymbol{\tau} = (\tau_{ij})_{i,j=1}^d$ and $\boldsymbol{\zeta} = (\zeta_{ij})_{i,j=1}^d$, we let $\mathbf{div}(\boldsymbol{\tau})$ be the divergence operator div acting along the rows of $\boldsymbol{\tau}$ and define the tensor inner product as

$$\boldsymbol{\tau} : \boldsymbol{\zeta} := \sum_{i,j=1}^d \tau_{ij}\,\zeta_{ij}\,.$$

In what follows, when no confusion arises, $|\cdot|$ denotes the Euclidean norm in R^d or $\mathrm{R}^{d\times d}$. In addition, in the sequel we will make use of the well-known Hölder inequality given by

$$\int_\Omega |f\,g| \leq \|f\|_{\mathrm{L}^\mathrm{p}(\Omega)}\,\|g\|_{\mathrm{L}^\mathrm{q}(\Omega)} \quad \forall\, f\in \mathrm{L}^\mathrm{p}(\Omega),\, \forall\, g\in \mathrm{L}^\mathrm{q}(\Omega), \quad \text{with} \quad \frac{1}{\mathrm{p}}+\frac{1}{\mathrm{q}} = 1\,, \tag{1.1}$$

which in the particular case when $\mathrm{p}=\mathrm{q}=2$, corresponds to the Cauchy–Schwarz inequality

$$\int_\Omega |f\,g| \leq \|f\|_{\mathrm{L}^2(\Omega)}\|g\|_{\mathrm{L}^2(\Omega)} \qquad \forall\, f, g\in \mathrm{L}^2(\Omega)\,, \tag{1.2}$$

and the Young inequality, for $a, b\geq 0$, $1/\mathrm{p}+1/\mathrm{q}=1$, and $\delta>0$,

$$ab \,\leq\, \frac{\delta^{\mathrm{p}/2}}{\mathrm{p}}\,a^\mathrm{p} + \frac{1}{\mathrm{q}\,\delta^{\mathrm{q}/2}}\,b^\mathrm{q}\,. \tag{1.3}$$

2 The model problem and its mixed-primal variational formulation

In this section, we introduce the stationary Biot–Brinkman–Forchheimer model and rewrite it in a form that is convenient for the analysis to follow. We then derive its associated variational formulation.

2.1 The model problem

Let $\Omega\subset\mathrm{R}^d$, $d\in\{2,3\}$, be a bounded Lipschitz domain occupied by a deformable porous medium, with boundary $\Gamma := \partial\Omega$. We consider a Biot–Brinkman–Forchheimer system describing the interaction between the deformation of the porous skeleton and a viscous fluid flowing through its pore network, including the nonlinear inertial resistance modeled by the Forchheimer term. Let $\nu>0$ be the fluid viscosity, $\mathtt{D}>0$ the Darcy coefficient, $\mathtt{F}\geq 0$ the Forchheimer coefficient, $m\in[3,4]$, $\alpha\in(0,1]$ the Biot–Willis constant, and $s_0>0$ the storage coefficient. In addition, let $\mathbf{f}_p:\Omega\to\mathrm{R}^d$ denote the body force acting on the porous skeleton, let $\mathbf{g}:\Omega\to\mathrm{R}^d$ denote the force acting on the fluid, and let $g:\Omega\to\mathrm{R}$ be the scalar source term in the mass balance equation. Then, the governing equations read

$$\begin{gathered}
-\mathbf{div}(\boldsymbol{\sigma}_p) = \mathbf{f}_p\,, \quad -\nu\,\Delta\mathbf{u} + \mathtt{D}\,\mathbf{u} + \mathtt{F}\,|\mathbf{u}|^{m-2}\mathbf{u} + \nabla p = \mathbf{g} \quad \text{in} \quad \Omega\,,\\
s_0\,p + \alpha\,\mathrm{div}(\boldsymbol{\eta}) + \mathrm{div}(\mathbf{u}) = g \quad \text{in} \quad \Omega\,,\\
\boldsymbol{\eta} = \mathbf{0}, \quad \mathbf{u} = \mathbf{0} \quad \text{on} \quad \Gamma\,,
\end{gathered} \tag{2.1}$$

where $\boldsymbol{\eta}$ denotes the displacement of the solid skeleton, $\mathbf{u}$ the fluid velocity, p the pore pressure, and $\boldsymbol{\sigma}_p$ the poroelastic stress tensor. The latter is given by Hooke's law as

$$\boldsymbol{\sigma}_p := 2\mu\,\boldsymbol{\varepsilon}(\boldsymbol{\eta}) + \lambda\,\mathrm{div}(\boldsymbol{\eta})\,\mathbb{I} - \alpha\,p\,\mathbb{I} \quad \text{in} \quad \Omega\,, \tag{2.2}$$

where $\mathbb{I}$ stands for the identity tensor and $\boldsymbol{\varepsilon}(\boldsymbol{\eta}) := \dfrac{1}{2}\big(\nabla\boldsymbol{\eta} + (\nabla\boldsymbol{\eta})^{\mathtt{t}}\big)$ is the infinitesimal strain tensor, while $\mu>0$ and $\lambda>0$ are the Lamé parameters.

To obtain a formulation that remains well defined in the limiting case $s_0\to 0^+$, we impose the normalization condition

$$(p, 1)_\Omega = 0\,. \tag{2.3}$$

Moreover, integrating the second equation of (2.1) over Ω and using the boundary conditions satisfied by $\boldsymbol{\eta}$ and $\mathbf{u}$, we obtain the following compatibility condition:

$$(g, 1)_\Omega = 0\,. \tag{2.4}$$

Following the locking-free strategy for poroelasticity developed in [37], we introduce the total pressure

$$\theta := \alpha\, p - \lambda\, \mathrm{div}(\boldsymbol{\eta}) \quad \text{in} \quad \Omega\,. \tag{2.5}$$

This change of variable allows us to rewrite the mechanical equation in terms of θ and to derive stability estimates that do not deteriorate in the nearly incompressible limit $\lambda \to \infty$. In addition, using (2.3), the divergence theorem, and the homogeneous Dirichlet boundary condition for $\boldsymbol{\eta}$, we obtain

$$(\theta, 1)_\Omega = \alpha (p, 1)_\Omega - \lambda (\mathrm{div}(\boldsymbol{\eta}), 1)_\Omega = \alpha (p, 1)_\Omega - \lambda \langle \boldsymbol{\eta} \cdot \mathbf{n}, 1 \rangle_\Gamma = 0\,. \tag{2.6}$$

Hence, using (2.1)–(2.6), the Biot–Brinkman–Forchheimer system can be equivalently rewritten as follows: Find $((\boldsymbol{\eta}, \mathbf{u}), (\theta, p))$ in suitable spaces such that

$$-\mathbf{div}\big(2\mu\, \boldsymbol{\varepsilon}(\boldsymbol{\eta}) - \theta\, \mathbb{I}\big) = \mathbf{f}_p\,, \quad -\nu\, \Delta \mathbf{u} + \mathtt{D}\, \mathbf{u} + \mathtt{F}\, |\mathbf{u}|^{m-2} \mathbf{u} + \nabla p = \mathbf{g} \quad \text{in} \quad \Omega\,, \tag{2.7a}$$

$$\frac{1}{\lambda} \theta - \frac{\alpha}{\lambda}\, p + \mathrm{div}(\boldsymbol{\eta}) = 0\,, \quad \left(s_0 + \frac{\alpha^2}{\lambda} \right) p - \frac{\alpha}{\lambda} \theta + \mathrm{div}(\mathbf{u}) = g \quad \text{in} \quad \Omega\,, \tag{2.7b}$$

$$(\theta, 1)_\Omega = 0\,, \quad (p, 1)_\Omega = 0\,, \quad \text{and} \quad \boldsymbol{\eta} = \mathbf{0}\,, \quad \mathbf{u} = \mathbf{0} \quad \text{on} \quad \Gamma\,. \tag{2.7c}$$

2.2 The mixed-primal variational formulation

We now derive a variational formulation associated with the reformulated Biot–Brinkman–Forchheimer system (2.7). To this end, the homogeneous Dirichlet boundary conditions imposed on $\boldsymbol{\eta}$ and $\mathbf{u}$ (cf. (2.7c)) naturally lead to test functions in $\mathbf{H}^1_0(\Omega) := \big\{ \mathbf{v} \in \mathbf{H}^1(\Omega) : \quad \mathbf{v} = \mathbf{0} \quad \text{on} \quad \Gamma \big\}$. Accordingly, we test the mechanical equilibrium and Brinkman–Forchheimer equations in (2.7a) with $\boldsymbol{\xi}, \mathbf{v} \in \mathbf{H}^1_0(\Omega)$, respectively. Integrating by parts and using $\boldsymbol{\xi} = \mathbf{0}$ and $\mathbf{v} = \mathbf{0}$ on Γ, we obtain

$$2\mu\, (\boldsymbol{\varepsilon}(\boldsymbol{\eta}), \boldsymbol{\varepsilon}(\boldsymbol{\xi}))_\Omega - (\theta, \mathrm{div}(\boldsymbol{\xi}))_\Omega = (\mathbf{f}_p, \boldsymbol{\xi})_\Omega \qquad \forall\, \boldsymbol{\xi} \in \mathbf{H}^1_0(\Omega)\,, \tag{2.8}$$

and

$$\nu\, (\nabla \mathbf{u}, \nabla \mathbf{v})_\Omega + \mathtt{D}\, (\mathbf{u}, \mathbf{v})_\Omega + \mathtt{F}\, (|\mathbf{u}|^{m-2} \mathbf{u}, \mathbf{v})_\Omega - (p, \mathrm{div}(\mathbf{v}))_\Omega = (\mathbf{g}, \mathbf{v})_\Omega \qquad \forall\, \mathbf{v} \in \mathbf{H}^1_0(\Omega)\,. \tag{2.9}$$

The weak identities (2.8)–(2.9) confirm that $\mathbf{H}^1_0(\Omega)$ is the natural search space for both $\boldsymbol{\eta}$ and $\mathbf{u}$. Indeed, this space provides the regularity required by the terms involving $\boldsymbol{\varepsilon}(\boldsymbol{\eta})$, $\nabla \mathbf{u}$, $\mathrm{div}(\boldsymbol{\eta})$, and $\mathrm{div}(\mathbf{u})$, while incorporating the homogeneous Dirichlet boundary conditions in the sense of traces. Thus, all terms in (2.8)–(2.9) are well defined for $\boldsymbol{\eta}, \mathbf{u} \in \mathbf{H}^1_0(\Omega)$ and $p, \theta \in \mathrm{L}^2(\Omega)$. Moreover, the nonlinear Forchheimer term is well defined in this setting. Indeed, since $m \in [3, 4]$, the continuous embedding $\mathbf{i}_m : \mathbf{H}^1(\Omega) \hookrightarrow \mathbf{L}^m(\Omega)$, together with Hlder's inequality, gives

$$\big| (|\mathbf{u}|^{m-2} \mathbf{u}, \mathbf{v})_\Omega \big| \le \|\mathbf{u}\|^{m-1}_{\mathbf{L}^m(\Omega)}\, \|\mathbf{v}\|_{\mathbf{L}^m(\Omega)} \le \|\mathbf{i}_m\|^m\, \|\mathbf{u}\|^{m-1}_{\mathbf{H}^1(\Omega)}\, \|\mathbf{v}\|_{\mathbf{H}^1(\Omega)} \qquad \forall\, \mathbf{u}, \mathbf{v} \in \mathbf{H}^1(\Omega)\,,$$

with $\|\mathbf{i}_m\|$ denoting the norm of the embedding $\mathbf{i}_m$.

We next derive the weak form of the scalar equations. Testing the definition of the total pressure and the reformulated mass balance equation (cf. (2.7b)) with $\psi, q \in \mathrm{L}^2(\Omega)$, respectively, yields

$$\frac{1}{\lambda} (\theta, \psi)_\Omega - \frac{\alpha}{\lambda}\, (p, \psi)_\Omega + (\mathrm{div}(\boldsymbol{\eta}), \psi)_\Omega = 0 \qquad \forall\, \psi \in \mathrm{L}^2(\Omega)\,, \tag{2.10}$$

and

$$\left(s_0 + \frac{\alpha^2}{\lambda} \right) (p, q)_\Omega - \frac{\alpha}{\lambda} (\theta, q)_\Omega + (\mathrm{div}(\mathbf{u}), q)_\Omega = (g, q)_\Omega \qquad \forall\, q \in \mathrm{L}^2(\Omega)\,. \tag{2.11}$$

At this point, the scalar equations have been written with test functions in $\mathrm{L}^2(\Omega)$. However, the conditions (2.3) and (2.6) imply that the scalar unknowns p and θ are sought in $\mathrm{L}^2_0(\Omega) := \big\{q \in \mathrm{L}^2(\Omega) : \quad (q,1)_\Omega = 0\big\}$. Consequently, it is enough to test (2.10) and (2.11) with functions in $\mathrm{L}^2_0(\Omega)$. Indeed, using the decomposition $\mathrm{L}^2(\Omega) = \mathrm{L}^2_0(\Omega) \oplus \mathrm{R}$, together with the fact $(\mathrm{div}(\boldsymbol{\eta}),1)_\Omega = 0$ and $(\mathrm{div}(\mathbf{u}),1)_\Omega = 0$, which follow from the divergence theorem and the homogeneous Dirichlet boundary conditions, the constant part of (2.10) is automatically satisfied. On the other hand, the constant part of (2.11) reduces to the compatibility condition (2.4). Therefore, throughout the paper we assume that $g \in \mathrm{L}^2_0(\Omega)$. Consequently, testing the scalar equations with functions in $\mathrm{L}^2(\Omega)$ is equivalent to testing them with functions in $\mathrm{L}^2_0(\Omega)$.

Next, in order to rewrite the above formulation in a more suitable form for the analysis below, we introduce the product spaces

$$\mathbb{H} := \mathbf{H}^1_0(\Omega) \times \mathbf{H}^1_0(\Omega) \quad \text{and} \quad \mathbb{Q} := \mathrm{L}^2_0(\Omega) \times \mathrm{L}^2_0(\Omega)\,,$$

endowed with the norms

$$\|(\boldsymbol{\xi},\mathbf{v})\|^2_{\mathbb{H}} := \|\boldsymbol{\xi}\|^2_{\mathbf{H}^1(\Omega)} + \|\mathbf{v}\|^2_{\mathbf{H}^1(\Omega)} \quad \forall\,(\boldsymbol{\xi},\mathbf{v}) \in \mathbb{H} \quad \text{and} \quad \|(\psi,q)\|^2_{\mathbb{Q}} := \|\psi\|^2_{\mathrm{L}^2(\Omega)} + \|q\|^2_{\mathrm{L}^2(\Omega)} \quad \forall\,(\psi,q) \in \mathbb{Q}\,.$$

Then, adding (2.8) and (2.9), and also adding (2.10) and (2.11), we arrive at the following mixed-primal formulation for the Biot–Brinkman–Forchheimer system: Find $((\boldsymbol{\eta},\mathbf{u}),(\theta,p)) \in \mathbb{H}\times\mathbb{Q}$ such that

$$\begin{aligned}
[\mathcal{A}(\boldsymbol{\eta},\mathbf{u}),(\boldsymbol{\xi},\mathbf{v})] \;+\; [\mathcal{B}^{\mathrm{t}}(\theta,p),(\boldsymbol{\xi},\mathbf{v})] \;&=\; [\mathbf{F},(\boldsymbol{\xi},\mathbf{v})] \quad \forall\,(\boldsymbol{\xi},\mathbf{v}) \in \mathbb{H}\,,\\
-[\mathcal{B}(\boldsymbol{\eta},\mathbf{u}),(\psi,q)] \;+\; [\mathcal{C}(\theta,p),(\psi,q)] \;&=\; [\mathbf{G},(\psi,q)] \quad \forall\,(\psi,q) \in \mathbb{Q}\,,
\end{aligned} \tag{2.12}$$

where the operators $\mathcal{A} : \mathbb{H} \to \mathbb{H}'$, $\mathcal{B} : \mathbb{H} \to \mathbb{Q}'$, and $\mathcal{C} : \mathbb{Q} \to \mathbb{Q}'$ are defined by

$$[\mathcal{A}(\boldsymbol{\eta},\mathbf{u}),(\boldsymbol{\xi},\mathbf{v})] := 2\mu\,(\boldsymbol{\varepsilon}(\boldsymbol{\eta}),\boldsymbol{\varepsilon}(\boldsymbol{\xi}))_\Omega + \nu\,(\nabla\mathbf{u},\nabla\mathbf{v})_\Omega + \mathtt{D}\,(\mathbf{u},\mathbf{v})_\Omega + \mathtt{F}\,(|\mathbf{u}|^{m-2}\mathbf{u},\mathbf{v})_\Omega\,, \tag{2.13}$$

$$[\mathcal{B}(\boldsymbol{\xi},\mathbf{v}),(\psi,q)] := -(\mathrm{div}(\boldsymbol{\xi}),\psi)_\Omega - (\mathrm{div}(\mathbf{v}),q)_\Omega\,, \tag{2.14}$$

$$[\mathcal{C}(\theta,p),(\psi,q)] := \frac{1}{\lambda}(\theta-\alpha p,\psi-\alpha q)_\Omega + s_0(p,q)_\Omega\,. \tag{2.15}$$

In addition, the linear functionals $\mathbf{F} \in \mathbb{H}'$ and $\mathbf{G} \in \mathbb{Q}'$ are given by

$$[\mathbf{F},(\boldsymbol{\xi},\mathbf{v})] := (\mathbf{f}_p,\boldsymbol{\xi})_\Omega + (\mathbf{g},\mathbf{v})_\Omega \quad \text{and} \quad [\mathbf{G},(\psi,q)] := (g,q)_\Omega\,. \tag{2.16}$$

Throughout, the notation $[\cdot,\cdot]$ denotes the duality pairing associated with the corresponding operator. Finally, we define $\mathcal{B}^{\mathrm{t}} : \mathbb{Q} \to \mathbb{H}'$ as the adjoint of $\mathcal{B}$, satisfying $[\mathcal{B}^{\mathrm{t}}(\psi,q),(\boldsymbol{\xi},\mathbf{v})] = [\mathcal{B}(\boldsymbol{\xi},\mathbf{v}),(\psi,q)]$ for all $((\boldsymbol{\xi},\mathbf{v}),(\psi,q)) \in \mathbb{H}\times\mathbb{Q}$.

3 Analysis of the continuous problem

We now address the well-posedness of the variational problem (2.12). We begin by establishing some auxiliary results that provide the main ingredients for the subsequent solvability analysis.

3.1 Preliminaries

In order to prove the existence and uniqueness of a solution to (2.12), we first recall the abstract result on which our analysis relies, namely the Browder–Minty theorem [38, Theorem 10.49]. Afterwards, we establish the stability and monotonicity properties of the operators involved in the present formulation.

Let V be a Banach space. We say that an operator $\mathcal{S} : V \to V'$ is hemicontinuous if, for each $u, v, z \in V$, the function

$$\mathrm{R} \ni t \longmapsto [\mathcal{S}(u + tv), z] \in \mathrm{R}$$

is continuous. Clearly, the continuity of $\mathcal{S} : V \to V'$ is a sufficient condition for hemicontinuity. In addition, $\mathcal{S}$ is said to be coercive if

$$\lim_{\|u\|_V \to +\infty} \frac{[\mathcal{S}(u), u]}{\|u\|_V} = +\infty. \tag{3.1}$$

Moreover, $\mathcal{S}$ is strictly monotone if

$$[\mathcal{S}(u) - \mathcal{S}(v), u - v] > 0 \qquad \forall\, u, v \in V,\, u \neq v,$$

and $\mathcal{S}$ is strongly monotone if there exists a constant $c > 0$ such that

$$[\mathcal{S}(u) - \mathcal{S}(v), u - v] \geq c\|u - v\|_V^2 \qquad \forall\, u, v \in V.$$

It is easy to see that strong monotonicity implies both strict monotonicity and coerciveness. In fact, applying the previous inequality with $v = 0$, we obtain

$$c\|u\|_V^2 \leq [\mathcal{S}(u) - \mathcal{S}(0), u] \leq [\mathcal{S}(u), u] + \|\mathcal{S}(0)\|_{V'}\|u\|_V,$$

and hence

$$\frac{[\mathcal{S}(u), u]}{\|u\|_V} \geq c\|u\|_V - \|\mathcal{S}(0)\|_{V'} \qquad \forall\, u \in V, \quad u \neq 0\,, \tag{3.2}$$

which implies (3.1). In particular, if $\mathcal{S}(0)$ is the null functional of V', then (3.2) becomes

$$[\mathcal{S}(u), u] \geq c\|u\|_V^2 \qquad \forall\, u \in V\,,$$

and in the linear case is called ellipticity and yields strong monotonicity. Indeed, by linearity of $\mathcal{S}$, for all $u, v \in V$,

$$[\mathcal{S}(u) - \mathcal{S}(v), u - v] = [\mathcal{S}(u - v), u - v] \geq c\|u - v\|_V^2\,.$$

We next recall the Browder–Minty theorem [38, Theorem 10.49].

Theorem 3.1 *Let V be a real separable reflexive Banach space and let $\mathcal{S} : V \to V'$ be a coercive, hemicontinuous, and monotone operator. Then $\mathcal{S}$ is surjective, that is, for each $f \in V'$ there exists $u \in V$ such that $\mathcal{S}(u) = f$. Moreover, if $\mathcal{S}$ is strictly monotone, then $\mathcal{S}$ is injective.*

As a direct consequence of the Browder–Minty theorem and the previous discussion, we have the following result.

Corollary 3.2 *Let V be a real separable reflexive Banach space and let $\mathcal{S} : V \to V'$ be a continuous and strongly monotone operator. Then $\mathcal{S}$ is bijective, that is, for each $f \in V'$ there exists a unique $u \in V$ such that $\mathcal{S}(u) = f$.*

We next verify the properties required to apply Corollary 3.2 to the operator associated with (2.12). We begin with the linear operators $\mathcal{B}$ and $\mathcal{C}$, and with the right-hand side functionals $\mathbf{F}$ and $\mathbf{G}$. From their definitions (cf. (2.14), (2.15), and (2.16)), it is clear that $\mathcal{B}$, $\mathcal{C}$, $\mathbf{F}$, and $\mathbf{G}$ are linear. Moreover, using the Cauchy–Schwarz inequality, we obtain

$$
\begin{aligned}
&|[\mathcal{B}(\boldsymbol{\xi},\mathbf{v}),(\psi,q)]| \le \sqrt{d}\,\|(\boldsymbol{\xi},\mathbf{v})\|_{\mathbb{H}}\,\|(\psi,q)\|_{\mathbb{Q}} && \forall\,((\boldsymbol{\xi},\mathbf{v}),(\psi,q)) \in \mathbb{H}\times\mathbb{Q}\,,\\
&|[\mathcal{C}(\theta,p),(\psi,q)]| \le 2\max\left\{\frac{1}{\lambda},\frac{\alpha}{\lambda},s_0+\frac{\alpha^2}{\lambda}\right\}\|(\theta,p)\|_{\mathbb{Q}}\,\|(\psi,q)\|_{\mathbb{Q}} && \forall\,(\theta,p),(\psi,q)\in\mathbb{Q}\,,\\
&|[\mathbf{F},(\boldsymbol{\xi},\mathbf{v})]| \le \Big(\|\mathbf{f}_p\|^2_{\mathbf{L}^2(\Omega)}+\|\mathbf{g}\|^2_{\mathbf{L}^2(\Omega)}\Big)^{1/2}\,\|(\boldsymbol{\xi},\mathbf{v})\|_{\mathbb{H}} && \forall\,(\boldsymbol{\xi},\mathbf{v})\in\mathbb{H}\,,\\
&|[\mathbf{G},(\psi,q)]| \le \|g\|_{\mathrm{L}^2(\Omega)}\|(\psi,q)\|_{\mathbb{Q}} && \forall\,(\psi,q)\in\mathbb{Q}\,.
\end{aligned}
\tag{3.3}
$$

Therefore, $\mathcal{B}$, $\mathcal{C}$, $\mathbf{F}$, and $\mathbf{G}$ are bounded and continuous.

We now establish the main properties of the nonlinear operator $\mathcal{A}$ and of the linear operator $\mathcal{C}$.

Lemma 3.3 *The nonlinear operator $\mathcal{A}:\mathbb{H}\to\mathbb{H}'$ satisfies the following properties:*

(i) $\mathcal{A}$ is bounded, in the sense that there exists a positive constant $C_{\mathcal{A}}$ such that

$$
|[\mathcal{A}(\boldsymbol{\eta},\mathbf{u}),(\boldsymbol{\xi},\mathbf{v})]| \le C_{\mathcal{A}}\Big(\|\boldsymbol{\eta}\|^2_{\mathbf{H}^1(\Omega)}+\|\mathbf{u}\|^2_{\mathbf{H}^1(\Omega)}+\|\mathbf{u}\|^{2(m-1)}_{\mathbf{H}^1(\Omega)}\Big)^{1/2}\|(\boldsymbol{\xi},\mathbf{v})\|_{\mathbb{H}} \tag{3.4}
$$

for all $(\boldsymbol{\eta},\mathbf{u}),(\boldsymbol{\xi},\mathbf{v})\in\mathbb{H}$.

(ii) $\mathcal{A}$ is continuous. More precisely, there exists a positive constant $L_{\mathcal{A}}$ such that

$$
\|\mathcal{A}(\boldsymbol{\eta},\mathbf{u})-\mathcal{A}(\boldsymbol{\zeta},\mathbf{w})\|_{\mathbb{H}'} \le L_{\mathcal{A}}\Big(1+\big(\|\mathbf{u}\|_{\mathbf{H}^1(\Omega)}+\|\mathbf{w}\|_{\mathbf{H}^1(\Omega)}\big)^{m-2}\Big)\|(\boldsymbol{\eta},\mathbf{u})-(\boldsymbol{\zeta},\mathbf{w})\|_{\mathbb{H}} \tag{3.5}
$$

for all $(\boldsymbol{\eta},\mathbf{u}),(\boldsymbol{\zeta},\mathbf{w})\in\mathbb{H}$.

(iii) $\mathcal{A}$ is strongly monotone, that is, there exists a positive constant $\alpha_{\mathcal{A}}$ such that

$$
[\mathcal{A}(\boldsymbol{\eta},\mathbf{u})-\mathcal{A}(\boldsymbol{\zeta},\mathbf{w}),(\boldsymbol{\eta}-\boldsymbol{\zeta},\mathbf{u}-\mathbf{w})] \ge \alpha_{\mathcal{A}}\|(\boldsymbol{\eta},\mathbf{u})-(\boldsymbol{\zeta},\mathbf{w})\|^2_{\mathbb{H}} \tag{3.6}
$$

for all $(\boldsymbol{\eta},\mathbf{u}),(\boldsymbol{\zeta},\mathbf{w})\in\mathbb{H}$.

Proof. We first prove the boundedness of $\mathcal{A}$. Let $(\boldsymbol{\eta},\mathbf{u}),(\boldsymbol{\xi},\mathbf{v})\in\mathbb{H}$. From the definition of $\mathcal{A}$ (cf. (2.13)), the Cauchy–Schwarz and Hölder inequalities (cf. (1.2) and (1.1)), and the continuous embedding $\mathbf{i}_m:\mathbf{H}^1(\Omega)\hookrightarrow\mathbf{L}^m(\Omega)$, we obtain

$$
\begin{aligned}
|[\mathcal{A}(\boldsymbol{\eta},\mathbf{u}),(\boldsymbol{\xi},\mathbf{v})]| &\le 2\mu\,\|\boldsymbol{\eta}\|_{\mathbf{H}^1(\Omega)}\|\boldsymbol{\xi}\|_{\mathbf{H}^1(\Omega)}+(\nu+\mathtt{D})\,\|\mathbf{u}\|_{\mathbf{H}^1(\Omega)}\|\mathbf{v}\|_{\mathbf{H}^1(\Omega)}\\
&\quad+\mathtt{F}\,\|\mathbf{i}_m\|^m\|\mathbf{u}\|^{m-1}_{\mathbf{H}^1(\Omega)}\|\mathbf{v}\|_{\mathbf{H}^1(\Omega)}\,.
\end{aligned}
$$

Hence, by the Cauchy–Schwarz inequality, we deduce (3.4) with

$$
C_{\mathcal{A}} := \sqrt{2}\,\max\{2\mu,\nu+\mathtt{D},\mathtt{F}\|\mathbf{i}_m\|^m\}\,.
$$

We now prove the continuity of $\mathcal{A}$. Let $(\boldsymbol{\eta},\mathbf{u}),(\boldsymbol{\zeta},\mathbf{w}),(\boldsymbol{\xi},\mathbf{v})\in\mathbb{H}$. From the definition of $\mathcal{A}$, the Cauchy–Schwarz inequality, and Hölder's inequality, we first have

$$
|[\mathcal{A}(\boldsymbol{\eta},\mathbf{u})-\mathcal{A}(\boldsymbol{\zeta},\mathbf{w}),(\boldsymbol{\xi},\mathbf{v})]|
$$

$$\leq 2\mu\,\|\boldsymbol{\eta}-\boldsymbol{\zeta}\|_{\mathbf{H}^1(\Omega)}\|\boldsymbol{\xi}\|_{\mathbf{H}^1(\Omega)} + (\nu+\mathtt{D})\,\|\mathbf{u}-\mathbf{w}\|_{\mathbf{H}^1(\Omega)}\|\mathbf{v}\|_{\mathbf{H}^1(\Omega)}$$
$$+\,\mathtt{F}\,\||\mathbf{u}|^{m-2}\mathbf{u}-|\mathbf{w}|^{m-2}\mathbf{w}\|_{\mathbf{L}^{m/(m-1)}(\Omega)}\|\mathbf{v}\|_{\mathbf{L}^m(\Omega)}\,. \tag{3.7}$$

To control the nonlinear term, we employ [4, eq. (2.1a) of Lemma 2.1] (see also [28, Proposition 5.3]), which gives

$$\big||\mathbf{u}|^{m-2}\mathbf{u}-|\mathbf{w}|^{m-2}\mathbf{w}\big| \leq C_m\big(|\mathbf{u}|+|\mathbf{w}|\big)^{m-2}|\mathbf{u}-\mathbf{w}|\,, \tag{3.8}$$

where $C_m>0$ depends on m. Then, by Hölder's inequality and the embedding $\mathbf{i}_m:\mathbf{H}^1(\Omega)\hookrightarrow\mathbf{L}^m(\Omega)$, we get

$$\begin{aligned}&\||\mathbf{u}|^{m-2}\mathbf{u}-|\mathbf{w}|^{m-2}\mathbf{w}\|_{\mathbf{L}^{m/(m-1)}(\Omega)}\|\mathbf{v}\|_{\mathbf{L}^m(\Omega)}\\&\quad\leq C_m\|\mathbf{i}_m\|^m\left(\|\mathbf{u}\|_{\mathbf{H}^1(\Omega)}+\|\mathbf{w}\|_{\mathbf{H}^1(\Omega)}\right)^{m-2}\|\mathbf{u}-\mathbf{w}\|_{\mathbf{H}^1(\Omega)}\|\mathbf{v}\|_{\mathbf{H}^1(\Omega)}\,.\end{aligned} \tag{3.9}$$

Combining (3.7) with (3.9), we arrive at

$$\begin{aligned}|[\mathcal{A}(\boldsymbol{\eta},\mathbf{u})-\mathcal{A}(\boldsymbol{\zeta},\mathbf{w}),(\boldsymbol{\xi},\mathbf{v})]| \leq \Big(&2\mu\|\boldsymbol{\eta}-\boldsymbol{\zeta}\|_{\mathbf{H}^1(\Omega)}+(\nu+\mathtt{D})\|\mathbf{u}-\mathbf{w}\|_{\mathbf{H}^1(\Omega)}\\&+C_m\mathtt{F}\|\mathbf{i}_m\|^m\left(\|\mathbf{u}\|_{\mathbf{H}^1(\Omega)}+\|\mathbf{w}\|_{\mathbf{H}^1(\Omega)}\right)^{m-2}\|\mathbf{u}-\mathbf{w}\|_{\mathbf{H}^1(\Omega)}\Big)\|(\boldsymbol{\xi},\mathbf{v})\|_{\mathbb{H}}\,.\end{aligned}$$

Taking the supremum over all nonzero $(\boldsymbol{\xi},\mathbf{v})\in\mathbb{H}$, we obtain (3.5) with

$$L_{\mathcal{A}} := \sqrt{2}\max\left\{2\mu+\nu+\mathtt{D},\,C_m\mathtt{F}\|\mathbf{i}_m\|^m\right\}\,. \tag{3.10}$$

It remains to prove the strong monotonicity. By [4, eq. (2.1b) of Lemma 2.1], there exists a constant $\widetilde{C}_m>0$, depending only on m, such that

$$\left(|\mathbf{u}|^{m-2}\mathbf{u}-|\mathbf{w}|^{m-2}\mathbf{w},\mathbf{u}-\mathbf{w}\right)_\Omega \geq \widetilde{C}_m\|\mathbf{u}-\mathbf{w}\|^m_{\mathbf{L}^m(\Omega)}\,. \tag{3.11}$$

Therefore, from the definition of $\mathcal{A}$ (cf. (2.13)) and (3.11), we obtain

$$\begin{aligned}&[\mathcal{A}(\boldsymbol{\eta},\mathbf{u})-\mathcal{A}(\boldsymbol{\zeta},\mathbf{w}),(\boldsymbol{\eta}-\boldsymbol{\zeta},\mathbf{u}-\mathbf{w})]\\&\quad\geq 2\mu\|\boldsymbol{\varepsilon}(\boldsymbol{\eta}-\boldsymbol{\zeta})\|^2_{\mathbb{L}^2(\Omega)}+\nu\|\nabla(\mathbf{u}-\mathbf{w})\|^2_{\mathbb{L}^2(\Omega)}+\mathtt{D}\|\mathbf{u}-\mathbf{w}\|^2_{\mathbf{L}^2(\Omega)}+\mathtt{F}\,\widetilde{C}_m\|\mathbf{u}-\mathbf{w}\|^m_{\mathbf{L}^m(\Omega)}.\end{aligned} \tag{3.12}$$

Dropping the last nonnegative term in (3.12) and using Korn's inequality,

$$\|\boldsymbol{\varepsilon}(\boldsymbol{\xi})\|^2_{\mathbb{L}^2(\Omega)} \geq c_k\|\boldsymbol{\xi}\|^2_{\mathbf{H}^1(\Omega)} \qquad \forall\,\boldsymbol{\xi}\in\mathbf{H}^1_0(\Omega),$$

we infer from (3.12) that

$$\begin{aligned}&[\mathcal{A}(\boldsymbol{\eta},\mathbf{u})-\mathcal{A}(\boldsymbol{\zeta},\mathbf{w}),(\boldsymbol{\eta}-\boldsymbol{\zeta},\mathbf{u}-\mathbf{w})]\\&\quad\geq 2\mu c_k\|\boldsymbol{\eta}-\boldsymbol{\zeta}\|^2_{\mathbf{H}^1(\Omega)}+\nu\|\nabla(\mathbf{u}-\mathbf{w})\|^2_{\mathbb{L}^2(\Omega)}+\mathtt{D}\|\mathbf{u}-\mathbf{w}\|^2_{\mathbf{L}^2(\Omega)}\geq\alpha_{\mathcal{A}}\|(\boldsymbol{\eta},\mathbf{u})-(\boldsymbol{\zeta},\mathbf{w})\|^2_{\mathbb{H}},\end{aligned}$$

where

$$\alpha_{\mathcal{A}} := \min\left\{2\mu c_k,\nu,\mathtt{D}\right\}\,. \tag{3.13}$$

□

Lemma 3.4 *The linear operator $\mathcal{C}:\mathbb{Q}\to\mathbb{Q}'$ is elliptic in $\mathbb{Q}$. More precisely, there exists a positive constant $\alpha_{\mathcal{C}}$, depending on λ, s_0, and α, such that*

$$[\mathcal{C}(\psi,q),(\psi,q)] \geq \alpha_{\mathcal{C}}\|(\psi,q)\|^2_{\mathbb{Q}} \qquad \forall\,(\psi,q)\in\mathbb{Q}\,. \tag{3.14}$$

Proof. Let $(\psi,q)\in\mathbb{Q}$. From the definition of $\mathcal{C}$ (cf. (2.15)), we have

$$[\mathcal{C}(\psi,q),(\psi,q)]=\frac{1}{\lambda}\|\psi-\alpha q\|^2_{\mathrm{L}^2(\Omega)}+s_0\|q\|^2_{\mathrm{L}^2(\Omega)}\,.$$

On the other hand, by the triangle and Young inequalities (cf. (1.3)), we obtain

$$\|\psi\|^2_{\mathrm{L}^2(\Omega)}\leq 2\|\psi-\alpha q\|^2_{\mathrm{L}^2(\Omega)}+2\alpha^2\|q\|^2_{\mathrm{L}^2(\Omega)}\,,$$

which implies

$$\begin{aligned}\|(\psi,q)\|^2_{\mathbb{Q}}&=\|\psi\|^2_{\mathrm{L}^2(\Omega)}+\|q\|^2_{\mathrm{L}^2(\Omega)}\leq 2\|\psi-\alpha q\|^2_{\mathrm{L}^2(\Omega)}+(1+2\alpha^2)\|q\|^2_{\mathrm{L}^2(\Omega)}\\&\leq\max\left\{2\lambda,\frac{(1+2\alpha^2)}{s_0}\right\}\left(\frac{1}{\lambda}\|\psi-\alpha\,q\|^2_{\mathrm{L}^2(\Omega)}+s_0\|q\|^2_{\mathrm{L}^2(\Omega)}\right)\,,\end{aligned}$$

and after simple computations, there holds (3.14) with

$$\alpha_{\mathcal{C}}:=\min\left\{\frac{1}{2\lambda},\frac{s_0}{1+2\alpha^2}\right\}\,.$$

□

Finally, we recall the inf-sup condition associated with the operator $\mathcal{B}$ (cf. (2.14)). Although this condition is not required to establish the existence and uniqueness of a solution to (2.12), it will be instrumental in deriving estimates for θ and p in which the dependence on the storage coefficient s_0 is explicitly identified.

Lemma 3.5 *There exists a positive constant β such that*

$$\sup_{\mathbf{0}\neq(\boldsymbol{\xi},\mathbf{v})\in\mathbb{H}}\frac{[\mathcal{B}(\boldsymbol{\xi},\mathbf{v}),(\psi,q)]}{\|(\boldsymbol{\xi},\mathbf{v})\|_{\mathbb{H}}}\geq\beta\|(\psi,q)\|_{\mathbb{Q}}\qquad\forall\,(\psi,q)\in\mathbb{Q}\,.\tag{3.15}$$

Proof. The result follows from the surjectivity of the divergence operator div : $\mathbf{H}^1_0(\Omega)\to\mathrm{L}^2_0(\Omega)$ [21, Corollary B.71]. Applying this result componentwise, according to the definition of $\mathcal{B}$ and the product structure of $\mathbb{H}$ and $\mathbb{Q}$, gives the stated inf-sup condition. □

3.2 Well-posedness of the mixed-primal formulation

Now, in order to establish the existence of a unique solution to (2.12), we introduce the operator $\mathcal{J}:\mathbb{H}\times\mathbb{Q}\to(\mathbb{H}\times\mathbb{Q})'$ defined by

$$\begin{aligned}&[\mathcal{J}((\boldsymbol{\eta},\mathbf{u}),(\theta,p)),((\boldsymbol{\xi},\mathbf{v}),(\psi,q))]\\&\quad:=[\mathcal{A}(\boldsymbol{\eta},\mathbf{u}),(\boldsymbol{\xi},\mathbf{v})]+[\mathcal{B}^{\mathrm{t}}(\theta,p),(\boldsymbol{\xi},\mathbf{v})]-[\mathcal{B}(\boldsymbol{\eta},\mathbf{u}),(\psi,q)]+[\mathcal{C}(\theta,p),(\psi,q)]\,.\end{aligned}$$

Then, solving (2.12) is equivalent to finding $((\boldsymbol{\eta},\mathbf{u}),(\theta,p))\in\mathbb{H}\times\mathbb{Q}$ such that

$$[\mathcal{J}((\boldsymbol{\eta},\mathbf{u}),(\theta,p)),((\boldsymbol{\xi},\mathbf{v}),(\psi,q))]=[\mathbf{F},(\boldsymbol{\xi},\mathbf{v})]+[\mathbf{G},(\psi,q)]\qquad\forall\,((\boldsymbol{\xi},\mathbf{v}),(\psi,q))\in\mathbb{H}\times\mathbb{Q}\,.\tag{3.16}$$

We begin by observing that $\mathcal{J}$ is continuous. Indeed, by its definition, this follows directly from the continuity of $\mathcal{A}$ (cf. (3.5)) and the boundedness of the linear operators $\mathcal{B}$ and $\mathcal{C}$ established in (3.3). Next, let $((\boldsymbol{\eta},\mathbf{u}),(\theta,p))$ and $((\boldsymbol{\zeta},\mathbf{w}),(\varphi,r))$ be in $\mathbb{H}\times\mathbb{Q}$. From the definition of $\mathcal{J}$, we have

$$[\mathcal{J}((\boldsymbol{\eta},\mathbf{u}),(\theta,p))-\mathcal{J}((\boldsymbol{\zeta},\mathbf{w}),(\varphi,r)),((\boldsymbol{\eta},\mathbf{u}),(\theta,p))-((\boldsymbol{\zeta},\mathbf{w}),(\varphi,r))]$$

$$= [\mathcal{A}(\boldsymbol{\eta},\mathbf{u}) - \mathcal{A}(\boldsymbol{\zeta},\mathbf{w}), (\boldsymbol{\eta},\mathbf{u}) - (\boldsymbol{\zeta},\mathbf{w})] + [\mathcal{C}((\theta,p)-(\varphi,r)), (\theta,p)-(\varphi,r)]\,.$$

Using the strong monotonicity of $\mathcal{A}$ and the ellipticity of $\mathcal{C}$, we obtain

$$\begin{aligned}&[\mathcal{J}((\boldsymbol{\eta},\mathbf{u}),(\theta,p)) - \mathcal{J}((\boldsymbol{\zeta},\mathbf{w}),(\varphi,r)), ((\boldsymbol{\eta}-\boldsymbol{\zeta},\mathbf{u}-\mathbf{w}),(\theta-\varphi,p-r))]\\ &\quad\geq \alpha_{\mathcal{A}}\|(\boldsymbol{\eta},\mathbf{u}) - (\boldsymbol{\zeta},\mathbf{w})\|^2_{\mathbb{H}} + \alpha_{\mathcal{C}}\|(\theta,p)-(\varphi,r)\|^2_{\mathbb{Q}} \geq \alpha_{\mathcal{J}}\,\|((\boldsymbol{\eta},\mathbf{u}),(\theta,p)) - ((\boldsymbol{\zeta},\mathbf{w}),(\varphi,r))\|^2_{\mathbb{H}\times\mathbb{Q}}\,,\end{aligned}$$

where $\alpha_{\mathcal{J}} := \min\{\alpha_{\mathcal{A}}, \alpha_{\mathcal{C}}\} > 0$. Consequently, $\mathcal{J}$ is strongly monotone.

Hence, we are in a position to conclude the main result of this section.

Theorem 3.6 *For each $(\mathbf{F},\mathbf{G}) \in \mathbb{H}'\times\mathbb{Q}'$ defined by (2.16), there exists a unique $((\boldsymbol{\eta},\mathbf{u}),(\theta,p)) \in \mathbb{H}\times\mathbb{Q}$ satisfying (3.16) (equivalently, (2.12)). Moreover, there exists a positive constant $C_{\mathtt{st}}$, independent of s_0 and λ, such that*

$$\|(\boldsymbol{\eta},\mathbf{u})\|_{\mathbb{H}} + \|(\theta,p)\|_{\mathbb{Q}} \leq C_{\mathtt{st}} \sum_{j\in\{1,m-1\}} \left(\|\mathbf{f}_p\|_{\mathbf{L}^2(\Omega)} + \|\mathbf{g}\|_{\mathbf{L}^2(\Omega)} + \frac{1}{\sqrt{s_0}}\|g\|_{\mathrm{L}^2(\Omega)}\right)^j. \tag{3.17}$$

Proof. Since $\mathcal{J} : \mathbb{H}\times\mathbb{Q} \to (\mathbb{H}\times\mathbb{Q})'$ is continuous and strongly monotone, Corollary 3.2 implies that $\mathcal{J}$ is bijective. Hence, for each $(\mathbf{F},\mathbf{G}) \in \mathbb{H}'\times\mathbb{Q}'$, there exists a unique $((\boldsymbol{\eta},\mathbf{u}),(\theta,p)) \in \mathbb{H}\times\mathbb{Q}$ satisfying (3.16) (equivalently, (2.12)).

It remains to establish the estimate (3.17). To this end, we take $(\boldsymbol{\xi},\mathbf{v}) = (\boldsymbol{\eta},\mathbf{u})$ in the first equation of (2.12), and $(\psi,q) = (\theta,p)$ in the second one. Then, adding both identities, we obtain

$$\begin{aligned}&2\mu\|\boldsymbol{\varepsilon}(\boldsymbol{\eta})\|^2_{\mathbb{L}^2(\Omega)} + \nu\|\nabla\mathbf{u}\|^2_{\mathbb{L}^2(\Omega)} + \mathtt{D}\|\mathbf{u}\|^2_{\mathbf{L}^2(\Omega)} + \mathtt{F}\|\mathbf{u}\|^m_{\mathbf{L}^m(\Omega)} + \frac{1}{\lambda}\|\theta-\alpha p\|^2_{\mathrm{L}^2(\Omega)} + s_0\|p\|^2_{\mathrm{L}^2(\Omega)}\\ &\quad= (\mathbf{f}_p,\boldsymbol{\eta})_\Omega + (\mathbf{g},\mathbf{u})_\Omega + (g,p)_\Omega\,.\end{aligned} \tag{3.18}$$

Using the Cauchy–Schwarz and Young inequalities, we have

$$(\mathbf{f}_p,\boldsymbol{\eta})_\Omega \leq \mu c_k\|\boldsymbol{\eta}\|^2_{\mathbf{H}^1(\Omega)} + \frac{1}{4\mu c_k}\|\mathbf{f}_p\|^2_{\mathbf{L}^2(\Omega)}\,, \tag{3.19}$$

where $c_k > 0$ is the Korn constant satisfying $\|\boldsymbol{\varepsilon}(\boldsymbol{\eta})\|^2_{\mathbb{L}^2(\Omega)} \geq c_k\|\boldsymbol{\eta}\|^2_{\mathbf{H}^1(\Omega)}$ for all $\boldsymbol{\eta} \in \mathbf{H}^1_0(\Omega)$. Similarly,

$$(\mathbf{g},\mathbf{u})_\Omega \leq \frac{\mathtt{D}}{2}\|\mathbf{u}\|^2_{\mathbf{L}^2(\Omega)} + \frac{1}{2\mathtt{D}}\|\mathbf{g}\|^2_{\mathbf{L}^2(\Omega)} \quad\text{and}\quad (g,p)_\Omega \leq \frac{s_0}{2}\|p\|^2_{\mathrm{L}^2(\Omega)} + \frac{1}{2s_0}\|g\|^2_{\mathrm{L}^2(\Omega)}\,. \tag{3.20}$$

Combining (3.18) with (3.19)–(3.20), and using Korn's inequality, gives

$$\begin{aligned}&\mu c_k\|\boldsymbol{\eta}\|^2_{\mathbf{H}^1(\Omega)} + \nu\|\nabla\mathbf{u}\|^2_{\mathbb{L}^2(\Omega)} + \frac{\mathtt{D}}{2}\|\mathbf{u}\|^2_{\mathbf{L}^2(\Omega)} + \mathtt{F}\|\mathbf{u}\|^m_{\mathbf{L}^m(\Omega)} + \frac{1}{\lambda}\|\theta-\alpha p\|^2_{\mathrm{L}^2(\Omega)} + \frac{s_0}{2}\|p\|^2_{\mathrm{L}^2(\Omega)}\\ &\leq \frac{1}{4\mu c_k}\|\mathbf{f}_p\|^2_{\mathbf{L}^2(\Omega)} + \frac{1}{2\mathtt{D}}\|\mathbf{g}\|^2_{\mathbf{L}^2(\Omega)} + \frac{1}{2s_0}\|g\|^2_{\mathrm{L}^2(\Omega)}\,.\end{aligned} \tag{3.21}$$

Then, dropping the last three nonnegative terms on the left-hand side of (3.21), a straightforward computation gives

$$\|(\boldsymbol{\eta},\mathbf{u})\|_{\mathbb{H}} \leq C_1\left(\|\mathbf{f}_p\|_{\mathbf{L}^2(\Omega)} + \|\mathbf{g}\|_{\mathbf{L}^2(\Omega)} + \frac{1}{\sqrt{s_0}}\|g\|_{\mathrm{L}^2(\Omega)}\right), \tag{3.22}$$

where C_1 is a positive constant only depending on μ, c_k, $\mathtt{D}$, and ν.

We now derive a bound for (θ, p). From the inf-sup condition (3.15) (cf. Lemma 3.5), with $(\psi, q) = (\theta, p) \in \mathbb{Q}$, and using the first equation of (2.12), we get

$$\beta \|(\theta, p)\|_{\mathbb{Q}} \leq \sup_{\mathbf{0} \neq (\boldsymbol{\xi}, \mathbf{v}) \in \mathbb{H}} \frac{[\mathbf{F}, (\boldsymbol{\xi}, \mathbf{v})] - [\mathcal{A}(\boldsymbol{\eta}, \mathbf{u}), (\boldsymbol{\xi}, \mathbf{v})]}{\|(\boldsymbol{\xi}, \mathbf{v})\|_{\mathbb{H}}} \leq \|\mathbf{F}\|_{\mathbb{H}'} + \|\mathcal{A}(\boldsymbol{\eta}, \mathbf{u})\|_{\mathbb{H}'} \,. \tag{3.23}$$

Using the bounds for $\mathbf{F}$ and $\mathcal{A}$ given in (3.3) and (3.4), respectively, we infer from (3.23) that

$$\|(\theta, p)\|_{\mathbb{Q}} \leq C_2 \left(\|\mathbf{f}_p\|_{\mathbf{L}^2(\Omega)} + \|\mathbf{g}\|_{\mathbf{L}^2(\Omega)} + \|(\boldsymbol{\eta}, \mathbf{u})\|_{\mathbb{H}} + \|\mathbf{u}\|_{\mathbf{H}^1(\Omega)}^{m-1} \right) , \tag{3.24}$$

where $C_2 > 0$ depends only on β, μ, ν, $\mathtt{D}$, $\mathtt{F}$, and $\|\mathbf{i}_m\|$. Finally, combining (3.22) and (3.24), a simple algebraic manipulation gives (3.17). $\square$

Remark 3.1 *It is worth emphasizing that the dependence of the a priori estimate (3.17) on the storage coefficient s_0 is completely explicit. More precisely, s_0 appears only through the contribution $\frac{1}{\sqrt{s_0}}\|g\|_{\mathrm{L}^2(\Omega)}$ associated with the scalar source term in the mass balance equation. Hence, in the particular case $g = 0$, this dependence disappears from the estimate. In addition, the constant $C_{\mathtt{st}}$ in (3.17) is independent of the Lamé parameter λ. This feature is one of the main advantages of the present formulation, since it provides a robust estimate in the nearly incompressible regime of the porous skeleton.*

Remark 3.2 *The analysis developed in this paper can also be extended to nonhomogeneous Dirichlet boundary conditions. Indeed, by introducing suitable liftings for the displacement and velocity fields, the problem can be rewritten in the present homogeneous setting, with appropriately modified right-hand side functionals.*

4 The Galerkin scheme

This section is devoted to the Galerkin approximation of the mixed-primal formulation (2.12). Since the discrete spaces considered below are conforming subspaces of the continuous ones, the well-posedness analysis follows the same arguments as those presented in Section 3.2.

4.1 Discrete setting

Let $\{\mathcal{T}_h\}_{h>0}$ be a shape-regular family of triangulations of $\overline{\Omega}$, made of triangles when $d = 2$ and tetrahedra when $d = 3$. For each $T \in \mathcal{T}_h$, we denote by h_T its diameter and set $h := \max\{h_T : \ T \in \mathcal{T}_h\}$. We consider finite-dimensional conforming subspaces

$$\mathbf{H}_h^{\boldsymbol{\eta}} \subset \mathbf{H}_0^1(\Omega) \,, \qquad \mathrm{Q}_h^{\theta} \subset \mathrm{L}_0^2(\Omega) \,, \qquad \mathbf{H}_h^{\mathbf{u}} \subset \mathbf{H}_0^1(\Omega) \,, \qquad \mathrm{Q}_h^{p} \subset \mathrm{L}_0^2(\Omega) \,,$$

chosen so that $(\mathbf{H}_h^{\boldsymbol{\eta}}, \mathrm{Q}_h^{\theta})$ and $(\mathbf{H}_h^{\mathbf{u}}, \mathrm{Q}_h^{p})$ are Stokes-stable finite element pairs (cf. [6, 7]). We then define

$$\mathbb{H}_h := \mathbf{H}_h^{\boldsymbol{\eta}} \times \mathbf{H}_h^{\mathbf{u}} \,, \qquad \mathbb{Q}_h := \mathrm{Q}_h^{\theta} \times \mathrm{Q}_h^{p} \,,$$

endowed with the norms inherited from $\mathbb{H}$ and $\mathbb{Q}$, respectively. By the choice of these finite element pairs, there exists a constant $\beta_{\mathtt{d}} > 0$, independent of h, such that

$$\sup_{\mathbf{0} \neq (\boldsymbol{\xi}_h, \mathbf{v}_h) \in \mathbb{H}_h} \frac{[\mathcal{B}(\boldsymbol{\xi}_h, \mathbf{v}_h), (\psi_h, q_h)]}{\|(\boldsymbol{\xi}_h, \mathbf{v}_h)\|_{\mathbb{H}}} \geq \beta_{\mathtt{d}} \|(\psi_h, q_h)\|_{\mathbb{Q}} \qquad \forall \, (\psi_h, q_h) \in \mathbb{Q}_h \,. \tag{4.1}$$

In particular, we focus on Taylor–Hood finite elements [40] for the pairs $(\boldsymbol{\eta},\theta)$ and $(\mathbf{u},p)$. More precisely, given an integer $\ell \geq 0$ and a subset S of R^d, we denote by $\mathrm{P}_\ell(S)$ the space of polynomials of total degree at most ℓ defined on S. Then, for any integer $k \geq 1$, we consider

$$\mathbf{H}_h^\star := \Big\{ \mathbf{w}_h \in [C(\overline{\Omega})]^d : \quad \mathbf{w}_h|_T \in [\mathrm{P}_{k+1}(T)]^d \quad \forall\, T \in \mathcal{T}_h \Big\} \cap \mathbf{H}_0^1(\Omega)\,, \qquad \star \in \{\boldsymbol{\eta}, \mathbf{u}\}\,,$$

$$\mathrm{Q}_h^\star := \Big\{ \psi_h \in C(\overline{\Omega}) : \quad \psi_h|_T \in \mathrm{P}_k(T) \quad \forall\, T \in \mathcal{T}_h \Big\} \cap \mathrm{L}_0^2(\Omega)\,, \qquad \star \in \{\theta, p\}\,.$$

The Galerkin scheme associated with (2.12) then reads as follows: Find $((\boldsymbol{\eta}_h,\mathbf{u}_h),(\theta_h,p_h)) \in \mathbb{H}_h \times \mathbb{Q}_h$ such that

$$\begin{aligned} [\mathcal{A}(\boldsymbol{\eta}_h,\mathbf{u}_h),(\boldsymbol{\xi}_h,\mathbf{v}_h)] \;&+\; [\mathcal{B}^{\mathtt{t}}(\theta_h,p_h),(\boldsymbol{\xi}_h,\mathbf{v}_h)] &=\; [\mathbf{F},(\boldsymbol{\xi}_h,\mathbf{v}_h)] \qquad &\forall\,(\boldsymbol{\xi}_h,\mathbf{v}_h) \in \mathbb{H}_h\,,\\ -[\mathcal{B}(\boldsymbol{\eta}_h,\mathbf{u}_h),(\psi_h,q_h)] \;&+\; [\mathcal{C}(\theta_h,p_h),(\psi_h,q_h)] &=\; [\mathbf{G},(\psi_h,q_h)] \qquad &\forall\,(\psi_h,q_h) \in \mathbb{Q}_h\,. \end{aligned} \tag{4.2}$$

Remark 4.1 *Alternatively to the Taylor–Hood elements, other conforming Stokes inf-sup stable finite element pairs can also be employed within the present framework. For instance, one may consider the classical MINI element [6, Sections 8.4.2, 8.6 and 8.7]. The only requirement is that the chosen pairs* $(\mathbf{H}_h^{\boldsymbol{\eta}},\mathrm{Q}_h^\theta)$ *and* $(\mathbf{H}_h^{\mathbf{u}},\mathrm{Q}_h^p)$ *satisfy the discrete inf-sup condition (4.1).*

We now state the discrete analogue of Theorem 3.6. Its proof follows the same strategy as in the continuous case, using the conforming character of the finite element spaces and the discrete inf-sup condition (4.1).

Theorem 4.1 *For each* $(\mathbf{F},\mathbf{G}) \in \mathbb{H}' \times \mathbb{Q}'$ *defined by (2.16), there exists a unique* $((\boldsymbol{\eta}_h,\mathbf{u}_h),(\theta_h,p_h)) \in \mathbb{H}_h \times \mathbb{Q}_h$ *satisfying (4.2). Moreover, there exists a positive constant* $C_{\mathtt{st_d}}$*, independent of* s_0*,* λ*, and* h*, such that*

$$\|(\boldsymbol{\eta}_h,\mathbf{u}_h)\|_{\mathbb{H}} + \|(\theta_h,p_h)\|_{\mathbb{Q}} \leq C_{\mathtt{st_d}} \sum_{j\in\{1,m-1\}} \left(\|\mathbf{f}_p\|_{\mathbf{L}^2(\Omega)} + \|\mathbf{g}\|_{\mathbf{L}^2(\Omega)} + \frac{1}{\sqrt{s_0}}\|g\|_{\mathrm{L}^2(\Omega)} \right)^j . \tag{4.3}$$

Proof. Let $\mathcal{J}_{\mathtt{d}} : \mathbb{H}_h \times \mathbb{Q}_h \to (\mathbb{H}_h \times \mathbb{Q}_h)'$ denote the restriction of the operator $\mathcal{J}$ (cf. (3.16)) to the discrete space $\mathbb{H}_h \times \mathbb{Q}_h$. Since $\mathbb{H}_h \subset \mathbb{H}$ and $\mathbb{Q}_h \subset \mathbb{Q}$, the boundedness, continuity, and strong monotonicity of $\mathcal{A}$, as well as the ellipticity of $\mathcal{C}$, remain valid at the discrete level. In addition, the coupling operator satisfies the discrete inf-sup condition (4.1). Therefore, arguing as in the proof of the continuous well-posedness result, we deduce that $\mathcal{J}_{\mathtt{d}}$ is continuous and strongly monotone on $\mathbb{H}_h \times \mathbb{Q}_h$. Consequently, Corollary 3.2 implies that $\mathcal{J}_{\mathtt{d}}$ is bijective. Hence, for each $(\mathbf{F},\mathbf{G}) \in \mathbb{H}' \times \mathbb{Q}'$, there exists a unique $((\boldsymbol{\eta}_h,\mathbf{u}_h),(\theta_h,p_h)) \in \mathbb{H}_h \times \mathbb{Q}_h$ satisfying (4.2).

Finally, the estimate (4.3) follows by repeating the argument used in the proof of Theorem 3.6, taking $(\boldsymbol{\xi}_h,\mathbf{v}_h) = (\boldsymbol{\eta}_h,\mathbf{u}_h)$ and $(\psi_h,q_h) = (\theta_h,p_h)$ in (4.2), and using the discrete inf-sup condition (4.1). The constants involved are independent of h and λ, and the dependence on s_0 is the one explicitly displayed in (4.3). □

4.2 A priori error analysis

Following a standard approach in error analysis, we introduce the total error components

$$\begin{aligned} \mathbf{e}_{\boldsymbol{\eta}} &:= \boldsymbol{\eta} - \boldsymbol{\eta}_h, \qquad & \mathbf{e}_{\mathbf{u}} &:= \mathbf{u} - \mathbf{u}_h,\\ \mathbf{e}_\theta &:= \theta - \theta_h, \qquad & \mathbf{e}_p &:= p - p_h. \end{aligned} \tag{4.4}$$

In order to derive the error equations, we subtract the discrete mixed-primal formulation (4.2) from the continuous one (2.12), tested with discrete functions. This yields the following error system:

$$\begin{aligned} [\mathcal{A}(\boldsymbol{\eta},\mathbf{u})-\mathcal{A}(\boldsymbol{\eta}_h,\mathbf{u}_h),(\boldsymbol{\xi}_h,\mathbf{v}_h)] \quad &+ \quad [\mathcal{B}^{\mathrm{t}}(\mathbf{e}_\theta,\mathbf{e}_p),(\boldsymbol{\xi}_h,\mathbf{v}_h)] \quad = \quad 0 \qquad \forall\,(\boldsymbol{\xi}_h,\mathbf{v}_h)\in\mathbb{H}_h,\\ -[\mathcal{B}(\mathbf{e}_{\boldsymbol{\eta}},\mathbf{e}_{\mathbf{u}}),(\psi_h,q_h)] \quad &+ \quad [\mathcal{C}(\mathbf{e}_\theta,\mathbf{e}_p),(\psi_h,q_h)] \quad = \quad 0 \qquad \forall\,(\psi_h,q_h)\in\mathbb{Q}_h. \end{aligned} \tag{4.5}$$

Let $\widehat{\theta}_h\in\mathrm{Q}_h^\theta$ and $\widehat{p}_h\in\mathrm{Q}_h^p$ denote the respective $\mathrm{L}^2(\Omega)$-orthogonal projections of θ and p. Using this fixed pair, we introduce the discrete constraint set

$$\mathbb{K}_h := \Big\{(\widehat{\boldsymbol{\eta}}_h,\widehat{\mathbf{u}}_h)\in\mathbb{H}_h : \quad \mathcal{B}(\widehat{\boldsymbol{\eta}}_h,\widehat{\mathbf{u}}_h)=\mathcal{C}(\widehat{\theta}_h,\widehat{p}_h)-\mathbf{G} \quad \text{in} \quad \mathbb{Q}_h'\Big\}, \tag{4.6}$$

where $\mathbf{G}\in\mathbb{Q}_h'$ denotes the restriction to $\mathbb{Q}_h$ of the functional defined in (2.16). Notice that $\mathbb{K}_h$ is nonempty, since the discrete inf–sup condition (4.1) implies that the operator induced by $\mathcal{B}$ from $\mathbb{H}_h$ onto $\mathbb{Q}_h'$ is surjective.

We then decompose each total error into its approximation and discrete components. More precisely, given $(\widehat{\boldsymbol{\eta}}_h,\widehat{\mathbf{u}}_h)\in\mathbb{K}_h$, for the vector unknowns we write

$$\mathbf{e}_{\boldsymbol{\eta}} = \big(\boldsymbol{\eta}-\widehat{\boldsymbol{\eta}}_h\big)+\big(\widehat{\boldsymbol{\eta}}_h-\boldsymbol{\eta}_h\big) =: \mathbf{e}_{\boldsymbol{\eta}}^I+\mathbf{e}_{\boldsymbol{\eta}}^h, \tag{4.7}$$

$$\mathbf{e}_{\mathbf{u}} = \big(\mathbf{u}-\widehat{\mathbf{u}}_h\big)+\big(\widehat{\mathbf{u}}_h-\mathbf{u}_h\big) =: \mathbf{e}_{\mathbf{u}}^I+\mathbf{e}_{\mathbf{u}}^h. \tag{4.8}$$

For the scalar unknowns, we use the fixed projected pair $(\widehat{\theta}_h,\widehat{p}_h)$ and set

$$\mathbf{e}_\theta = \big(\theta-\widehat{\theta}_h\big)+\big(\widehat{\theta}_h-\theta_h\big) =: \mathbf{e}_\theta^I+\mathbf{e}_\theta^h, \tag{4.9}$$

$$\mathbf{e}_p = \big(p-\widehat{p}_h\big)+\big(\widehat{p}_h-p_h\big) =: \mathbf{e}_p^I+\mathbf{e}_p^h. \tag{4.10}$$

Here, $\mathbf{e}_{\boldsymbol{\eta}}^I$, $\mathbf{e}_{\mathbf{u}}^I$, $\mathbf{e}_\theta^I$, and $\mathbf{e}_p^I$ denote the approximation errors, whereas $\mathbf{e}_{\boldsymbol{\eta}}^h$, $\mathbf{e}_{\mathbf{u}}^h$, $\mathbf{e}_\theta^h$, and $\mathbf{e}_p^h$ denote the corresponding discrete errors.

Notice that, since $(\widehat{\boldsymbol{\eta}}_h,\widehat{\mathbf{u}}_h)\in\mathbb{K}_h$ and $(\boldsymbol{\eta}_h,\mathbf{u}_h)\in\mathbb{H}_h$ satisfies the second equation of (4.2), it follows that

$$[\mathcal{B}((\mathbf{e}_{\boldsymbol{\eta}}^h,\mathbf{e}_{\mathbf{u}}^h)),(\psi_h,q_h)] = [\mathcal{C}(\mathbf{e}_\theta^h,\mathbf{e}_p^h),(\psi_h,q_h)] \qquad \forall\,(\psi_h,q_h)\in\mathbb{Q}_h. \tag{4.11}$$

Then, taking $(\psi_h,q_h)=(\mathbf{e}_\theta^h,\mathbf{e}_p^h)$ in (4.11) and recalling the ellipticity of $\mathcal{C}$ (cf. (3.14)), we obtain

$$[\mathcal{B}((\mathbf{e}_{\boldsymbol{\eta}}^h,\mathbf{e}_{\mathbf{u}}^h)),(\mathbf{e}_\theta^h,\mathbf{e}_p^h)] \geq 0. \tag{4.12}$$

We conclude this discussion by recalling the following standard best-approximation properties of the finite element subspaces $\mathbf{H}_h^{\boldsymbol{\eta}}$, $\mathbf{H}_h^{\mathbf{u}}$, Q_h^θ, and Q_h^p (see, e.g., [21, Proposition 1.134]):

$(\mathbf{AP}_h^{\boldsymbol{\zeta}})$ There exists a positive constant C, independent of h, such that, for each $s\in[1,k+1]$ and for each $\boldsymbol{\zeta}\in\mathbf{H}^{s+1}(\Omega)\cap\mathbf{H}_0^1(\Omega)$, there holds

$$\inf_{\boldsymbol{\zeta}_h\in\mathbf{H}_h^\star}\|\boldsymbol{\zeta}-\boldsymbol{\zeta}_h\|_{\mathbf{H}^1(\Omega)} \leq Ch^s\|\boldsymbol{\zeta}\|_{\mathbf{H}^{1+s}(\Omega)}, \qquad \star\in\{\boldsymbol{\eta},\mathbf{u}\}.$$

$(\mathbf{AP}_h^{\psi})$ There exists a positive constant C, independent of h, such that, for each $s\in[0,k+1]$ and for each $\psi\in\mathrm{H}^s(\Omega)\cap\mathrm{L}_0^2(\Omega)$, there holds

$$\inf_{\psi_h\in\mathrm{Q}_h^\star}\|\psi-\psi_h\|_{\mathrm{L}^2(\Omega)} \leq Ch^s\|\psi\|_{\mathrm{H}^s(\Omega)}, \qquad \star\in\{\theta,p\}.$$

Since $\widehat{\theta}_h$ and $\widehat{p}_h$ are the respective $\mathrm{L}^2(\Omega)$-orthogonal projections, $(\mathbf{AP}_h^{\psi})$ implies

$$\|(\theta,p)-(\widehat{\theta}_h,\widehat{p}_h)\|_{\mathbb{Q}} \le C h^s\Big(\|\theta\|_{\mathrm{H}^s(\Omega)}+\|p\|_{\mathrm{H}^s(\Omega)}\Big). \tag{4.13}$$

In addition, the following approximation property, whose proof is provided in Appendix A, holds:

$$\begin{aligned}
&\inf_{(\widehat{\boldsymbol{\eta}}_h,\widehat{\mathbf{u}}_h)\in\mathbb{K}_h} \|(\boldsymbol{\eta},\mathbf{u})-(\widehat{\boldsymbol{\eta}}_h,\widehat{\mathbf{u}}_h)\|_{\mathbb{H}} \\
&\quad\le C\,h^s\left(\left(1+\frac{\|\mathcal{B}\|}{\beta_{\mathtt{d}}}\right)\Big(\|\boldsymbol{\eta}\|_{\mathbf{H}^{1+s}(\Omega)}+\|\mathbf{u}\|_{\mathbf{H}^{1+s}(\Omega)}\Big)+\frac{\|\mathcal{C}\|}{\beta_{\mathtt{d}}}\Big(\|\theta\|_{\mathrm{H}^s(\Omega)}+\|p\|_{\mathrm{H}^s(\Omega)}\Big)\right),
\end{aligned}\tag{4.14}$$

where $C>0$ is independent of h.

We are now in a position to state the main result of this section.

Theorem 4.2 *Let $m\in[3,4]$. Let $((\boldsymbol{\eta},\mathbf{u}),(\theta,p))\in\mathbb{H}\times\mathbb{Q}$ be the unique solution of (2.12), and let $((\boldsymbol{\eta}_h,\mathbf{u}_h),(\theta_h,p_h))\in\mathbb{H}_h\times\mathbb{Q}_h$ be the unique solution of (4.2). Assume further that there exists $s\in[1,k+1]$ such that $\boldsymbol{\eta},\mathbf{u}\in\mathbf{H}^{1+s}(\Omega)$ and $\theta,p\in\mathrm{H}^s(\Omega)$. Then, there exists a positive constant C, independent of h, such that*

$$\begin{aligned}
\|(\mathbf{e}_{\boldsymbol{\eta}},\mathbf{e}_{\mathbf{u}})\|_{\mathbb{H}}+\|(\mathbf{e}_\theta,\mathbf{e}_p)\|_{\mathbb{Q}} \;\le\; C\Bigg\{ & h^s\Big(\|\boldsymbol{\eta}\|_{\mathbf{H}^{1+s}(\Omega)}+\|\mathbf{u}\|_{\mathbf{H}^{1+s}(\Omega)}+\|\theta\|_{\mathrm{H}^s(\Omega)}+\|p\|_{\mathrm{H}^s(\Omega)}\Big) \\
&+h^{s(m-1)}\Big(\|\boldsymbol{\eta}\|_{\mathbf{H}^{1+s}(\Omega)}+\|\mathbf{u}\|_{\mathbf{H}^{1+s}(\Omega)}+\|\theta\|_{\mathrm{H}^s(\Omega)}+\|p\|_{\mathrm{H}^s(\Omega)}\Big)^{m-1}\Bigg\}.
\end{aligned}\tag{4.15}$$

Proof. We begin by testing the first row of (4.5) with $(\boldsymbol{\xi}_h,\mathbf{v}_h)=(\mathbf{e}^h_{\boldsymbol{\eta}},\mathbf{e}^h_{\mathbf{u}})$, using the decompositions (4.9)–(4.10), and the fact that $[\mathcal{B}^{\mathtt{t}}(\mathbf{e}^h_\theta,\mathbf{e}^h_p),(\mathbf{e}^h_{\boldsymbol{\eta}},\mathbf{e}^h_{\mathbf{u}})]\ge 0$ (cf. (4.12)), we obtain

$$[\mathcal{A}(\boldsymbol{\eta},\mathbf{u})-\mathcal{A}(\boldsymbol{\eta}_h,\mathbf{u}_h),(\mathbf{e}^h_{\boldsymbol{\eta}},\mathbf{e}^h_{\mathbf{u}})]+[\mathcal{B}^{\mathtt{t}}(\mathbf{e}^I_\theta,\mathbf{e}^I_p),(\mathbf{e}^h_{\boldsymbol{\eta}},\mathbf{e}^h_{\mathbf{u}})]\le 0\,. \tag{4.16}$$

Using the definition of $\mathcal{A}$ (cf. (2.13)), after adding and subtracting the term $|\widehat{\mathbf{u}}_h|^{m-2}\widehat{\mathbf{u}}_h$, the monotonicity inequality (3.11), and the decompositions (4.7)–(4.8), we deduce from (4.16) that

$$\begin{aligned}
&2\mu\,\|\boldsymbol{\varepsilon}(\mathbf{e}^h_{\boldsymbol{\eta}})\|^2_{\mathbb{L}^2(\Omega)}+\nu\,\|\nabla\mathbf{e}^h_{\mathbf{u}}\|^2_{\mathbb{L}^2(\Omega)}+\mathtt{D}\,\|\mathbf{e}^h_{\mathbf{u}}\|^2_{\mathbf{L}^2(\Omega)}+\mathtt{F}\,\widetilde{C}_m\,\|\mathbf{e}^h_{\mathbf{u}}\|^m_{\mathbf{L}^m(\Omega)} \\
&\quad\le -2\mu\,(\boldsymbol{\varepsilon}(\mathbf{e}^I_{\boldsymbol{\eta}}),\boldsymbol{\varepsilon}(\mathbf{e}^h_{\boldsymbol{\eta}}))_\Omega-\nu\,(\nabla\mathbf{e}^I_{\mathbf{u}},\nabla\mathbf{e}^h_{\mathbf{u}})_\Omega-\mathtt{D}\,(\mathbf{e}^I_{\mathbf{u}},\mathbf{e}^h_{\mathbf{u}})_\Omega \\
&\quad-\mathtt{F}\big(|\mathbf{u}|^{m-2}\mathbf{u}-|\widehat{\mathbf{u}}_h|^{m-2}\widehat{\mathbf{u}}_h,\mathbf{e}^h_{\mathbf{u}}\big)_\Omega+(\mathbf{e}^I_\theta,\mathrm{div}(\mathbf{e}^h_{\boldsymbol{\eta}}))_\Omega+(\mathbf{e}^I_p,\mathrm{div}(\mathbf{e}^h_{\mathbf{u}}))_\Omega\,.
\end{aligned}\tag{4.17}$$

Here, $\widetilde{C}_m>0$ denotes a monotonicity constant depending only on m. In turn, to bound the fourth term on the right-hand side of (4.17), we use the Lipschitz-type estimate (3.8) for the Forchheimer term. More precisely, by [4, Lemma 2.1], there exists a positive constant c_m, depending on m, such that

$$\begin{aligned}
&\||\mathbf{u}|^{m-2}\mathbf{u}-|\widehat{\mathbf{u}}_h|^{m-2}\widehat{\mathbf{u}}_h\|_{\mathbf{L}^2(\Omega)} \\
&\quad\le c_m\Big(\|\mathbf{u}\|_{\mathbf{L}^{2(m-1)}(\Omega)}+\|\widehat{\mathbf{u}}_h\|_{\mathbf{L}^{2(m-1)}(\Omega)}\Big)^{m-2}\,\|\mathbf{e}^I_{\mathbf{u}}\|_{\mathbf{L}^{2(m-1)}(\Omega)}\,.
\end{aligned}\tag{4.18}$$

Hence, employing the Cauchy–Schwarz inequality, the continuous embedding $\mathbf{i}_{2(m-1)}:\mathbf{H}^1(\Omega)\hookrightarrow\mathbf{L}^{2(m-1)}(\Omega)$, with $2(m-1)\in[4,6]$, the identity $\widehat{\mathbf{u}}_h=\mathbf{u}-\mathbf{e}^I_{\mathbf{u}}$, and Young's inequality with parameter $\delta>0$, we obtain

$$\mathtt{F}\left|\big(|\mathbf{u}|^{m-2}\mathbf{u}-|\widehat{\mathbf{u}}_h|^{m-2}\widehat{\mathbf{u}}_h,\mathbf{e}^h_{\mathbf{u}}\big)_\Omega\right|$$

$$
\begin{aligned}
&\le \mathtt{F}\, c_m \left(\|\mathbf{u}\|_{\mathbf{L}^{2(m-1)}(\Omega)} + \|\widehat{\mathbf{u}}_h\|_{\mathbf{L}^{2(m-1)}(\Omega)}\right)^{m-2} \|\mathbf{e}_{\mathbf{u}}^I\|_{\mathbf{L}^{2(m-1)}(\Omega)}\|\mathbf{e}_{\mathbf{u}}^h\|_{\mathbf{L}^2(\Omega)}\\
&\le \mathtt{F}\, c_m \left(2\|\mathbf{u}\|_{\mathbf{L}^{2(m-1)}(\Omega)} + \|\mathbf{e}_{\mathbf{u}}^I\|_{\mathbf{L}^{2(m-1)}(\Omega)}\right)^{m-2} \|\mathbf{e}_{\mathbf{u}}^I\|_{\mathbf{L}^{2(m-1)}(\Omega)}\|\mathbf{e}_{\mathbf{u}}^h\|_{\mathbf{L}^2(\Omega)}\\
&\le \widetilde{C}\left(\|\mathbf{u}\|_{\mathbf{H}^1(\Omega)}^{m-2} + \|\mathbf{e}_{\mathbf{u}}^I\|_{\mathbf{H}^1(\Omega)}^{m-2}\right)\|\mathbf{e}_{\mathbf{u}}^I\|_{\mathbf{H}^1(\Omega)}\|\mathbf{e}_{\mathbf{u}}^h\|_{\mathbf{L}^2(\Omega)}\\
&\le \frac{2\widetilde{C}}{\delta}\left(\|\mathbf{u}\|_{\mathbf{H}^1(\Omega)}^{2(m-2)}\|\mathbf{e}_{\mathbf{u}}^I\|_{\mathbf{H}^1(\Omega)}^2 + \|\mathbf{e}_{\mathbf{u}}^I\|_{\mathbf{H}^1(\Omega)}^{2(m-1)}\right) + \frac{\delta}{4}\|\mathbf{e}_{\mathbf{u}}^h\|_{\mathbf{L}^2(\Omega)}^2\,,
\end{aligned}
\tag{4.19}
$$

where $\delta > 0$ is arbitrary, and $\widetilde{C} > 0$ depends on m, $\mathtt{F}$, and $\|\mathbf{i}_{2(m-1)}\|$, but is independent of h.

Then, combining (4.19) with (4.17), taking $\delta = \mathtt{D}$, and applying Young's inequality to the remaining terms, together with Korn's inequality and the bound $\|\mathrm{div}(\mathbf{z})\|_{\mathrm{L}^2(\Omega)} \le \sqrt{d}\,\|\mathbf{z}\|_{\mathbf{H}^1(\Omega)}$, we deduce

$$
\begin{aligned}
&\frac{\mu}{2}\,\|\boldsymbol{\varepsilon}(\mathbf{e}_{\boldsymbol{\eta}}^h)\|_{\mathbb{L}^2(\Omega)}^2 + \frac{\nu}{2}\,\|\nabla\mathbf{e}_{\mathbf{u}}^h\|_{\mathbb{L}^2(\Omega)}^2 + \frac{\mathtt{D}}{2}\,\|\mathbf{e}_{\mathbf{u}}^h\|_{\mathbf{L}^2(\Omega)}^2 + \widetilde{C}_m\frac{\mathtt{F}}{2}\,\|\mathbf{e}_{\mathbf{u}}^h\|_{\mathbf{L}^m(\Omega)}^m\\
&\quad\le \mu\,\|\boldsymbol{\varepsilon}(\mathbf{e}_{\boldsymbol{\eta}}^I)\|_{\mathbb{L}^2(\Omega)}^2 + \nu\,\|\nabla\mathbf{e}_{\mathbf{u}}^I\|_{\mathbb{L}^2(\Omega)}^2 + \mathtt{D}\,\|\mathbf{e}_{\mathbf{u}}^I\|_{\mathbf{L}^2(\Omega)}^2 + \frac{d}{2\mu c_k}\,\|\mathbf{e}_{\theta}^I\|_{\mathrm{L}^2(\Omega)}^2 + \frac{d}{\nu}\,\|\mathbf{e}_{p}^I\|_{\mathrm{L}^2(\Omega)}^2\\
&\quad+ \frac{2\widetilde{C}}{\mathtt{D}}\left(\|\mathbf{u}\|_{\mathbf{H}^1(\Omega)}^{2(m-2)}\|\mathbf{e}_{\mathbf{u}}^I\|_{\mathbf{H}^1(\Omega)}^2 + \|\mathbf{e}_{\mathbf{u}}^I\|_{\mathbf{H}^1(\Omega)}^{2(m-1)}\right).
\end{aligned}
\tag{4.20}
$$

Thus, taking the minimum of the constants on the left-hand side of (4.20) and using Korn's inequality for $\mathbf{e}_{\boldsymbol{\eta}}^h$, we infer that there exists a positive constant C, independent of h, such that

$$
\begin{aligned}
\|(\mathbf{e}_{\boldsymbol{\eta}}^h, \mathbf{e}_{\mathbf{u}}^h)\|_{\mathbb{H}}^2 \le C\Bigg(&\|\mathbf{e}_{\boldsymbol{\eta}}^I\|_{\mathbf{H}^1(\Omega)}^2 + \|\mathbf{e}_{\mathbf{u}}^I\|_{\mathbf{H}^1(\Omega)}^2 + \|\mathbf{e}_{\theta}^I\|_{\mathrm{L}^2(\Omega)}^2 + \|\mathbf{e}_{p}^I\|_{\mathrm{L}^2(\Omega)}^2\\
&+ \|\mathbf{u}\|_{\mathbf{H}^1(\Omega)}^{2(m-2)}\|\mathbf{e}_{\mathbf{u}}^I\|_{\mathbf{H}^1(\Omega)}^2 + \|\mathbf{e}_{\mathbf{u}}^I\|_{\mathbf{H}^1(\Omega)}^{2(m-1)}\Bigg).
\end{aligned}
$$

Thanks to the a priori estimate of $\mathbf{u}$ (cf. (3.17)), we conclude that there exists a positive constant C, independent of h, such that

$$
\begin{aligned}
\|(\mathbf{e}_{\boldsymbol{\eta}}, \mathbf{e}_{\mathbf{u}})\|_{\mathbb{H}} &\le \|(\mathbf{e}_{\boldsymbol{\eta}}^I, \mathbf{e}_{\mathbf{u}}^I)\|_{\mathbb{H}} + \|(\mathbf{e}_{\boldsymbol{\eta}}^h, \mathbf{e}_{\mathbf{u}}^h)\|_{\mathbb{H}}\\
&\le C\Big(\|(\mathbf{e}_{\boldsymbol{\eta}}^I, \mathbf{e}_{\mathbf{u}}^I)\|_{\mathbb{H}} + \|(\mathbf{e}_{\theta}^I, \mathbf{e}_{p}^I)\|_{\mathbb{Q}} + \|(\mathbf{e}_{\boldsymbol{\eta}}^I, \mathbf{e}_{\mathbf{u}}^I)\|_{\mathbb{H}}^{m-1}\Big).
\end{aligned}
\tag{4.21}
$$

We now estimate the errors associated with θ and p. From the discrete inf-sup condition (4.1), with $(\psi_h, q_h) = (\mathbf{e}_{\theta}^h, \mathbf{e}_{p}^h) \in \mathbb{Q}_h$, we obtain

$$
\beta_{\mathtt{d}}\|(\mathbf{e}_{\theta}^h, \mathbf{e}_{p}^h)\|_{\mathbb{Q}} \le \sup_{\mathbf{0}\neq(\boldsymbol{\xi}_h,\mathbf{v}_h)\in\mathbb{H}_h} \frac{[\mathcal{B}^{\mathtt{t}}(\mathbf{e}_{\theta}^h, \mathbf{e}_{p}^h), (\boldsymbol{\xi}_h, \mathbf{v}_h)]}{\|(\boldsymbol{\xi}_h, \mathbf{v}_h)\|_{\mathbb{H}}}.
\tag{4.22}
$$

On the other hand, using the decomposition $(\mathbf{e}_{\theta}, \mathbf{e}_{p}) = (\mathbf{e}_{\theta}^I, \mathbf{e}_{p}^I) + (\mathbf{e}_{\theta}^h, \mathbf{e}_{p}^h)$ and the first row of the error equation, we have

$$
[\mathcal{B}^{\mathtt{t}}(\mathbf{e}_{\theta}^h, \mathbf{e}_{p}^h), (\boldsymbol{\xi}_h, \mathbf{v}_h)] = -[\mathcal{A}(\boldsymbol{\eta}, \mathbf{u}) - \mathcal{A}(\boldsymbol{\eta}_h, \mathbf{u}_h), (\boldsymbol{\xi}_h, \mathbf{v}_h)] - [\mathcal{B}^{\mathtt{t}}(\mathbf{e}_{\theta}^I, \mathbf{e}_{p}^I), (\boldsymbol{\xi}_h, \mathbf{v}_h)].
\tag{4.23}
$$

Therefore, by the boundedness of $\mathcal{B}$ (cf. (3.3)) and the continuity estimate for $\mathcal{A}$ given in Lemma 3.3, we deduce from (4.22)–(4.23) that

$$
\|(\mathbf{e}_{\theta}^h, \mathbf{e}_{p}^h)\|_{\mathbb{Q}} \le C\Big(\left(1 + \|\mathbf{u}\|_{\mathbf{H}^1(\Omega)}^{m-2} + \|\mathbf{u}_h\|_{\mathbf{H}^1(\Omega)}^{m-2}\right)\|(\mathbf{e}_{\boldsymbol{\eta}}, \mathbf{e}_{\mathbf{u}})\|_{\mathbb{H}} + \|(\mathbf{e}_{\theta}^I, \mathbf{e}_{p}^I)\|_{\mathbb{Q}}\Big),
\tag{4.24}
$$

where $C > 0$ is independent of h. More precisely, C depends on μ, ν, $\mathtt{D}$, $\mathtt{F}$, m, d, C_m, $\beta_{\mathtt{d}}$, and the norm of the embedding $\mathbf{i}_m : \mathbf{H}^1(\Omega) \hookrightarrow \mathbf{L}^m(\Omega)$. Hence, combining (4.21) and (4.24), and using the a priori bounds for $\mathbf{u}$ and $\mathbf{u}_h$ (cf. (3.17) and (4.3)), we get

$$\|(\mathbf{e}_\theta, \mathbf{e}_p)\|_{\mathbb{Q}} \leq C\Big(\|(\mathbf{e}^I_{\boldsymbol{\eta}}, \mathbf{e}^I_{\mathbf{u}})\|_{\mathbb{H}} + \|(\mathbf{e}^I_\theta, \mathbf{e}^I_p)\|_{\mathbb{Q}} + \|(\mathbf{e}^I_{\boldsymbol{\eta}}, \mathbf{e}^I_{\mathbf{u}})\|^{m-1}_{\mathbb{H}}\Big), \tag{4.25}$$

with $C > 0$ independent of h.

Combining (4.21) and (4.25), we obtain, for every $(\widehat{\boldsymbol{\eta}}_h, \widehat{\mathbf{u}}_h) \in \mathbb{K}_h$,

$$\|(\mathbf{e}_{\boldsymbol{\eta}}, \mathbf{e}_{\mathbf{u}})\|_{\mathbb{H}} + \|(\mathbf{e}_\theta, \mathbf{e}_p)\|_{\mathbb{Q}} \leq C\Big(\|(\mathbf{e}^I_{\boldsymbol{\eta}}, \mathbf{e}^I_{\mathbf{u}})\|_{\mathbb{H}} + \|(\mathbf{e}^I_\theta, \mathbf{e}^I_p)\|_{\mathbb{Q}} + \|(\mathbf{e}^I_{\boldsymbol{\eta}}, \mathbf{e}^I_{\mathbf{u}})\|^{m-1}_{\mathbb{H}}\Big). \tag{4.26}$$

Finally, taking the infimum over $(\widehat{\boldsymbol{\eta}}_h, \widehat{\mathbf{u}}_h) \in \mathbb{K}_h$ in (4.26), and using (4.13) and (4.14), we conclude (4.15). $\square$

Remark 4.2 *We point out that the dependence of the constant in (4.15) on the storage coefficient s_0 can be traced through the a priori bounds for the continuous and discrete velocities. More precisely, this dependence enters the estimate when controlling the nonlinear Forchheimer contribution through the bounds for $\mathbf{u}$ and $\mathbf{u}_h$. In view of (3.17) and (4.3), it is associated with the term*

$$\frac{1}{\sqrt{s_0}}\|g\|_{\mathrm{L}^2(\Omega)},$$

which arises from the scalar source in the mass balance equation. Hence, if $g = 0$, the explicit dependence on negative powers of s_0 disappears from the error constant. On the other hand, the constant in (4.15) is not strictly independent of the first Lamé parameter λ, since its dependence on λ enters through the continuity constant of $\mathcal{C}$, given by

$$\|\mathcal{C}\| = 2\max\left\{\frac{1}{\lambda}, \frac{\alpha}{\lambda}, s_0 + \frac{\alpha^2}{\lambda}\right\}.$$

Nevertheless, this dependence does not compromise the robustness of the estimate in the nearly incompressible limit. Indeed,

$$\|\mathcal{C}\| \longrightarrow 2s_0 \qquad as \qquad \lambda \to \infty.$$

Therefore, the constant in (4.15) remains uniformly bounded for large values of λ, and the Galerkin scheme is locking-free in the nearly incompressible limit.

5 A residual-based a posteriori error estimator

In this section, we derive a reliable and efficient residual-based a posteriori error estimator for the Galerkin scheme (4.2). To this end, we employ the notation and auxiliary results collected in Appendix B. Let $((\boldsymbol{\eta}, \mathbf{u}), (\theta, p)) \in \mathbb{H} \times \mathbb{Q}$ and $((\boldsymbol{\eta}_h, \mathbf{u}_h), (\theta_h, p_h)) \in \mathbb{H}_h \times \mathbb{Q}_h$ be the unique solutions of the continuous and discrete problems (2.12) and (4.2), respectively.

We begin by introducing the global residual-based error estimator

$$\boldsymbol{\Xi} := \left(\sum_{T\in\mathcal{T}_h}\left(\boldsymbol{\Xi}^2_{1,T} + \boldsymbol{\Xi}^2_{2,T}\right)\right)^{1/2}, \tag{5.1}$$

where, for each $T \in \mathcal{T}_h$, the local error indicators $\Xi_{i,T}$, $i \in \{1,2\}$, are defined as follows:

$$\Xi_{1,T}^2 := h_T^2 \, \|\mathbf{f}_p + \mathbf{div}(2\mu\, \boldsymbol{\varepsilon}(\boldsymbol{\eta}_h) - \theta_h \mathbb{I})\|_{\mathbf{L}^2(T)}^2 + h_T^2 \, \big\|\mathbf{g} + \nu\, \Delta \mathbf{u}_h - \mathtt{D}\,\mathbf{u}_h - \mathtt{F}|\mathbf{u}_h|^{m-2}\mathbf{u}_h - \nabla p_h\big\|_{\mathbf{L}^2(T)}^2$$
$$+ \sum_{e \in \mathcal{E}_{h,T}(\Omega)} h_e \, \|[\![(\nu \nabla \mathbf{u}_h - p_h \mathbb{I})\mathbf{n}]\!]\|_{\mathbf{L}^2(e)}^2 + \sum_{e \in \mathcal{E}_{h,T}(\Omega)} h_e \, \|[\![(2\mu\, \boldsymbol{\varepsilon}(\boldsymbol{\eta}_h) - \theta_h \mathbb{I})\mathbf{n}]\!]\|_{\mathbf{L}^2(e)}^2 \,, \tag{5.2}$$

and

$$\Xi_{2,T}^2 := \left\| \frac{1}{\lambda}\theta_h - \frac{\alpha}{\lambda} p_h + \operatorname{div}(\boldsymbol{\eta}_h) \right\|_{\mathrm{L}^2(T)}^2 + \left\| g - \left(s_0 + \frac{\alpha^2}{\lambda} \right) p_h + \frac{\alpha}{\lambda}\theta_h - \operatorname{div}(\mathbf{u}_h) \right\|_{\mathrm{L}^2(T)}^2 \,, \tag{5.3}$$

where the jump operator $[\![\cdot]\!]$ is defined by (B.1).

Recalling the total error components defined in (4.4), the main goal of the present section is to prove the existence of positive constants $C_{\mathtt{eff}}$ and $C_{\mathtt{rel}}$, independent of the mesh parameter h and the continuous and discrete solutions, such that

$$C_{\mathtt{eff}} \Xi + \mathtt{h.o.t.} \le \|(\mathbf{e}_{\boldsymbol{\eta}}, \mathbf{e}_{\mathbf{u}})\|_{\mathbb{H}} + \|(\mathbf{e}_\theta, \mathbf{e}_p)\|_{\mathbb{Q}} \le C_{\mathtt{rel}} \Xi \,, \tag{5.4}$$

where $\mathtt{h.o.t.}$ is a generic expression denoting one or several terms of higher order. The upper and lower bounds in (5.4), which are known as the reliability and efficiency of Ξ, are derived below in Sections 5.1 and 5.2, respectively.

5.1 Reliability of the a posteriori error estimator

In this section we derive the reliability estimate for the residual-based a posteriori error estimator introduced in (5.1), that is, we establish the upper bound in (5.4). To this end, we prove several results that are instrumental for this purpose.

Lemma 5.1 *There exists a positive constant C_1, independent of λ and h, such that*

$$\|(\mathbf{e}_{\boldsymbol{\eta}}, \mathbf{e}_{\mathbf{u}})\|_{\mathbb{H}} + \|(\mathbf{e}_\theta, \mathbf{e}_p)\|_{\mathbb{Q}} \le C_1 \left(\|\mathcal{R}_1\|_{\mathbb{H}'} + \|\mathcal{R}_2\|_{\mathbb{Q}'} \right) \,, \tag{5.5}$$

where the residual functionals $\mathcal{R}_1 \in \mathbb{H}'$ and $\mathcal{R}_2 \in \mathbb{Q}'$ are defined by

$$[\mathcal{R}_1, (\boldsymbol{\xi}, \mathbf{v})] := [\mathbf{F}, (\boldsymbol{\xi}, \mathbf{v})] - [\mathcal{A}(\boldsymbol{\eta}_h, \mathbf{u}_h), (\boldsymbol{\xi}, \mathbf{v})] - [\mathcal{B}^{\mathtt{t}}(\theta_h, p_h), (\boldsymbol{\xi}, \mathbf{v})] \,, \tag{5.6}$$

$$[\mathcal{R}_2, (\psi, q)] := [\mathbf{G}, (\psi, q)] + [\mathcal{B}(\boldsymbol{\eta}_h, \mathbf{u}_h), (\psi, q)] - [\mathcal{C}(\theta_h, p_h), (\psi, q)] \,. \tag{5.7}$$

Proof. From the continuous formulation (2.12) and the definitions of $\mathcal{R}_1$ and $\mathcal{R}_2$ (cf. (5.6) and (5.7), respectively), we have the residual identities

$$[\mathcal{R}_1, (\boldsymbol{\xi}, \mathbf{v})] = [\mathcal{A}(\boldsymbol{\eta}, \mathbf{u}) - \mathcal{A}(\boldsymbol{\eta}_h, \mathbf{u}_h), (\boldsymbol{\xi}, \mathbf{v})] + [\mathcal{B}^{\mathtt{t}}(\mathbf{e}_\theta, \mathbf{e}_p), (\boldsymbol{\xi}, \mathbf{v})] \,, \tag{5.8}$$

$$[\mathcal{R}_2, (\psi, q)] = -[\mathcal{B}(\mathbf{e}_{\boldsymbol{\eta}}, \mathbf{e}_{\mathbf{u}}), (\psi, q)] + [\mathcal{C}(\mathbf{e}_\theta, \mathbf{e}_p), (\psi, q)] \,. \tag{5.9}$$

Then, using the strong monotonicity of $\mathcal{A}$ (cf. (3.6)) and taking $(\boldsymbol{\xi}, \mathbf{v}) = (\mathbf{e}_{\boldsymbol{\eta}}, \mathbf{e}_{\mathbf{u}})$ in (5.8), we obtain

$$\alpha_{\mathcal{A}} \|(\mathbf{e}_{\boldsymbol{\eta}}, \mathbf{e}_{\mathbf{u}})\|_{\mathbb{H}}^2 \le [\mathcal{A}(\boldsymbol{\eta}, \mathbf{u}) - \mathcal{A}(\boldsymbol{\eta}_h, \mathbf{u}_h), (\mathbf{e}_{\boldsymbol{\eta}}, \mathbf{e}_{\mathbf{u}})] = [\mathcal{R}_1, (\mathbf{e}_{\boldsymbol{\eta}}, \mathbf{e}_{\mathbf{u}})] - [\mathcal{B}(\mathbf{e}_{\boldsymbol{\eta}}, \mathbf{e}_{\mathbf{u}}), (\mathbf{e}_\theta, \mathbf{e}_p)] \,, \tag{5.10}$$

where $\alpha_{\mathcal{A}}$ is defined in (3.13). On the other hand, taking $(\psi, q) = (\mathbf{e}_\theta, \mathbf{e}_p)$ in (5.9), we get

$$-[\mathcal{B}(\mathbf{e}_{\boldsymbol{\eta}}, \mathbf{e}_{\mathbf{u}}), (\mathbf{e}_\theta, \mathbf{e}_p)] = [\mathcal{R}_2, (\mathbf{e}_\theta, \mathbf{e}_p)] - [\mathcal{C}(\mathbf{e}_\theta, \mathbf{e}_p), (\mathbf{e}_\theta, \mathbf{e}_p)] \,. \tag{5.11}$$

Since $\mathcal{C}$ is elliptic in $\mathbb{Q}$ (cf. (3.14)), from (5.11), we have

$$-[\mathcal{B}(\mathbf{e}_{\boldsymbol{\eta}}, \mathbf{e}_{\mathbf{u}}), (\mathbf{e}_\theta, \mathbf{e}_p)] \leq [\mathcal{R}_2, (\mathbf{e}_\theta, \mathbf{e}_p)]\,.$$

Substituting this bound into (5.10), and using the definition of the dual norms, we deduce

$$\alpha_{\mathcal{A}} \|(\mathbf{e}_{\boldsymbol{\eta}}, \mathbf{e}_{\mathbf{u}})\|_{\mathbb{H}}^2 \leq \|\mathcal{R}_1\|_{\mathbb{H}'} \|(\mathbf{e}_{\boldsymbol{\eta}}, \mathbf{e}_{\mathbf{u}})\|_{\mathbb{H}} + \|\mathcal{R}_2\|_{\mathbb{Q}'} \|(\mathbf{e}_\theta, \mathbf{e}_p)\|_{\mathbb{Q}}\,. \tag{5.12}$$

Next, we estimate the scalar error $\|(\mathbf{e}_\theta, \mathbf{e}_p)\|_{\mathbb{Q}}$. Indeed, by means of the inf-sup condition (3.15), there holds

$$\beta \|(\mathbf{e}_\theta, \mathbf{e}_p)\|_{\mathbb{Q}} \leq \sup_{\mathbf{0} \neq (\boldsymbol{\xi}, \mathbf{v}) \in \mathbb{H}} \frac{[\mathcal{B}^{\mathrm{t}}(\mathbf{e}_\theta, \mathbf{e}_p), (\boldsymbol{\xi}, \mathbf{v})]}{\|(\boldsymbol{\xi}, \mathbf{v})\|_{\mathbb{H}}}\,,$$

and using (5.8), we deduce

$$\beta \|(\mathbf{e}_\theta, \mathbf{e}_p)\|_{\mathbb{Q}} \leq \|\mathcal{R}_1\|_{\mathbb{H}'} + \|\mathcal{A}(\boldsymbol{\eta}, \mathbf{u}) - \mathcal{A}(\boldsymbol{\eta}_h, \mathbf{u}_h)\|_{\mathbb{H}'}\,. \tag{5.13}$$

By the continuity estimate for $\mathcal{A}$ (cf. (3.5)), we have

$$\|\mathcal{A}(\boldsymbol{\eta}, \mathbf{u}) - \mathcal{A}(\boldsymbol{\eta}_h, \mathbf{u}_h)\|_{\mathbb{H}'} \leq L_{\mathcal{A}} \left(1 + \left(\|\mathbf{u}\|_{\mathbf{H}^1(\Omega)} + \|\mathbf{u}_h\|_{\mathbf{H}^1(\Omega)}\right)^{m-2}\right) \|(\mathbf{e}_{\boldsymbol{\eta}}, \mathbf{e}_{\mathbf{u}})\|_{\mathbb{H}}\,, \tag{5.14}$$

where $L_{\mathcal{A}}$ is defined in (3.10). In particular, by the continuous and discrete a priori estimates (3.17) and (4.3), established in Theorems 3.6 and 4.1, respectively, the factor depending on $\|\mathbf{u}\|_{\mathbf{H}^1(\Omega)}$ and $\|\mathbf{u}_h\|_{\mathbf{H}^1(\Omega)}$ can be bounded in terms of

$$C_\star \sum_{j \in \{1, m-1\}} \left(\|\mathbf{f}_p\|_{\mathbf{L}^2(\Omega)} + \|\mathbf{g}\|_{\mathbf{L}^2(\Omega)} + \frac{1}{\sqrt{s_0}} \|g\|_{\mathrm{L}^2(\Omega)}\right)^j \quad \star \in \{\mathtt{st}, \mathtt{st}_{\mathtt{d}}\}\,.$$

Consequently, there exists a positive constant C_{data}, depending on the quantities displayed above, but independent of λ and h, such that, combining (5.13) with (5.14), we obtain

$$\|(\mathbf{e}_\theta, \mathbf{e}_p)\|_{\mathbb{Q}} \leq \frac{1}{\beta} \|\mathcal{R}_1\|_{\mathbb{H}'} + \frac{L_{\mathcal{A}} C_{\mathrm{data}}}{\beta} \|(\mathbf{e}_{\boldsymbol{\eta}}, \mathbf{e}_{\mathbf{u}})\|_{\mathbb{H}}\,. \tag{5.15}$$

Inserting (5.15) into (5.12), we obtain

$$\alpha_{\mathcal{A}} \|(\mathbf{e}_{\boldsymbol{\eta}}, \mathbf{e}_{\mathbf{u}})\|_{\mathbb{H}}^2 \leq \|\mathcal{R}_1\|_{\mathbb{H}'} \|(\mathbf{e}_{\boldsymbol{\eta}}, \mathbf{e}_{\mathbf{u}})\|_{\mathbb{H}} + \frac{1}{\beta} \|\mathcal{R}_1\|_{\mathbb{H}'} \|\mathcal{R}_2\|_{\mathbb{Q}'} + \frac{L_{\mathcal{A}} C_{\mathrm{data}}}{\beta} \|\mathcal{R}_2\|_{\mathbb{Q}'} \|(\mathbf{e}_{\boldsymbol{\eta}}, \mathbf{e}_{\mathbf{u}})\|_{\mathbb{H}}. \tag{5.16}$$

Applying Young's inequality to the three terms on the right-hand side yields

$$\frac{\alpha_{\mathcal{A}}}{2} \|(\mathbf{e}_{\boldsymbol{\eta}}, \mathbf{e}_{\mathbf{u}})\|_{\mathbb{H}}^2 \leq \left(\frac{1}{\alpha_{\mathcal{A}}} + \frac{1}{2\beta}\right) \|\mathcal{R}_1\|_{\mathbb{H}'}^2 + \left(\frac{L_{\mathcal{A}}^2 C_{\mathrm{data}}^2}{\alpha_{\mathcal{A}} \beta^2} + \frac{1}{2\beta}\right) \|\mathcal{R}_2\|_{\mathbb{Q}'}^2. \tag{5.17}$$

Consequently, there exists a positive constant $C_{\mathbb{H}}$, independent of λ and h, such that

$$\|(\mathbf{e}_{\boldsymbol{\eta}}, \mathbf{e}_{\mathbf{u}})\|_{\mathbb{H}} \leq C_{\mathbb{H}} \left(\|\mathcal{R}_1\|_{\mathbb{H}'} + \|\mathcal{R}_2\|_{\mathbb{Q}'}\right). \tag{5.18}$$

Finally, combining (5.18) and (5.15), we conclude that (5.5) holds with a positive constant C_1 independent of λ and h. □

We now proceed to bound the terms on the right-hand side of (5.5). We begin with the residual functional $\mathcal{R}_2$. A direct application of the Cauchy–Schwarz inequality gives the following estimate.

Lemma 5.2 *There holds*

$$\|\mathcal{R}_2\|_{\mathbb{Q}'} \leq \left(\sum_{T\in\mathcal{T}_h} \boldsymbol{\Xi}_{2,T}^2\right)^{1/2},$$

where $\boldsymbol{\Xi}_{2,T}$ is defined in (5.3).

We continue the reliability analysis by deriving a suitable bound for the norm of the residual functional $\mathcal{R}_1$ (cf. (5.6)).

Lemma 5.3 *There exists a positive constant C_2, independent of λ and h, such that*

$$\|\mathcal{R}_1\|_{\mathbb{H}'} \leq C_2 \left(\sum_{T\in\mathcal{T}_h} \boldsymbol{\Xi}_{1,T}^2\right)^{1/2}, \tag{5.19}$$

where $\boldsymbol{\Xi}_{1,T}$ is defined in (5.2).

Proof. We proceed as in [19, Lemma 3.12]. Let $(\boldsymbol{\xi},\mathbf{v}) \in \mathbb{H}$ and set $(\widehat{\boldsymbol{\xi}},\widehat{\mathbf{v}}) := (\boldsymbol{\xi} - \boldsymbol{\mathcal{I}}_h(\boldsymbol{\xi}), \mathbf{v} - \boldsymbol{\mathcal{I}}_h(\mathbf{v}))$, where $\boldsymbol{\mathcal{I}}_h$ denotes the vector-valued Clément interpolation operator introduced in Appendix B. Since $[\mathcal{R}_1,(\boldsymbol{\xi}_h,\mathbf{v}_h)] = 0$ for all $(\boldsymbol{\xi}_h,\mathbf{v}_h) \in \mathbb{H}_h$, we have $[\mathcal{R}_1,(\boldsymbol{\xi},\mathbf{v})] = [\mathcal{R}_1,(\widehat{\boldsymbol{\xi}},\widehat{\mathbf{v}})]$. Then, using the definition of $\mathcal{R}_1$ (cf. (5.6)) and integrating by parts elementwise, we obtain

$$\begin{aligned}
[\mathcal{R}_1,(\widehat{\boldsymbol{\xi}},\widehat{\mathbf{v}})] &= \sum_{T\in\mathcal{T}_h} \Big(\mathbf{f}_p + \mathbf{div}(2\mu\,\boldsymbol{\varepsilon}(\boldsymbol{\eta}_h) - \theta_h\mathbb{I}), \widehat{\boldsymbol{\xi}}\Big)_T - \sum_{e\in\mathcal{E}_h(\Omega)} \Big\langle [\![(2\mu\,\boldsymbol{\varepsilon}(\boldsymbol{\eta}_h) - \theta_h\mathbb{I})\mathbf{n}]\!], \widehat{\boldsymbol{\xi}}\Big\rangle_e \\
&\quad + \sum_{T\in\mathcal{T}_h} \Big(\mathbf{g} + \nu\,\Delta\mathbf{u}_h - \mathtt{D}\,\mathbf{u}_h - \mathtt{F}|\mathbf{u}_h|^{m-2}\mathbf{u}_h - \nabla p_h, \widehat{\mathbf{v}}\Big)_T - \sum_{e\in\mathcal{E}_h(\Omega)} \langle [\![(\nu\nabla\mathbf{u}_h - p_h\mathbb{I})\mathbf{n}]\!], \widehat{\mathbf{v}}\rangle_e\,.
\end{aligned}$$

Hence, by the Cauchy–Schwarz inequality and the approximation and trace estimates for the Clément operator established in Lemma B.1 (cf. (B.2) and (B.3)), we conclude (5.19), where $C_2 > 0$ depends only on the constants in the Clément interpolation estimates. In particular, C_2 is independent of h, λ, and the problem data. □

The main result of this section, namely the reliability of the *a posteriori* error estimator $\boldsymbol{\Xi}$ defined in (5.1), is stated next.

Theorem 5.4 *Let $((\boldsymbol{\eta},\mathbf{u}),(\theta,p)) \in \mathbb{H}\times\mathbb{Q}$ and $((\boldsymbol{\eta}_h,\mathbf{u}_h),(\theta_h,p_h)) \in \mathbb{H}_h\times\mathbb{Q}_h$ be the unique solutions of (2.12) and (4.2), respectively. Then $\boldsymbol{\Xi}$ is reliable. More precisely, there exists a positive constant $C_{\mathtt{rel}}$, independent of λ and h, such that*

$$\|(\mathbf{e}_{\boldsymbol{\eta}},\mathbf{e}_{\mathbf{u}})\|_{\mathbb{H}} + \|(\mathbf{e}_\theta,\mathbf{e}_p)\|_{\mathbb{Q}} \leq C_{\mathtt{rel}}\,\boldsymbol{\Xi}\,.$$

Proof. The result follows from the abstract reliability estimate (5.5), together with the residual bounds provided by Lemmas 5.3 and 5.2. □

5.2 Efficiency of the a posteriori error estimator

We now turn to the efficiency analysis of the global *a posteriori* error estimator $\boldsymbol{\Xi}$ (cf. (5.1)). More precisely, we prove the lower bound in (5.4). The arguments rely on the notation and auxiliary results collected in Appendix C, as well as on the strong form of the reformulated system (2.7). In particular, the proof is based on suitable local test functions and on reversing the integration by parts arguments used in the derivation of the residual estimator.

Throughout this section, we assume that $\mathbf{f}_p$, $\mathbf{g}$, and g are piecewise polynomial functions. If this is not the case, but the data are sufficiently smooth, the analysis can be carried out along the same lines as in [16, Section 6.2]. In that situation, additional higher-order terms arising from suitable polynomial approximations of the data appear in the lower bound of (5.4), which accounts for the presence of the `h.o.t.` contribution in that estimate.

We begin the proof of the global efficiency estimate in (5.4) by establishing a sequence of local lower bounds. The first one concerns the terms entering $\Xi_{2,T}$ (cf. (5.3)).

Lemma 5.5 *There exists a positive constant C_3, independent of h, such that*

$$\Xi_{2,T}^2 \leq C_3\Big\{\|\mathrm{div}(\mathbf{e}_{\boldsymbol{\eta}})\|^2_{\mathrm{L}^2(T)} + \|\mathrm{div}(\mathbf{e}_{\mathbf{u}})\|^2_{\mathrm{L}^2(T)} + \|\mathbf{e}_\theta\|^2_{\mathrm{L}^2(T)} + \|\mathbf{e}_p\|^2_{\mathrm{L}^2(T)}\Big\}. \tag{5.20}$$

Proof. Recalling the scalar equations in the strong form (2.7b), we have

$$\frac{1}{\lambda}\theta - \frac{\alpha}{\lambda}p + \mathrm{div}(\boldsymbol{\eta}) = 0 \quad \text{and} \quad \left(s_0 + \frac{\alpha^2}{\lambda}\right)p - \frac{\alpha}{\lambda}\theta + \mathrm{div}(\mathbf{u}) = g \quad \text{in} \quad \Omega\,.$$

Subtracting these identities from the corresponding discrete residuals in the definition of $\Xi_{2,T}$, cf. (5.3), and applying the triangle and Cauchy–Schwarz inequalities, we obtain (5.20), with $C_3 > 0$ depending on λ^{-1}, α, and s_0, but independent of h. $\square$

Now we proceed by deriving the estimates for the terms defining $\Xi_{1,T}$ (cf. (5.2)).

Lemma 5.6 *There exists a positive constant C_4, independent of h, such that for all $T \in \mathcal{T}_h$,*

$$h_T^2\,\|\mathbf{f}_p + \mathbf{div}\,(2\mu\,\boldsymbol{\varepsilon}(\boldsymbol{\eta}_h) - \theta_h\mathbb{I})\|^2_{\mathbf{L}^2(T)} \leq C_4\left\{\|\mathbf{e}_{\boldsymbol{\eta}}\|^2_{\mathbf{H}^1(T)} + \|\mathbf{e}_\theta\|^2_{\mathrm{L}^2(T)}\right\}. \tag{5.21}$$

Proof. Define

$$\boldsymbol{\chi}_T := \mathbf{f}_p + \mathbf{div}\,(2\mu\boldsymbol{\varepsilon}(\boldsymbol{\eta}_h) - \theta_h\mathbb{I}) \quad \text{in} \quad T\,.$$

Thanks to the assumption that $\mathbf{f}_p$ is piecewise polynomial, and since $\boldsymbol{\eta}_h$ and θ_h are finite element functions, there exists a nonnegative integer $\widetilde{k}$, depending on k and on the polynomial degree of $\mathbf{f}_p$, such that $\boldsymbol{\chi}_T \in \mathbf{P}_{\widetilde{k}}(T)$. Then, using the vector version of (C.4) in Lemma C.1, we have

$$\|\boldsymbol{\chi}_T\|^2_{\mathbf{L}^2(T)} \leq c_1\|\phi_T^{1/2}\boldsymbol{\chi}_T\|^2_{\mathbf{L}^2(T)} = c_1(\boldsymbol{\chi}_T, \phi_T\boldsymbol{\chi}_T)_T\,. \tag{5.22}$$

On the other hand, from the first equation of (2.7a), the exact solution satisfies

$$\mathbf{f}_p + \mathbf{div}\,(2\mu\boldsymbol{\varepsilon}(\boldsymbol{\eta}) - \theta\mathbb{I}) = \mathbf{0} \quad \text{in} \quad T\,,$$

which yields

$$\boldsymbol{\chi}_T = \mathbf{div}\,(2\mu\boldsymbol{\varepsilon}(\boldsymbol{\eta}_h - \boldsymbol{\eta}) - (\theta_h - \theta)\mathbb{I}) = -\mathbf{div}\,(2\mu\boldsymbol{\varepsilon}(\mathbf{e}_{\boldsymbol{\eta}}) - \mathbf{e}_\theta\mathbb{I})\,.$$

Consequently, integrating by parts and using that $\phi_T = 0$ on ∂T (cf. (C.1)), we get

$$(\boldsymbol{\chi}_T, \phi_T\boldsymbol{\chi}_T)_T = -\left(\mathbf{div}\,(2\mu\boldsymbol{\varepsilon}(\mathbf{e}_{\boldsymbol{\eta}}) - \mathbf{e}_\theta\mathbb{I})\,, \phi_T\boldsymbol{\chi}_T\right)_T = \left(2\mu\boldsymbol{\varepsilon}(\mathbf{e}_{\boldsymbol{\eta}}) - \mathbf{e}_\theta\mathbb{I}, \nabla(\phi_T\boldsymbol{\chi}_T)\right)_T\,.$$

Thus, by the Cauchy–Schwarz inequality and the identity $\|\mathbf{e}_\theta\mathbb{I}\|_{\mathbb{L}^2(T)} = \sqrt{d}\,\|\mathbf{e}_\theta\|_{\mathrm{L}^2(T)}$, we obtain

$$|(\boldsymbol{\chi}_T, \phi_T\boldsymbol{\chi}_T)_T| \leq \Big(2\mu\|\boldsymbol{\varepsilon}(\mathbf{e}_{\boldsymbol{\eta}})\|_{\mathbb{L}^2(T)} + \sqrt{d}\,\|\mathbf{e}_\theta\|_{\mathrm{L}^2(T)}\Big)\,\|\nabla(\phi_T\boldsymbol{\chi}_T)\|_{\mathbb{L}^2(T)}. \tag{5.23}$$

Since $\phi_T\boldsymbol{\chi}_T$ is a polynomial on T, the inverse inequality (C.7), together with (C.4), yields

$$\|\nabla(\phi_T\boldsymbol{\chi}_T)\|_{\mathbb{L}^2(T)} \le C h_T^{-1}\|\phi_T\boldsymbol{\chi}_T\|_{\mathbf{L}^2(T)} \le C h_T^{-1}\|\boldsymbol{\chi}_T\|_{\mathbf{L}^2(T)}.$$

Replacing this estimate into (5.23) and then using (5.22), we deduce that

$$\|\boldsymbol{\chi}_T\|^2_{\mathbf{L}^2(T)} \le C h_T^{-1}\left(\|\mathbf{e}_{\boldsymbol{\eta}}\|_{\mathbf{H}^1(T)} + \|\mathbf{e}_\theta\|_{\mathrm{L}^2(T)}\right)\|\boldsymbol{\chi}_T\|_{\mathbf{L}^2(T)}.$$

After cancelling the common factor $\|\boldsymbol{\chi}_T\|_{\mathbf{L}^2(T)}$ and multiplying by h_T, it follows that

$$h_T\|\boldsymbol{\chi}_T\|_{\mathbf{L}^2(T)} \le C\left(\|\mathbf{e}_{\boldsymbol{\eta}}\|_{\mathbf{H}^1(T)} + \|\mathbf{e}_\theta\|_{\mathrm{L}^2(T)}\right).$$

Finally, squaring the last inequality yields (5.21). □

Lemma 5.7 *There exists a positive constant C_5, independent of h, such that*

$$\begin{aligned} &h_T^2\left\|\mathbf{g} + \nu\,\Delta\mathbf{u}_h - \mathtt{D}\,\mathbf{u}_h - \mathtt{F}|\mathbf{u}_h|^{m-2}\mathbf{u}_h - \nabla p_h\right\|^2_{\mathbf{L}^2(T)} \\ &\quad\le C_5\Big\{\|\mathbf{e}_{\mathbf{u}}\|^2_{\mathbf{H}^1(T)} + \|\mathbf{e}_p\|^2_{\mathrm{L}^2(T)} + h_T^2\big\||\mathbf{u}|^{m-2}\mathbf{u} - |\mathbf{u}_h|^{m-2}\mathbf{u}_h\big\|^2_{\mathbf{L}^2(T)}\Big\}. \end{aligned} \tag{5.24}$$

Proof. The proof follows the same bubble-function argument used in Lemma 5.6. Indeed, define

$$\boldsymbol{\chi}_T := \mathbf{g} + \nu\,\Delta\mathbf{u}_h - \mathtt{D}\,\mathbf{u}_h - \mathtt{F}|\mathbf{u}_h|^{m-2}\mathbf{u}_h - \nabla p_h \quad \text{in} \quad T.$$

For simplicity of exposition, throughout this argument we assume that the Forchheimer contribution $|\mathbf{u}_h|^{m-2}\mathbf{u}_h$ is polynomial on each element $T \in \mathcal{T}_h$. The general case can be treated by replacing this term with a suitable local polynomial projection. The corresponding projection error gives rise to additional higher-order terms in the efficiency estimate, which are omitted here for the sake of conciseness. Under this assumption, $\boldsymbol{\chi}_T$ belongs to a finite-dimensional polynomial space on T. Hence, using the vector-valued version of (C.4), we obtain

$$\|\boldsymbol{\chi}_T\|^2_{\mathbf{L}^2(T)} \le c_1(\boldsymbol{\chi}_T, \phi_T\boldsymbol{\chi}_T)_T.$$

Then, we employ the strong form of the Brinkman–Forchheimer equation (2.7a), namely,

$$-\nu\,\Delta\mathbf{u} + \mathtt{D}\,\mathbf{u} + \mathtt{F}\,|\mathbf{u}|^{m-2}\mathbf{u} + \nabla p = \mathbf{g} \quad \text{in} \quad \Omega.$$

Combining this equation with the definition of the discrete residual $\boldsymbol{\chi}_T$, testing the resulting residual identity with $\phi_T\boldsymbol{\chi}_T$, and integrating by parts over T, we obtain

$$\begin{aligned} (\boldsymbol{\chi}_T, \phi_T\boldsymbol{\chi}_T)_T &= \nu(\nabla\mathbf{e}_{\mathbf{u}}, \nabla(\phi_T\boldsymbol{\chi}_T))_T + \mathtt{D}(\mathbf{e}_{\mathbf{u}}, \phi_T\boldsymbol{\chi}_T)_T - (\mathbf{e}_p, \mathrm{div}(\phi_T\boldsymbol{\chi}_T))_T \\ &\quad + \mathtt{F}\big(|\mathbf{u}|^{m-2}\mathbf{u} - |\mathbf{u}_h|^{m-2}\mathbf{u}_h, \phi_T\boldsymbol{\chi}_T\big)_T. \end{aligned}$$

Using the standard bubble-function estimate, the Cauchy–Schwarz inequality, the inverse estimate (C.7), and the bound $0 \le \phi_T \le 1$, we deduce that

$$\begin{aligned} \|\boldsymbol{\chi}_T\|^2_{\mathbf{L}^2(T)} &\le C\Big(h_T^{-1}\|\nabla\mathbf{e}_{\mathbf{u}}\|_{\mathbb{L}^2(T)} + \|\mathbf{e}_{\mathbf{u}}\|_{\mathbf{L}^2(T)} + h_T^{-1}\|\mathbf{e}_p\|_{\mathrm{L}^2(T)} \\ &\quad + \big\||\mathbf{u}|^{m-2}\mathbf{u} - |\mathbf{u}_h|^{m-2}\mathbf{u}_h\big\|_{\mathbf{L}^2(T)}\Big)\|\boldsymbol{\chi}_T\|_{\mathbf{L}^2(T)}. \end{aligned}$$

After cancelling the common factor $\|\boldsymbol{\chi}_T\|_{\mathbf{L}^2(T)}$, multiplying the resulting inequality by h_T, and using $h_T\|\mathbf{e}_{\mathbf{u}}\|_{\mathbf{L}^2(T)} \le C\|\mathbf{e}_{\mathbf{u}}\|_{\mathbf{H}^1(T)}$, we obtain

$$h_T\|\boldsymbol{\chi}_T\|_{\mathbf{L}^2(T)} \le C\left(\|\mathbf{e}_{\mathbf{u}}\|_{\mathbf{H}^1(T)} + \|\mathbf{e}_p\|_{\mathrm{L}^2(T)} + h_T\big\||\mathbf{u}|^{m-2}\mathbf{u} - |\mathbf{u}_h|^{m-2}\mathbf{u}_h\big\|_{\mathbf{L}^2(T)}\right).$$

Finally, squaring the last inequality yields (5.24). □

Lemma 5.8 *There exists a positive constant C, independent of h, such that, for each $e \in \mathcal{E}_h(\Omega)$, there holds*

$$
\begin{aligned}
& h_e \, \| [\![(2\mu \, \boldsymbol{\varepsilon}(\boldsymbol{\eta}_h) - \theta_h \mathbb{I}) \mathbf{n}]\!] \|^2_{\mathbf{L}^2(e)} \\
& \quad \leq C \left\{ \sum_{T_e \in \omega_e} \left(h_T^2 \| \mathbf{f}_p + \mathbf{div} \, (2\mu \, \boldsymbol{\varepsilon}(\boldsymbol{\eta}_h) - \theta_h \mathbb{I}) \, \|^2_{\mathbf{L}^2(T_e)} + \| \mathbf{e}_{\boldsymbol{\eta}} \|^2_{\mathbf{H}^1(T_e)} + \| \mathbf{e}_\theta \|^2_{\mathrm{L}^2(T_e)} \right) \right\},
\end{aligned} \tag{5.25}
$$

and

$$
\begin{aligned}
h_e \, \| [\![(\nu \nabla \mathbf{u}_h - p_h \mathbb{I}) \mathbf{n}]\!] \|^2_{\mathbf{L}^2(e)} & \leq C \left\{ \sum_{T_e \in \omega_e} \left(h_T^2 \| \mathbf{g} + \nu \, \Delta \mathbf{u}_h - \mathtt{D} \, \mathbf{u}_h - \mathtt{F} |\mathbf{u}_h|^{m-2} \mathbf{u}_h - \nabla p_h \|^2_{\mathbf{L}^2(T_e)} \right. \right. \\
& \left. \left. + \| \mathbf{e}_{\mathbf{u}} \|^2_{\mathbf{H}^1(T_e)} + \| \mathbf{e}_p \|^2_{\mathrm{L}^2(T_e)} + h_e^2 \left\| |\mathbf{u}|^{m-2} \mathbf{u} - |\mathbf{u}_h|^{m-2} \mathbf{u}_h \right\|^2_{\mathbf{L}^2(T_e)} \right) \right\},
\end{aligned} \tag{5.26}
$$

where ω_e denotes the patch formed by the two elements of $\mathcal{T}_h$ sharing the edge/face e.

Proof. We prove only (5.26), since (5.25) follows analogously. Let $\boldsymbol{\chi}_e := [\![(\nu \nabla \mathbf{u}_h - p_h \mathbb{I}) \mathbf{n}]\!]$ on e. Proceeding as in [3, Lemma 4.5], we apply the vector-valued version of the facet-bubble estimate (C.5) and integrate by parts over each $T_e \in \omega_e$. This yields

$$
\begin{aligned}
\| \boldsymbol{\chi}_e \|^2_{\mathbf{L}^2(e)} & \leq c_2 \| \phi_e^{1/2} \boldsymbol{\chi}_e \|^2_{\mathbf{L}^2(e)} = c_2 \, \langle [\![(\nu \nabla \mathbf{u}_h - p_h \mathbb{I}) \mathbf{n}]\!] \, , \phi_e \, \mathbf{L}(\boldsymbol{\chi}_e) \rangle_e \\
& = c_2 \sum_{T_e \in \omega_e} \langle (\nu \nabla \mathbf{u}_h - p_h \mathbb{I}) \mathbf{n}_{T_e}, \phi_e \, \mathbf{L}(\boldsymbol{\chi}_e) \rangle_{\partial T_e} \\
& = c_2 \sum_{T_e \in \omega_e} \left\{ (\nu \nabla \mathbf{u}_h - p_h \mathbb{I}, \nabla (\phi_e \, \mathbf{L}(\boldsymbol{\chi}_e)))_{T_e} + (\nu \Delta \mathbf{u}_h - \nabla p_h, \phi_e \, \mathbf{L}(\boldsymbol{\chi}_e))_{T_e} \right\},
\end{aligned}
$$

where $\mathbf{L}$ denotes the vector-valued version of the extension operator L defined in (C.3). Now, from the Brinkman–Forchheimer equation in (2.7a), and then, integrating by parts once more on each $T_e \in \omega_e$, and adding and subtracting suitable terms, we get

$$
\begin{aligned}
\| \boldsymbol{\chi}_e \|^2_{\mathbf{L}^2(e)} \leq c_2 \sum_{T_e \in \omega_e} & \left\{ \left(\mathbf{g} + \nu \, \Delta \mathbf{u}_h - \mathtt{D} \, \mathbf{u}_h - \mathtt{F} |\mathbf{u}_h|^{m-2} \mathbf{u}_h - \nabla p_h, \phi_e \, \mathbf{L}(\boldsymbol{\chi}_e) \right)_{T_e} \right. \\
& + (\nu \nabla (\mathbf{u}_h - \mathbf{u}) - (p_h - p) \mathbb{I}, \nabla (\phi_e \, \mathbf{L}(\boldsymbol{\chi}_e)))_{T_e} \\
& \left. + \left(\mathtt{D} (\mathbf{u}_h - \mathbf{u}) + \mathtt{F} \left(|\mathbf{u}_h|^{m-2} \mathbf{u}_h - |\mathbf{u}|^{m-2} \mathbf{u} \right), \phi_e \, \mathbf{L}(\boldsymbol{\chi}_e) \right)_{T_e} \right\}.
\end{aligned}
$$

Then, applying the Cauchy–Schwarz inequality, we first obtain

$$
\begin{aligned}
\| \boldsymbol{\chi}_e \|^2_{\mathrm{L}^2(e)} \leq c_2 \sum_{T_e \in \omega_e} & \left\{ \left\| \mathbf{g} + \nu \, \Delta \mathbf{u}_h - \mathtt{D} \, \mathbf{u}_h - \mathtt{F} |\mathbf{u}_h|^{m-2} \mathbf{u}_h - \nabla p_h \right\|_{\mathbf{L}^2(T_e)} \| \phi_e \mathbf{L}(\boldsymbol{\chi}_e) \|_{\mathbf{L}^2(T_e)} \right. \\
& + \left(\nu \| \nabla \mathbf{e}_{\mathbf{u}} \|_{\mathbb{L}^2(T_e)} + \| \mathbf{e}_p \|_{\mathrm{L}^2(T_e)} \right) \| \nabla (\phi_e \mathbf{L}(\boldsymbol{\chi}_e)) \|_{\mathbb{L}^2(T_e)} \\
& \left. + \left(\mathtt{D} \| \mathbf{e}_{\mathbf{u}} \|_{\mathbf{L}^2(T_e)} + \mathtt{F} \left\| |\mathbf{u}|^{m-2} \mathbf{u} - |\mathbf{u}_h|^{m-2} \mathbf{u}_h \right\|_{\mathbf{L}^2(T_e)} \right) \| \phi_e \mathbf{L}(\boldsymbol{\chi}_e) \|_{\mathbf{L}^2(T_e)} \right\}.
\end{aligned} \tag{5.27}
$$

On the other hand, by the inverse inequality (C.7), applied with $\ell = 1$ and $m = 0$, by the face-bubble estimate (C.6), using that $0 \leq \phi_e \leq 1$ (cf. (C.2)), and that $h_e \leq h_{T_e}$, we have, for each $T_e \in \omega_e$,

$$
\| \phi_e \mathbf{L}(\boldsymbol{\chi}_e) \|_{\mathbf{L}^2(T_e)} \leq \| \phi_e^{1/2} \mathbf{L}(\boldsymbol{\chi}_e) \|_{\mathbf{L}^2(T_e)} \leq c_4 h_e^{1/2} \| \boldsymbol{\chi}_e \|_{\mathbf{L}^2(e)} \, , \tag{5.28}
$$

and

$$\|\nabla(\phi_e \mathbf{L}(\boldsymbol{\chi}_e))\|_{\mathbb{L}^2(T_e)} \leq C h_{T_e}^{-1} \|\phi_e \mathbf{L}(\boldsymbol{\chi}_e)\|_{\mathbf{L}^2(T_e)} \leq C h_{T_e}^{-1} h_e^{1/2} \|\boldsymbol{\chi}_e\|_{\mathbf{L}^2(e)} \leq C h_e^{-1/2} \|\boldsymbol{\chi}_e\|_{\mathbf{L}^2(e)} \,. \tag{5.29}$$

Consequently, replacing (5.28) and (5.29) into (5.27), dividing by $\|\boldsymbol{\chi}_e\|_{\mathbf{L}^2(e)}$, and multiplying by $h_e^{1/2}$, we infer that

$$\begin{aligned} h_e^{1/2} \|\boldsymbol{\chi}_e\|_{\mathbf{L}^2(e)} \leq C \sum_{T_e \in \omega_e} \Big\{ & h_{T_e} \left\| \mathbf{g} + \nu\, \Delta \mathbf{u}_h - \mathtt{D}\, \mathbf{u}_h - \mathtt{F} |\mathbf{u}_h|^{m-2} \mathbf{u}_h - \nabla p_h \right\|_{\mathbf{L}^2(T_e)} \\ & + \|\mathbf{e}_{\mathbf{u}}\|_{\mathbf{H}^1(T_e)} + \|\mathbf{e}_p\|_{\mathrm{L}^2(T_e)} + h_e \left\| |\mathbf{u}|^{m-2}\mathbf{u} - |\mathbf{u}_h|^{m-2}\mathbf{u}_h \right\|_{\mathbf{L}^2(T_e)} \Big\}. \end{aligned}$$

Squaring the previous estimate yields (5.26). The proof of (5.25) is obtained in the same way, using $\boldsymbol{\chi}_e := [\![(2\mu\, \boldsymbol{\varepsilon}(\boldsymbol{\eta}_h) - \theta_h \mathbb{I})\mathbf{n}]\!]$ on e, together with the mechanical equation in (2.7a). □

In order to complete the global efficiency estimate for $\boldsymbol{\Xi}$ (cf. (5.1)), it remains to control the nonlinear term appearing in the upper bound established in Lemma 5.7 and 5.8. To this end, using (4.18) and the continuous embedding $\mathbf{i}_{2(m-1)} : \mathbf{H}^1(\Omega) \hookrightarrow \mathbf{L}^{2(m-1)}(\Omega)$, we obtain

$$\begin{aligned} \sum_{T \in \mathcal{T}_h} \left\| |\mathbf{u}|^{m-2}\mathbf{u} - |\mathbf{u}_h|^{m-2}\mathbf{u}_h \right\|_{\mathbf{L}^2(T)}^2 &= \left\| |\mathbf{u}|^{m-2}\mathbf{u} - |\mathbf{u}_h|^{m-2}\mathbf{u}_h \right\|_{\mathbf{L}^2(\Omega)}^2 \\ &\leq C \left(\|\mathbf{u}\|_{\mathbf{L}^{2(m-1)}(\Omega)} + \|\mathbf{u}_h\|_{\mathbf{L}^{2(m-1)}(\Omega)} \right)^{2(m-2)} \|\mathbf{u} - \mathbf{u}_h\|_{\mathbf{L}^{2(m-1)}(\Omega)}^2 \\ &\leq C \left(\|\mathbf{u}\|_{\mathbf{H}^1(\Omega)} + \|\mathbf{u}_h\|_{\mathbf{H}^1(\Omega)} \right)^{2(m-2)} \|\mathbf{e}_{\mathbf{u}}\|_{\mathbf{H}^1(\Omega)}^2 \,. \end{aligned}$$

Furthermore, by the continuous and discrete a priori estimates (3.17) and (4.3), the factor involving $\|\mathbf{u}\|_{\mathbf{H}^1(\Omega)}$ and $\|\mathbf{u}_h\|_{\mathbf{H}^1(\Omega)}$ is bounded in terms of the data. Consequently,

$$\sum_{T \in \mathcal{T}_h} \left\| |\mathbf{u}|^{m-2}\mathbf{u} - |\mathbf{u}_h|^{m-2}\mathbf{u}_h \right\|_{\mathbf{L}^2(T)}^2 \leq C_{\mathrm{data}} \|\mathbf{e}_{\mathbf{u}}\|_{\mathbf{H}^1(\Omega)}^2 \,, \tag{5.30}$$

where $C_{\mathrm{data}} > 0$ is independent of h. Thus, we have arrived at the main result of this section.

Theorem 5.9 *Let $((\boldsymbol{\eta}, \mathbf{u}), (\theta, p)) \in \mathbb{H} \times \mathbb{Q}$ and $((\boldsymbol{\eta}_h, \mathbf{u}_h), (\theta_h, p_h)) \in \mathbb{H}_h \times \mathbb{Q}_h$ be the unique solutions of (2.12) and (4.2), respectively. Then $\boldsymbol{\Xi}$ is efficient. More precisely, there exists a positive constant $C_{\mathtt{eff}}$, independent of h, such that*

$$C_{\mathtt{eff}}\, \boldsymbol{\Xi} + \mathtt{h.o.t.} \leq \|(\mathbf{e}_{\boldsymbol{\eta}}, \mathbf{e}_{\mathbf{u}})\|_{\mathbb{H}} + \|(\mathbf{e}_\theta, \mathbf{e}_p)\|_{\mathbb{Q}} \,. \tag{5.31}$$

Proof. Assume first that $\mathbf{f}_p$, $\mathbf{g}$, and g are piecewise polynomial functions. In this case, the estimate follows directly from Lemmas 5.5, 5.6, 5.7, and 5.8, together with (5.30), after summing the corresponding local bounds over all $T \in \mathcal{T}_h$. If the data are not piecewise polynomial, the same argument can be carried out by using suitable local polynomial approximations of the data, as in [16, Section 6.2]. This gives the additional higher-order contribution denoted by $\mathtt{h.o.t.}$ in (5.31). □

Remark 5.1 *The continuous, discrete, and error analyses developed in this paper extend, with minor modifications, to spatially varying coefficients ν, $\mathtt{D}$, $\mathtt{F}$, and μ, while keeping s_0, α, and λ constant. It suffices to assume that ν, $\mathtt{D}$, and μ are essentially bounded and uniformly positive, and that $\mathtt{F}$ is essentially bounded and nonnegative. For the residual-based a posteriori analysis, suitable element-wise regularity is additionally required, and the residuals and normal-flux jumps must be written in divergence form. Related treatments can be found in [10]. Spatially varying coefficients $\lambda = \lambda(\mathbf{x})$ and $s_0 = s_0(\mathbf{x})$ are not directly covered by the present framework, since they affect the zero-mean and compatibility conditions imposed on the scalar unknowns (cf. (2.6)). Their treatment would require a suitable modification of the formulation and is left for future work.*

6 Numerical results

In this section, we assess the performance and accuracy of the mixed-primal scheme (4.2). In particular, we illustrate its locking-free behavior and the reliability and efficiency of the *a posteriori* error estimator $\boldsymbol{\Xi}$ (cf. (5.1)). The computational results were obtained using `FreeFEM` [29]. The nonlinear algebraic system arising from (4.2) is solved by means of a Newton–Raphson algorithm with fixed tolerance $\mathrm{tol} = 10^{-6}$. More precisely, the iterative process is stopped whenever the relative difference between two successive iterates of the full coefficient vector $\mathbf{coeff}^n$ and $\mathbf{coeff}^{n+1}$ satisfies

$$\frac{\|\mathbf{coeff}^{n+1} - \mathbf{coeff}^n\|_{\mathtt{DoF}}}{\|\mathbf{coeff}^{n+1}\|_{\mathtt{DoF}}} \leq \mathrm{tol}\,,$$

where $\|\cdot\|_{\mathtt{DoF}}$ denotes the standard Euclidean norm and $\mathtt{DoF}$ represents the total number of degrees of freedom associated with the finite element subspaces involved.

The individual and global errors, and the effectivity index for the estimator $\boldsymbol{\Xi}$ are defined as

$$\mathrm{e}(\boldsymbol{\eta}) := \|\boldsymbol{\eta} - \boldsymbol{\eta}_h\|_{\mathbf{H}^1(\Omega)}\,, \qquad \mathrm{e}(\mathbf{u}) := \|\mathbf{u} - \mathbf{u}_h\|_{\mathbf{H}^1(\Omega)}\,, \qquad \mathrm{e}(\theta) := \|\theta - \theta_h\|_{\mathrm{L}^2(\Omega)},$$

$$\mathrm{e}(p) := \|p - p_h\|_{\mathrm{L}^2(\Omega)}\,, \qquad \mathrm{e}_{\mathtt{tot}} := \big(\mathrm{e}(\boldsymbol{\eta})^2 + \mathrm{e}(\mathbf{u})^2 + \mathrm{e}(\theta)^2 + \mathrm{e}(p)^2\big)^{1/2}\,, \qquad \mathrm{eff} := \frac{\mathrm{e}_{\mathtt{tot}}}{\boldsymbol{\Xi}}\,.$$

Since $h \simeq \mathtt{DoF}^{-1/d}$ for quasi-uniform meshes, the experimental convergence rates are computed in terms of the total number of degrees of freedom. More precisely, for two consecutive meshes, we define

$$r(\star) := -d\,\frac{\log(\mathrm{e}(\star)/\mathrm{e}'(\star))}{\log(\mathtt{DoF}/\mathtt{DoF}')} \qquad \text{for each } \star \in \{\boldsymbol{\eta}, \mathbf{u}, \theta, p\}\,.$$

where $\mathtt{DoF}$ and $\mathtt{DoF}'$ denote the total degrees of freedom associated with two consecutive meshes with errors $\mathrm{e}(\star)$ and $\mathrm{e}'(\star)$, respectively. The convergence rate of the total error, denoted by $r_{\mathtt{tot}}$, is defined analogously by replacing $\mathrm{e}(\star)$ and $\mathrm{e}'(\star)$ with $\mathrm{e}_{\mathtt{tot}}$ and $\mathrm{e}'_{\mathtt{tot}}$, respectively.

Some of the numerical experiments presented below involve spatially varying model coefficients. In accordance with Remark 5.1, the tests with heterogeneous ν, $\mathtt{D}$, $\mathtt{F}$, or μ, but constant α and λ, are understood within the natural extension of the analysis to bounded and uniformly positive coefficients. Example 2 requires an additional qualification, since both Lamé coefficients, including $\lambda = \lambda(\mathbf{x})$, are obtained from the heterogeneous SPE10 porosity field [17]. Consequently, this experiment does not fall entirely within the theoretical framework established in the preceding sections. We nevertheless include it as an exploratory computational extension of the proposed method to a highly heterogeneous poroelastic medium. The resulting numerical behavior motivates the development of a modified total-pressure formulation and a corresponding analysis for spatially varying λ, which will be addressed in future work. For the experiments involving spatially varying coefficients, the corresponding differential operators and residual terms are understood in divergence form. In particular, when $\nu = \nu(\mathbf{x})$, the Brinkman diffusion operator is written as $-\mathrm{div}(\nu\nabla\mathbf{u})$, and the associated element residual and normal-flux jump are modified accordingly.

The adaptive procedure follows the standard strategy proposed in [42]:

(1) Start with a coarse mesh $\mathcal{T}_h$.

(2) Solve the nonlinear discrete problem (4.2) on the current mesh $\mathcal{T}_h$ by means of Newton's method.

(3) Compute the local indicator $\boldsymbol{\Xi}_T$ for each $T \in \mathcal{T}_h$, where

$$\boldsymbol{\Xi}_T := \boldsymbol{\Xi}_{1,T} + \boldsymbol{\Xi}_{2,T} \quad (\text{cf. (5.2) and (5.3)})\,.$$

(4) Check the stopping criterion and decide whether to finish or go to next step.

(5) Use the automatic meshing algorithm adaptmesh [30, Section 9.1.9] to refine each element $T' \in \mathcal{T}_h$ satisfying

$$\Xi_{T'} \geq C_{\mathtt{adm}} \frac{1}{\#\mathcal{T}_h} \sum_{T \in \mathcal{T}_h} \Xi_T, \qquad C_{\mathtt{adm}} \in (0,1),$$

where $\#\mathcal{T}_h$ denotes the number of elements of the current mesh.

(6) Replace $\mathcal{T}_h$ by the resulting refined mesh and return to step (2).

In particular, $C_{\mathtt{adm}}$ is chosen as 0.83 for Examples 3 and 4, whereas for Example 5 we consider 0.85.

Example 1: Robustness with respect to the nearly incompressible limit

We first validate the convergence rates and assess the robustness of the numerical method (4.2) in a two-dimensional setting. The main purpose of this example is to verify that the method does not suffer from locking when approaching the nearly incompressible regime. The computational domain is the unit square $\Omega := (0,1)^2$, and we set $m = 4$. The physical and model parameters are chosen as

$$s_0 = 1\,, \qquad \alpha = 0.9\,, \qquad \nu = 1\,, \qquad \mathtt{D} = 1\,, \qquad \mu = 1\,, \qquad \mathtt{F} = 10\,.$$

The robustness with respect to incompressibility is tested by varying the Lamé parameter $\lambda \in \{1, 10^3, 10^6, 10^{12}\}$. Hence, the largest value corresponds to a regime very close to incompressibility. The data are manufactured so that the exact solution is given by the following smooth functions. For $\mathbf{x} = (x_1, x_2) \in \Omega$, let

$$\psi(\mathbf{x}) := \prod_{i=1}^{2} x_i(1 - x_i)\,.$$

The displacement field is defined by

$$\boldsymbol{\eta}(\mathbf{x}) := \begin{pmatrix} \pi \sin^2(\pi x_1)\sin(2\pi x_2) \\ -\pi \sin^2(\pi x_2)\sin(2\pi x_1) \end{pmatrix} + \frac{1}{2\lambda}\psi(\mathbf{x}) \begin{pmatrix} 1 \\ 1 \end{pmatrix}.$$

The velocity field and the pressure are given by

$$\mathbf{u}(\mathbf{x}) := \begin{pmatrix} \sin^2(\pi x_1)\sin(\pi x_2) \\ -\sin(\pi x_1)\sin^2(\pi x_2) \end{pmatrix} \quad \text{and} \quad p(\mathbf{x}) := \sin(\pi x_1)\cos\left(\frac{\pi x_2}{2}\right) - \frac{4}{\pi^2}.$$

Notice that $\boldsymbol{\eta} = \mathbf{0}$ and $\mathbf{u} = \mathbf{0}$ on $\partial\Omega$. In addition, the pressure has zero mean over Ω. The dominant part of the displacement field is divergence-free, whereas the compressible perturbation is scaled by λ^{-1}. Therefore, as $\lambda^{-1} \to 0$, the exact solution remains smooth while the problem approaches the nearly incompressible limit.

We consider two inf-sup stable finite element families: the MINI element $\mathbf{P}_{1,b} - \mathrm{P}_1$ and the Taylor–Hood element $\mathbf{P}_2 - \mathrm{P}_1$. For each value of λ, the problem is solved on a sequence of quasi-uniform meshes. The corresponding convergence histories are displayed in Figure 6.1. In each case, the dashed line represents the algebraic reference behavior $\mathtt{DoF}^{-k/2}$, which corresponds to an h^k convergence rate under quasi-uniform refinement, with $k = 1$ for the MINI element and $k = 2$ for the Taylor–Hood element. The results show that the expected convergence behavior is preserved as λ increases, providing numerical evidence of the locking-free character of the method.

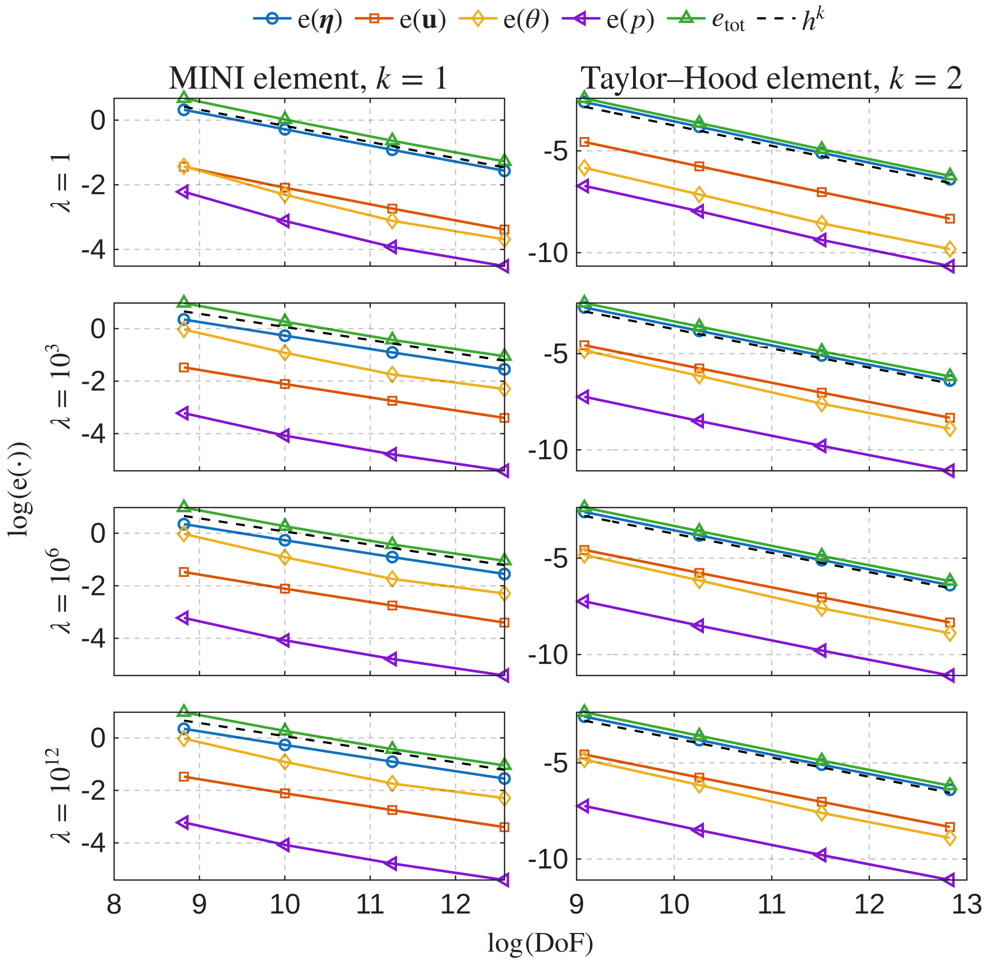

Figure 6.1: [Example 1] Convergence histories for the MINI element, $k = 1$, and the Taylor–Hood element, $k = 2$, for $\lambda \in \{1, 10^3, 10^6, 10^{12}\}$. The dashed lines represent the algebraic reference behavior $\texttt{DoF}^{-k/d}$, corresponding to an h^k convergence rate under quasi-uniform refinement.

We next investigate the sensitivity of the method with respect to the storage coefficient s_0. For this purpose, we fix $\lambda = 1$ and consider $s_0 \in \{10^{-3}, 10^{-6}, 10^{-12}\}$. This test assesses the behavior of the discretization as the storage coefficient approaches the degenerate limit $s_0 = 0$. The results are displayed in Figure 6.2. The left column corresponds to the MINI element, whereas the right column corresponds to the Taylor–Hood element. Each row represents one value of s_0, and the dashed lines denote the reference slopes h^k. We observe that the convergence histories are essentially unaffected by the variation of s_0. In particular, no visible loss of accuracy is observed when passing from $s_0 = 10^{-3}$ to $s_0 = 10^{-12}$. The expected convergence rates are preserved for both finite element families, and the behavior of the total error is consistent with the corresponding reference slopes. These results provide numerical evidence of the robustness of the proposed discretization with respect to small values of the storage coefficient.

Example 2: Flow through a strongly heterogeneous porous medium

In this example, we consider a two-dimensional heterogeneous benchmark based on the Society of Petroleum Engineers 10th Comparative Solution Project (SPE10) data set [17], accessed and processed

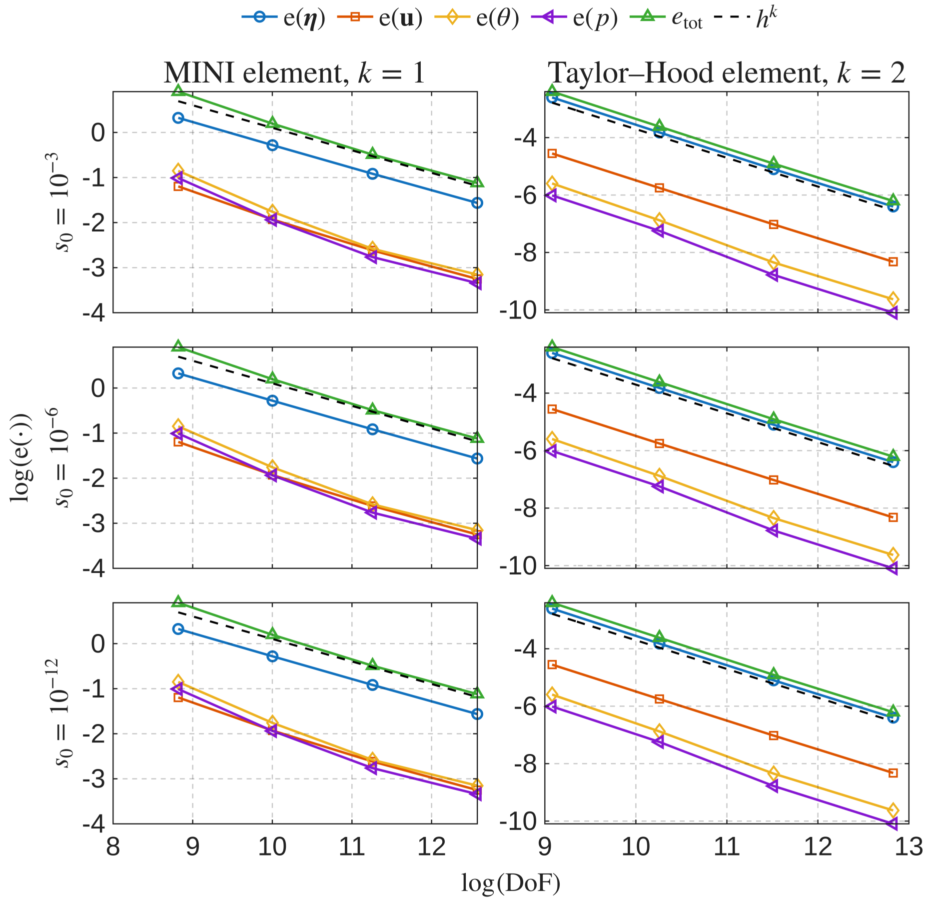

Figure 6.2: [Example 1] Convergence histories for the MINI element, $k = 1$, and the Taylor–Hood element, $k = 2$, for $s_0 \in \{10^{-3}, 10^{-6}, 10^{-12}\}$, with fixed $\lambda = 1$. The dashed lines represent the algebraic reference behavior $\mathtt{DoF}^{-k/d}$, corresponding to an h^k convergence rate under quasi-uniform refinement.

using the SPE10 module of the MATLAB Reservoir Simulation Toolbox (MRST) [34]. The design of the experiment is also motivated by the poroelasticity benchmarks presented in [32, 36]. The aim is to assess the behavior of the proposed scheme in a highly heterogeneous medium and to illustrate the interaction between permeability channels, nonlinear Forchheimer resistance, pressure gradients, fluid velocity, and poroelastic deformation.

Using MRST 2026a, we extract the 85th layer of the SPE10 model, which contains 60×220 cells. Since each cell has physical dimensions $20\,\text{ft} \times 10\,\text{ft}$, the computational domain is $\Omega = (0, 365.76) \times (0, 670.56)$, with lengths expressed in meters. Each rectangular cell is split into two triangles, yielding a mesh with 26,400 triangular elements. For the spatial discretization, we employ Taylor–Hood finite element spaces, consisting of continuous piecewise quadratic elements for the two vector-valued unknowns and continuous piecewise linear elements for the total and pore pressures. The scalar permeability used in the two-dimensional model is obtained from the horizontal SPE10 permeabilities as $\kappa = \sqrt{\kappa_x \kappa_y}$. Since κ spans several orders of magnitude, we introduce the normalized permeability $\widehat{\kappa} = \frac{\kappa}{\kappa_{\text{ref}}}$, $\kappa_{\text{ref}} = \exp\left(\frac{1}{|\Omega|}(\log \kappa, 1)_\Omega\right)$, and define the Darcy coefficient by $\mathtt{D} = \frac{\mathtt{D}_0}{\widehat{\kappa}}$. Here, $\mathtt{D}_0 > 0$ is a reference Darcy resistance parameter controlling the global flow regime, while $\widehat{\kappa}$ preserves the spatial variability and channelized structure of the SPE10 permeability field.

The SPE10 porosity field ϕ is also used to prescribe the spatially varying elastic properties of the porous skeleton. To this end, we consider the empirical porosity–Young modulus relation

$$E(\mathbf{x}) = E_0 \left(1 - \frac{\phi(\mathbf{x})}{\phi_{\mathrm{ref}}}\right)^{2.1}, \qquad E_0 = 10^2\,, \qquad \phi_{\mathrm{ref}} = 0.5\,.$$

The parameter E_0 denotes the reference Young's modulus used in the dimensionless simulation. The corresponding Lamé coefficients are defined by

$$\mu(\mathbf{x}) = \frac{E(\mathbf{x})}{2(1+\nu_s)} \quad \text{and} \quad \lambda(\mathbf{x}) = \frac{E(\mathbf{x})\nu_s}{(1+\nu_s)(1-2\nu_s)},$$

where the Poisson ratio is fixed as $\nu_s = 0.25$. Thus, regions with larger porosity exhibit a softer elastic response, whereas regions with lower porosity are comparatively stiffer.

We impose homogeneous boundary conditions on the whole boundary. The source term represents two injection wells and one production well located at

$$P_1 = (119, 578), \qquad P_2 = (155, 130), \qquad P_3 = (175, 360)\,.$$

More precisely, we define

$$g(\mathbf{x}) = 0.01 \exp\left(-\frac{|\mathbf{x} - P_1|^2}{1500}\right) + 0.01 \exp\left(-\frac{|\mathbf{x} - P_2|^2}{1500}\right) - 0.02 \exp\left(-\frac{|\mathbf{x} - P_3|^2}{1500}\right) - g_0\,,$$

where g_0 is chosen such that g has zero mean value. The denominator 1,500 corresponds to a smooth Gaussian regularization of the wells over several grid cells, avoiding point-source singularities while keeping the injection and production effects localized. The vector-valued source terms in the mechanical equilibrium and fluid momentum equations are set to zero, namely, $\mathbf{f}_p = \mathbf{0}$ and $\mathbf{g} = \mathbf{0}$ in Ω. The parameters used in the flow model are

$$s_0 = 10^{-6}, \quad \nu = 0.1, \quad \alpha = 0.95, \quad m = 3, \quad \text{and} \quad \mathtt{D}_0 = 5 \times 10^{-2}\,.$$

To investigate the influence of the nonlinear Forchheimer resistance, we consider the values $\mathtt{F} \in \{5, 0.5, 10^{-2}, 0\}$, while keeping all the remaining parameters fixed. The case $\mathtt{F} = 0$ corresponds to the Brinkman regime and is included as a reference, whereas the positive values of $\mathtt{F}$ allow us to assess the progressive damping induced by the nonlinear inertial correction.

Figure 6.3 displays the logarithm of the original permeability field, $\log_{10}(\kappa)$, together with the Lamé coefficients λ and μ. These fields reflect the mechanical heterogeneity induced by the SPE10 porosity distribution. Figure 6.4 shows a sweep with respect to the Forchheimer coefficient, namely $\mathtt{F} \in \{5, 0.5, 10^{-2}, 0\}$. The same color scale is used in all panels in order to make the comparison meaningful. For large values of $\mathtt{F}$, the nonlinear resistance term $\mathtt{F}|\mathbf{u}_h|^{m-2}\mathbf{u}_h$ strongly damps the flow, and the velocity remains concentrated mainly near the injection and production regions. As $\mathtt{F}$ decreases, the damping effect becomes weaker and the preferential paths associated with the high-permeability channels become progressively more visible. In the limiting case $\mathtt{F} = 0$, the velocity field exhibits the largest peaks and the most developed channelized structure. This comparison shows that the SPE10 permeability distribution determines the main flow pathways, whereas the Forchheimer term controls their intensity. In particular, increasing $\mathtt{F}$ does not create new preferential paths, but reduces the magnitude of the velocity along the existing high-permeability channels. Figure 6.5 displays the fluid pressure and displacement magnitude for the nonlinear case $\mathtt{F} = 10^{-2}$. The pressure field exhibits localized variations near the injection and production wells, whereas the displacement remains small in magnitude but reflects the coupled poroelastic response induced by the pressure distribution and the heterogeneous elastic coefficients.

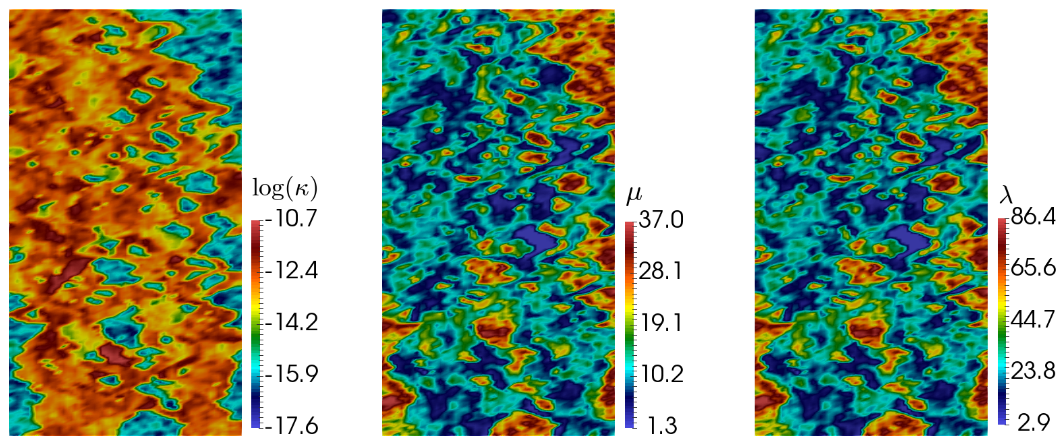

Figure 6.3: [Example 2] Heterogeneous fields used in the simulation. From left to right: logarithm of the permeability $\log_{10}(\kappa)$, Lamé coefficient μ, and Lamé coefficient λ.

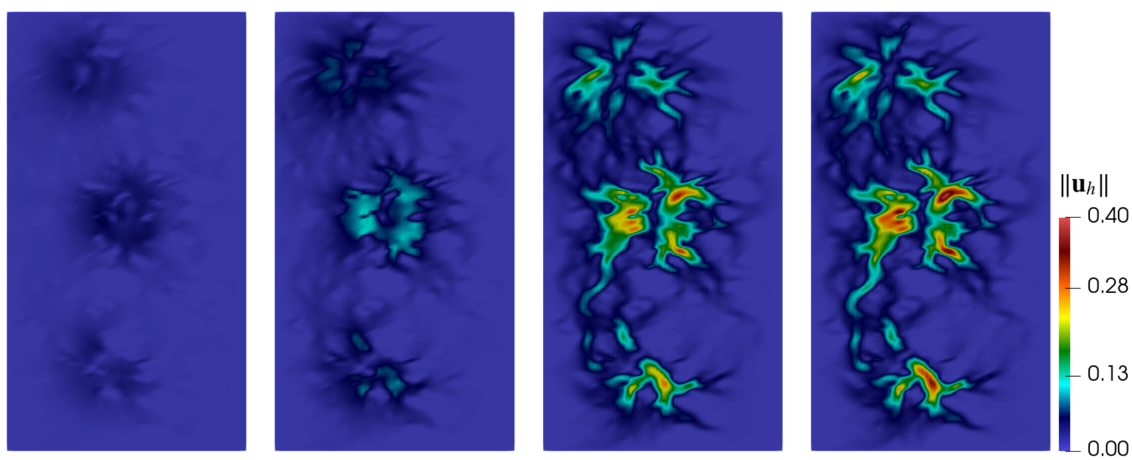

Figure 6.4: [Example 2] Computed velocity magnitude $\|\mathbf{u}_h\|$ for the heterogeneous porous-medium benchmark and different values of the Forchheimer coefficient. From left to right: $\mathtt{F} = 5$, $\mathtt{F} = 0.5$, $\mathtt{F} = 10^{-2}$, and $\mathtt{F} = 0$. The same color scale is used in all panels.

Example 3: Adaptive refinement on a two-dimensional L-shaped domain

We now assess the performance of the adaptive refinement strategy driven by the *a posteriori* error estimator $\boldsymbol{\Xi}$ on a two-dimensional L-shaped domain. The aim of this example is to test the ability of the estimator to identify and resolve localized regions of high pressure gradient in a nonconvex domain and under a nearly incompressible regime. We consider $\Omega := (-1,1)^2 \setminus \big((0,1) \times (-1,0)\big)$, whose reentrant corner is located at the origin. Homogeneous Dirichlet boundary conditions are imposed on the displacement and velocity fields, and we employ the Taylor–Hood finite element pair $\mathbf{P}_2 - \mathrm{P}_1$. The model parameters are chosen as

$$s_0 = 10^{-6}, \quad \alpha = 0.9, \quad \nu(\mathbf{x}) = \exp(-x_1 x_2), \quad \mathtt{D} = 10^2, \quad \lambda = 10^{12}, \quad \mu = 1, \quad \mathtt{F} = 10, \quad m = 4.$$

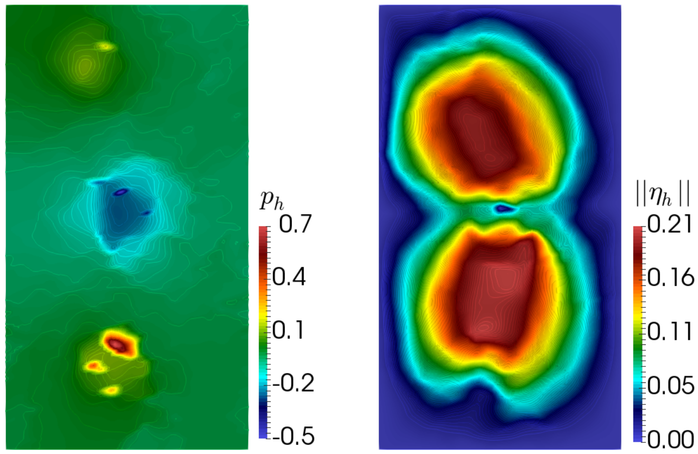

Figure 6.5: [Example 2] Computed fluid pressure p_h (left) and displacement magnitude $\|\boldsymbol{\eta}_h\|$ (right) for the nonlinear case $\mathtt{F} = 10^{-2}$.

The data are manufactured so that the exact solution is given by the following functions. For $\mathbf{x} = (x_1, x_2) \in \Omega$, let

$$\varphi(\mathbf{x}) := \prod_{i=1}^{2} x_i(1 - x_i^2).$$

The displacement field is defined by

$$\boldsymbol{\eta}(\mathbf{x}) := \begin{pmatrix} \partial_{x_2}(\varphi^2) \\ -\partial_{x_1}(\varphi^2) \end{pmatrix} + \frac{1}{\lambda} \begin{pmatrix} \varphi(\mathbf{x}) \sin(\pi x_1) \\ \varphi(\mathbf{x}) \cos(\pi x_2) \end{pmatrix},$$

whereas the velocity field and the pressure are given by

$$\mathbf{u}(\mathbf{x}) := \begin{pmatrix} \varphi(\mathbf{x}) \sin(\pi x_1) \\ \varphi(\mathbf{x}) \cos(\pi x_2) \end{pmatrix} \quad \text{and} \quad p(\mathbf{x}) := 10 \arctan\left(\frac{x_1 + x_2}{0.01}\right) + \frac{x_1 - 0.1}{(x_1 - 0.1)^2 + (x_2 + 0.1)^2} - p_0\,,$$

where p_0 is chosen so that p has zero mean in Ω. Notice that $\boldsymbol{\eta} = \mathbf{0}$ and $\mathbf{u} = \mathbf{0}$ on Γ. In addition, the first vector field in the definition of $\boldsymbol{\eta}$ is divergence-free, whereas the compressible perturbation is scaled by λ^{-1}. Therefore, $\lambda \mathrm{div}(\boldsymbol{\eta})$ remains uniformly bounded as λ increases. The total pressure is then defined by $\theta = \alpha p - \lambda \mathrm{div}(\boldsymbol{\eta})$ (cf. (2.5)), and the right-hand side data are obtained by substituting the exact solution into the governing equations. The pressure contains two distinct localized features. The arctangent term generates a steep internal layer along the diagonal $x_1 + x_2 = 0$, whereas the rational term produces a large pressure variation near the reentrant corner. Since the point $(0.1, -0.1)$ lies in the removed quadrant, its pole is outside the computational domain and p remains smooth throughout Ω.

Tables 6.1 and 6.2 compare the performance of uniform and adaptive refinement strategies. Both approaches reduce the error and estimator as the mesh is refined. However, the adaptive strategy is significantly more efficient in terms of degrees of freedom. Indeed, under uniform refinement, the smallest reported total error is 3.091×10^{-1}, obtained with 251,668 degrees of freedom. In contrast, the adaptive strategy already reaches a smaller total error, 1.356×10^{-1}, with only 22,382 degrees of freedom, and further reduces it to 5.537×10^{-2} with 42,940 degrees of freedom. This shows that the local refinement driven by $\boldsymbol{\Xi}$ concentrates the computational effort near the dominant high-gradient regions and avoids unnecessary refinement away from them.

Uniform refinement on the two-dimensional L-shaped domain								
DoF	h	it	$\mathrm{e}(\boldsymbol{\eta})$	$r(\boldsymbol{\eta})$	$\mathrm{e}(\mathbf{u})$	$r(\mathbf{u})$	$\mathrm{e}(\theta)$	$r(\theta)$
1,120	3.750e-01	3	3.295e+00	–	2.256e+00	–	9.303e+00	–
4,304	1.901e-01	3	2.535e+00	0.39	2.330e+00	-0.05	5.115e+00	0.89
16,162	9.943e-02	3	6.372e-01	2.09	7.824e-01	1.65	1.333e+00	2.03
63,638	5.240e-02	3	2.474e-01	1.38	3.924e-01	1.01	5.776e-01	1.22
251,668	2.731e-02	3	7.618e-02	1.71	1.241e-01	1.67	1.823e-01	1.68

$\mathrm{e}(p)$	$r(p)$	$\mathrm{e}_{\mathrm{tot}}$	r_{tot}	$\boldsymbol{\Xi}$	$\mathrm{eff}(\boldsymbol{\Xi})$
1.081e+01	–	1.481e+01	–	8.433e+01	0.1756
6.529e+00	0.75	8.980e+00	0.74	4.146e+01	0.2166
1.466e+00	2.26	2.223e+00	2.11	1.576e+01	0.1411
6.410e-01	1.21	9.797e-01	1.20	5.560e+00	0.1762
2.028e-01	1.67	3.091e-01	1.68	1.814e+00	0.1704

Table 6.1: [Example 3] Convergence history, estimator values and effectivity indices for the Taylor–Hood approximation under uniform refinement on the two-dimensional L-shaped domain. The rows of the second block follow the same order as those of the first block.

The effectivity indices remain of the same order for both refinement strategies, which indicates that the estimator captures the decay of the total error in a consistent way. This behavior is also reflected in Figure 6.6, where the refined meshes concentrate around the reentrant corner and along the steep pressure layer, consistently with the two localized high-gradient regions of the exact pressure. The computed fields in Figure 6.7 illustrate the corresponding pressure layer, together with the velocity and displacement magnitudes.

Example 4: Adaptive refinement on a three-dimensional L-shaped domain

We consider a three-dimensional extension of the adaptive test from Example 3. The purpose of this experiment is to assess the ability of the estimator $\boldsymbol{\Xi}$ to identify and resolve a localized region of high pressure gradient near a reentrant edge. The computational domain is given by

$$\Omega := \big\{\mathbf{x} = (x_1, x_2, x_3) \in (-0.5, 0.5) \times (0, 0.5) \times (-0.5, 0.5) : x_1 < 0 \text{ or } x_3 < 0\big\}.$$

Equivalently, Ω is obtained by extruding, along the x_2-direction, an L-shaped section in the (x_1, x_3)-plane. Hence, the nonconvex geometry contains the reentrant edge $\{(0, x_2, 0) : 0 < x_2 < 0.5\}$. As in the previous example, homogeneous Dirichlet boundary conditions are imposed on the whole boundary, and we employ the Taylor–Hood finite element pair $\mathbf{P}_2 - \mathrm{P}_1$. The model parameters are chosen as

$$s_0 = 10^{-2}, \quad \alpha = 0.9, \quad \nu(\mathbf{x}) = \exp(-x_1 x_2 x_3), \quad \mathtt{D} = 10^2, \quad \lambda = 10^2, \quad \mu = 10, \quad \mathtt{F} = 10, \quad m = 4.$$

The data are manufactured from smooth polynomial-trigonometric functions. To prescribe the exact solution, we introduce the scalar function

$$\gamma(\mathbf{x}) := x_2(0.5 - x_2) \prod_{i \in \{1,3\}} x_i(x_i + 0.5)(x_i - 0.5).$$

Adaptive refinement on the two-dimensional L-shaped domain								
DoF	h	it	$\mathrm{e}(\boldsymbol{\eta})$	$r(\boldsymbol{\eta})$	$\mathrm{e}(\mathbf{u})$	$r(\mathbf{u})$	$\mathrm{e}(\theta)$	$r(\theta)$
1,120	3.750e-01	3	3.295e+00	–	2.256e+00	–	9.303e+00	–
2,276	3.389e-01	3	9.199e-01	3.60	1.211e+00	1.75	1.906e+00	4.47
5,380	3.676e-01	3	2.960e-01	2.64	4.862e-01	2.12	6.785e-01	2.40
11,636	3.205e-01	3	9.847e-02	2.85	1.275e-01	3.47	2.788e-01	2.31
22,382	1.834e-01	3	3.244e-02	3.39	5.101e-02	2.80	8.150e-02	3.76
42,940	1.593e-01	3	1.496e-02	2.38	1.740e-02	3.30	3.416e-02	2.67
90,394	1.412e-01	3	7.656e-03	1.80	8.258e-03	2.00	1.577e-02	2.08
199,660	8.390e-02	3	2.723e-03	2.61	3.011e-03	2.55	6.980e-03	2.06
450,276	5.553e-02	3	1.291e-03	1.84	1.332e-03	2.01	3.086e-03	2.01

$\mathrm{e}(p)$	$r(p)$	$\mathrm{e}_{\mathrm{tot}}$	r_{tot}	$\boldsymbol{\Xi}$	$\mathrm{eff}(\boldsymbol{\Xi})$
1.081e+01	–	1.481e+01	–	8.433e+01	0.1756
2.092e+00	4.63	3.213e+00	4.31	2.160e+01	0.1488
7.476e-01	2.39	1.159e+00	2.37	6.297e+00	0.1841
3.045e-01	2.33	4.432e-01	2.49	2.021e+00	0.2193
9.001e-02	3.73	1.356e-01	3.62	9.599e-01	0.1413
3.704e-02	2.73	5.537e-02	2.75	4.656e-01	0.1189
1.672e-02	2.14	2.560e-02	2.07	2.218e-01	0.1154
7.583e-03	2.00	1.108e-02	2.11	9.818e-02	0.1128
3.321e-03	2.03	4.898e-03	2.01	4.395e-02	0.1115

Table 6.2: [Example 3] Convergence history, estimator values and effectivity indices for the adaptive Taylor–Hood approximation on the two-dimensional L-shaped domain. The rows of the second block follow the same order as those of the first block.

The exact displacement and velocity are given by

$$\boldsymbol{\eta}(\mathbf{x}) := \gamma(\mathbf{x}) \begin{pmatrix} \cos(\pi x_1) \\ \sin(\pi x_2) \\ \cos(\pi x_3) \end{pmatrix} \quad \text{and} \quad \mathbf{u}(\mathbf{x}) := \gamma(\mathbf{x}) \begin{pmatrix} \sin(\pi x_1) \\ \cos(\pi x_2) \\ \sin(\pi x_3) \end{pmatrix}.$$

Notice that $\boldsymbol{\eta} = \mathbf{0}$ and $\mathbf{u} = \mathbf{0}$ on Γ. The pressure is prescribed as

$$p(\mathbf{x}) = \frac{0.25}{\sqrt{(x_1 - 0.02)^2 + (x_3 - 0.02)^2 + 0.015^2}} - p_0,$$

where p_0 is chosen so that p has zero mean in Ω. The regularized line $\{(0.02, x_2, 0.02) : 0 < x_2 < 0.5\}$ lies in the removed part of the domain. Consequently, the pressure is smooth throughout Ω, but exhibits a strongly localized gradient near the reentrant edge. The total pressure θ is defined by (2.5), and the right-hand side data are obtained by substituting the exact solution into (2.7). Hence, the adaptive refinement is expected to concentrate in the region where the pressure variation is largest.

Tables 6.3 and 6.4 compare the uniform and adaptive refinement strategies. Both methods reduce the individual errors and the total error as the mesh is refined. However, the adaptive strategy is more efficient in terms of degrees of freedom. For instance, under uniform refinement, the total error is reduced to 4.075×10^{-2} with 286,258 degrees of freedom. In contrast, the adaptive method reaches

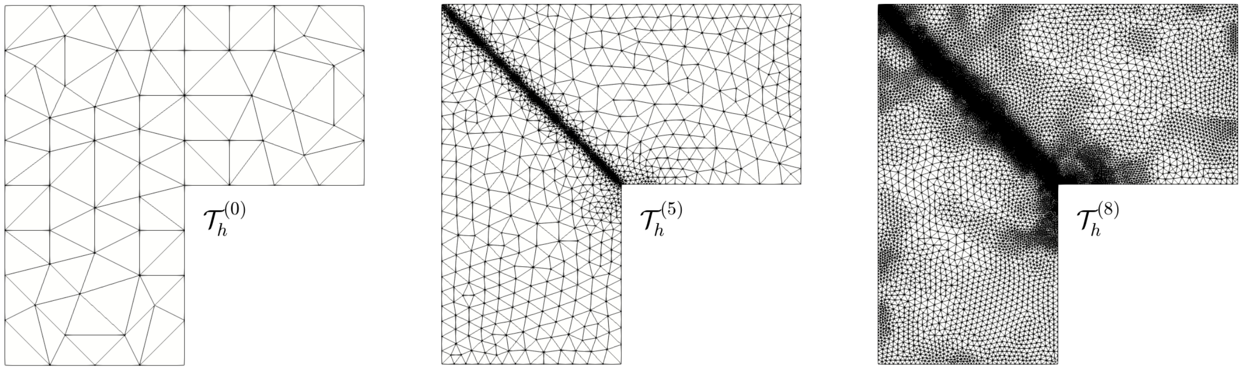

Figure 6.6: [Example 3] Initial mesh and two adaptively refined meshes for the two-dimensional L-shaped domain. From left to right: $\mathcal{T}_h^{(0)}$, $\mathcal{T}_h^{(5)}$, and $\mathcal{T}_h^{(8)}$.

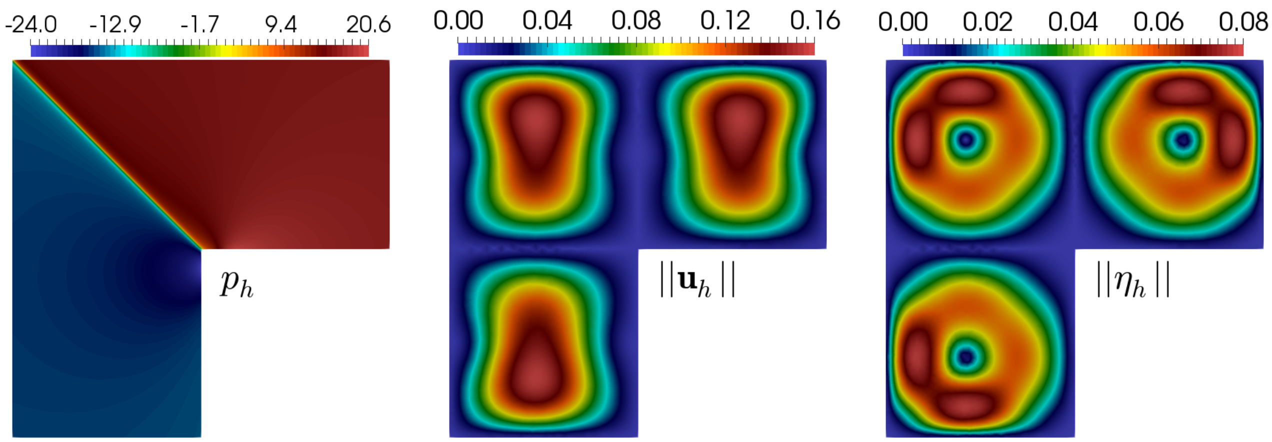

Figure 6.7: [Example 3] Computed fields for the two-dimensional adaptive test. From left to right: fluid pressure p_h, velocity magnitude $\|\mathbf{u}_h\|$, and displacement magnitude $\|\boldsymbol{\eta}_h\|$.

a smaller total error, 6.642×10^{-3}, with only 180,038 degrees of freedom. Similarly, the final adaptive mesh yields $\mathrm{e}_{\mathrm{tot}} = 2.048 \times 10^{-3}$ with 863,048 degrees of freedom, whereas the final uniform mesh gives $\mathrm{e}_{\mathrm{tot}} = 1.259 \times 10^{-2}$ even with 1,470,892 degrees of freedom.

The effectivity indices remain stable and of the same order for both refinement strategies. Nevertheless, the adaptive procedure achieves substantially smaller errors with fewer degrees of freedom, confirming that the estimator $\boldsymbol{\Xi}$ successfully concentrates the refinement near the dominant error region. This is also observed in Figure 6.8, where the sequence of meshes $\mathcal{T}_h^{(0)}$, $\mathcal{T}_h^{(3)}$, and $\mathcal{T}_h^{(4)}$ shows a progressive concentration of tetrahedra around the reentrant edge. The last panel displays the computed pressure p_h, whose largest variation occurs precisely near this edge. Hence, the adapted meshes are consistent with the structure of the pressure field and with the localization predicted by the estimator.

Example 5: A brain-shaped domain with a localized tumor-like source

We conclude with a three-dimensional test on an anatomical brain-shaped geometry. The aim of this example is to assess the behavior of the adaptive algorithm on a nontrivial realistic geometry

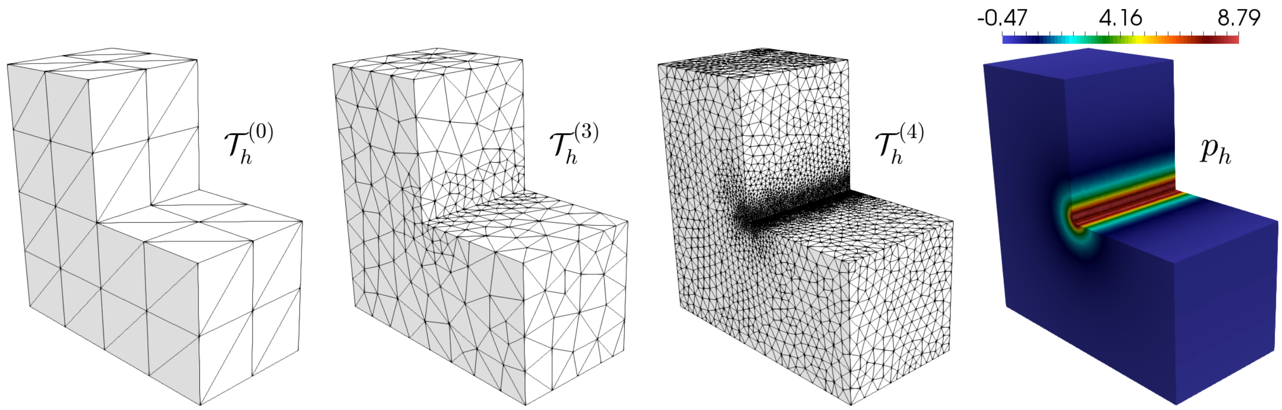

Figure 6.8: [Example 4] Three-dimensional adaptive test. From left to right: initial mesh $\mathcal{T}_h^{(0)}$, intermediate adapted mesh $\mathcal{T}_h^{(3)}$, final adapted mesh $\mathcal{T}_h^{(4)}$, and computed pore pressure p_h.

and in the presence of localized spatial data. The computational domain is obtained from an atlas-based segmentation by merging the gray and white matter regions. The initial mesh is intentionally coarse, with 1,309 vertices and 3,913 tetrahedra, leading to 33,952 degrees of freedom for the MINI discretization. This choice allows us to clearly observe the effect of the adaptive refinement process.

We consider a localized tumor-like perturbation placed inside the brain parenchyma. More precisely, the lesion is represented by the smooth ellipsoidal profile

$$T(\mathbf{x}) = \exp\left(-3\left[\left(\frac{x_1 - 0.55}{0.045}\right)^2 + \left(\frac{x_2 - 0.48}{0.055}\right)^2 + \left(\frac{x_3 - 0.55}{0.045}\right)^2\right]\right).$$

This function is used as a lesion marker and produces a highly localized material perturbation. In particular, it determines the region where the hydraulic resistance, Brinkman viscosity and Forchheimer coefficient are locally modified. The scalar source term is chosen slightly wider than the lesion marker. More precisely, we define

$$S(\mathbf{x}) = \exp\left(-\left[\left(\frac{x_1 - 0.55}{0.080}\right)^2 + \left(\frac{x_2 - 0.48}{0.100}\right)^2 + \left(\frac{x_3 - 0.55}{0.080}\right)^2\right]\right).$$

On each mesh, this profile is normalized as $\widehat{S} := \frac{S}{(S,1)_\Omega}$, so that $(\widehat{S},1)_\Omega = 1$. The compatible source term is then defined by $g(\mathbf{x}) = 0.5\,\widehat{S}(\mathbf{x}) - \frac{0.5}{|\Omega|}$, which satisfies $(g,1)_\Omega = 0$. The source term mimics a localized accumulation of fluid in the lesion region. We stress that this test is not intended to provide a patient-specific tumor-growth model; rather, it is a simplified computational setting in which localized data generate strong pressure and velocity gradients.

In order to incorporate spatially varying tissue properties, we consider space-dependent hydraulic coefficients. The Darcy resistance is defined by

$$\mathtt{D}(\mathbf{x}) = H(\mathbf{x}) + 30\,T(\mathbf{x}),$$

where

$$H(\mathbf{x}) = 1 + 0.20\sin(2\pi x_1)\sin(\pi x_2) + 0.10\cos(2\pi x_3)$$

represents a mild background heterogeneity of the healthy parenchyma. The term $30\,T(\mathbf{x})$ models an increased hydraulic resistance near the lesion. Similarly, the Brinkman viscosity is chosen as

$$\nu(\mathbf{x}) = 10^{-1}\left(1 + 0.25\,T(\mathbf{x}) + 0.10\,\sin(\pi x_1)\sin(\pi x_3)\right).$$

Uniform refinement on the three-dimensional L-shaped domain								
DoF	h	it	$\mathrm{e}(\boldsymbol{\eta})$	$r(\boldsymbol{\eta})$	$\mathrm{e}(\mathbf{u})$	$r(\mathbf{u})$	$\mathrm{e}(\theta)$	$r(\theta)$
2,078	4.330e-01	2	2.936e-03	–	4.031e-02	–	1.403e-01	–
12,802	2.165e-01	2	2.372e-03	0.35	3.760e-02	0.11	8.706e-02	0.79
60,868	1.237e-01	2	1.627e-03	0.73	2.745e-02	0.61	5.525e-02	0.87
286,258	7.217e-02	2	7.691e-04	1.45	1.351e-02	1.37	2.568e-02	1.48
1,470,892	4.124e-02	2	2.054e-04	2.42	3.927e-03	2.26	7.992e-03	2.14

$\mathrm{e}(p)$	$r(p)$	$\mathrm{e}_{\mathrm{tot}}$	r_{tot}	$\boldsymbol{\Xi}$	$\mathrm{eff}(\boldsymbol{\Xi})$
1.576e-01	–	2.148e-01	–	3.769e+00	0.0570
9.704e-02	0.80	1.357e-01	0.76	1.720e+00	0.0789
6.153e-02	0.88	8.715e-02	0.85	8.744e-01	0.0997
2.859e-02	1.48	4.075e-02	1.47	4.041e-01	0.1008
8.895e-03	2.14	1.259e-02	2.15	1.505e-01	0.0836

Table 6.3: [Example 4] Convergence history, estimator values and effectivity indices for the Taylor–Hood approximation under uniform refinement on the three-dimensional L-shaped domain.

For the present simulation, we consider the nonlinear Brinkman–Forchheimer regime by taking

$$\mathtt{F}(\mathbf{x}) = 10^{-1}\,(1 + 20T(\mathbf{x}))\ .$$

Thus, the nonlinear inertial resistance is enhanced near the lesion. The localized source generates a spatially concentrated fluid response, whereas the heterogeneous Darcy and Forchheimer coefficients modulate and damp the flow within the perturbed region.

The mechanical response of the poroelastic skeleton is described by constant effective Lam parameters. This choice is motivated by poroelastic brain-edema models in which the elastic coefficients are obtained from a Young modulus and a Poisson ratio; see, for instance, [33]. Since the present experiment is dimensionless, we do not use the dimensional values directly. Instead, we choose $\mu = 1$ and $\lambda = 10^2$, which preserves, at the level of order of magnitude, the scale separation associated with a nearly incompressible poroelastic response. The remaining dimensionless parameters are $s_0 = 10^{-4}$ and $\alpha = 0.9$. The external body force in the poroelastic equation and the external vector force in the Brinkman–Forchheimer equation are both set equal to zero. Hence, the coupled response is driven by the localized source term, the spatial variation of the hydraulic coefficients, and the nonlinear Forchheimer resistance.

In Table 6.5, we report the experimental convergence rate of the global estimator $\boldsymbol{\Xi}$ for six adapted meshes. Here, $r(\boldsymbol{\Xi})$ is defined analogously to the experimental error rates by replacing $\mathrm{e}(\star)$ and $\mathrm{e}'(\star)$ with $\boldsymbol{\Xi}$ and $\boldsymbol{\Xi}'$, respectively. Although the effectivity index cannot be computed for this example, the decay of $\boldsymbol{\Xi}$ illustrates the ability of the proposed indicator to guide the refinement towards the regions where the localized source term and the heterogeneous hydraulic coefficients generate the dominant response. We also observe that the number of Newton iterations remains stable throughout the refinement process. Figure 6.9 displays the computational domain, the lesion marker, the source profile, the pressure, the velocity magnitude, and the final adapted mesh.

Adaptive refinement on the three-dimensional L-shaped domain								
DoF	h	it	$\mathrm{e}(\boldsymbol{\eta})$	$r(\boldsymbol{\eta})$	$\mathrm{e}(\mathbf{u})$	$r(\mathbf{u})$	$\mathrm{e}(\theta)$	$r(\theta)$
2,078	4.330e-01	2	2.936e-03	–	4.031e-02	–	1.403e-01	–
6,254	3.536e-01	2	1.938e-03	1.13	3.033e-02	0.77	7.516e-02	1.70
28,642	2.324e-01	2	8.882e-04	1.54	1.510e-02	1.37	2.816e-02	1.94
180,038	1.444e-01	2	1.240e-04	3.21	2.180e-03	3.16	4.239e-03	3.09
863,048	8.701e-02	2	3.677e-05	2.33	6.532e-04	2.31	1.316e-03	2.24

$\mathrm{e}(p)$	$r(p)$	$\mathrm{e}_{\mathrm{tot}}$	r_{tot}	$\boldsymbol{\Xi}$	$\mathrm{eff}(\boldsymbol{\Xi})$
1.576e-01	–	2.148e-01	–	3.769e+00	0.0570
8.347e-02	1.73	1.164e-01	1.67	1.374e+00	0.0847
3.125e-02	1.94	4.470e-02	1.89	4.382e-01	0.1020
4.623e-03	3.12	6.642e-03	3.11	7.212e-02	0.0921
1.426e-03	2.25	2.048e-03	2.25	2.222e-02	0.0922

Table 6.4: [Example 4] Convergence history, estimator values and effectivity indices for the adaptive Taylor–Hood approximation on the three-dimensional L-shaped domain.

DoF it	33,952 3	60,160 4	112,444 4	186,872 4	272,700 4	382,282 4
$\boldsymbol{\Xi}$	4.17e+01	5.68e+00	2.25e+00	1.64e+00	1.35e+00	1.18e+00
$r(\boldsymbol{\Xi})$	–	10.45	4.44	1.89	1.52	1.18

Table 6.5: [Example 5] Brain-shaped adaptive test: number of degrees of freedom, Newton iteration count, global estimator $\boldsymbol{\Xi}$, and experimental convergence rate of the global estimator for the MINI element discretization.

7 Conclusions

In this paper, we introduced and analyzed a mixed-primal finite element formulation for the stationary Biot–Brinkman–Forchheimer problem. The formulation incorporates the total pressure as an additional unknown, together with the solid displacement, fluid velocity, and pore pressure. This choice allows the volumetric response of the porous skeleton to be treated separately from the pore pressure and provides a suitable framework for the analysis of the nearly incompressible regime. The existence and uniqueness of a solution to the continuous problem were established by exploiting the continuity and strong monotonicity of the nonlinear Brinkman–Forchheimer operator, together with the stability properties of the coupling terms. We also introduced conforming Galerkin approximations based on Stokes-stable finite element pairs and proved the well-posedness of the resulting nonlinear discrete problem. In addition, a priori error estimates were derived with constants independent of the first Lamé parameter λ. Consequently, the proposed method is locking-free and remains robust as the porous skeleton approaches the nearly incompressible limit. A residual-based a posteriori error estimator was also developed, and its reliability and efficiency up to higher-order terms were established. The numerical experiments confirmed the theoretical convergence behavior and the robustness of the method for large values of λ. They also showed that the estimator successfully guides the adaptive refinement towards regions characterized by large pressure gradients. Further tests involving strongly

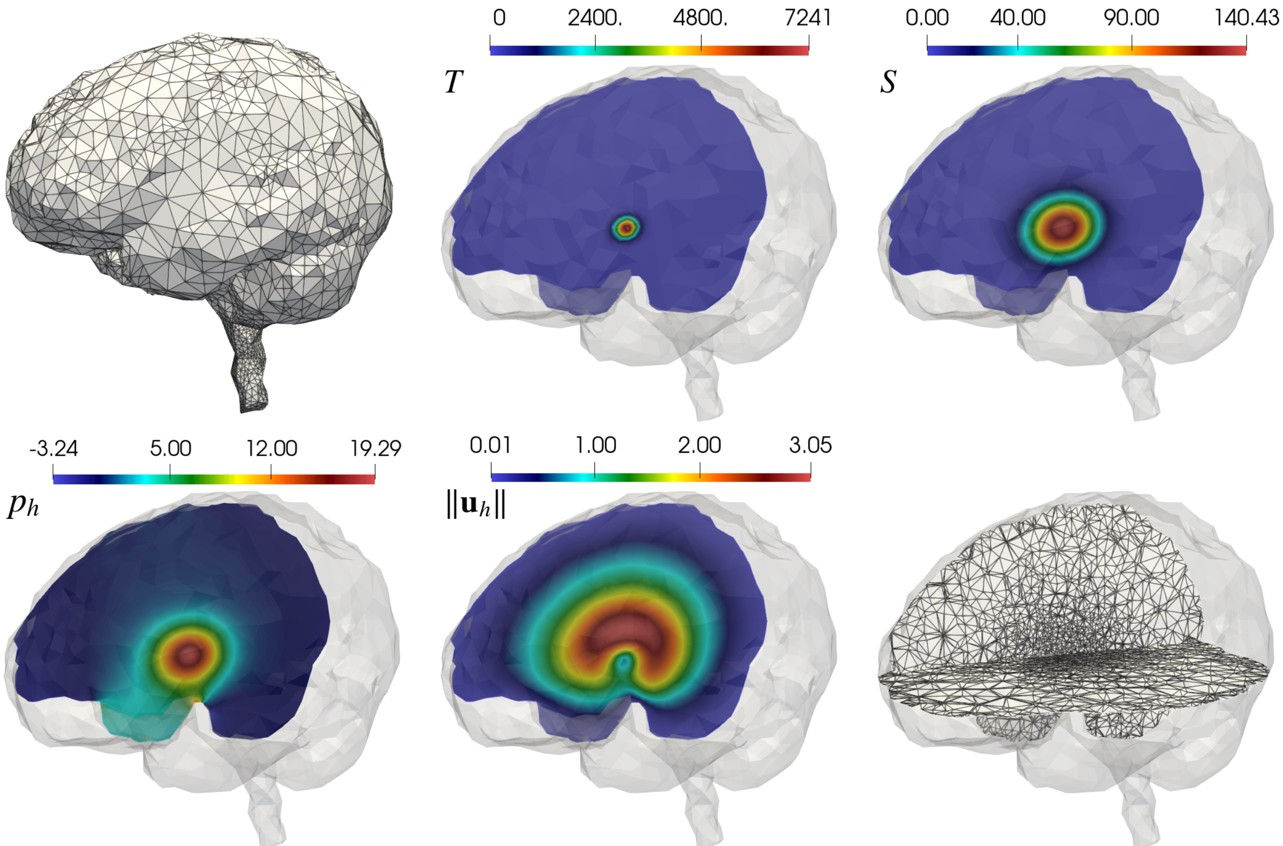

Figure 6.9: [Example 5] Brain-shaped adaptive test with a localized tumor-like source. Top: left, computational domain; middle, lesion marker T; right, source profile S. Bottom: left, computed pressure p_h; middle, velocity magnitude $\|\mathbf{u}_h\|$; right, final adapted mesh. The mesh refinement is concentrated near the localized source region, indicating that the adaptive strategy successfully captures the main features induced by the tumor-like perturbation.

heterogeneous permeability fields and complex two- and three-dimensional geometries illustrated the flexibility of the proposed formulation in computationally challenging configurations.

A A discrete approximation result

The following lemma establishes the discrete approximation property used in the a priori error analysis.

Lemma A.1 *Let* $((\boldsymbol{\eta}, \mathbf{u}), (\theta, p)) \in \mathbb{H} \times \mathbb{Q}$ *be the solution of* (2.12). *Let* $\widehat{\theta}_h \in \mathrm{Q}_h^\theta$ *and* $\widehat{p}_h \in \mathrm{Q}_h^p$ *be the respective* $\mathrm{L}^2(\Omega)$*-orthogonal projections of* θ *and* p*, and let* $\mathbb{K}_h$ *be defined by* (4.6). *Assume that, for some* $s \in [1, k+1]$, $\boldsymbol{\eta}, \mathbf{u} \in \mathbf{H}^{1+s}(\Omega)$ *and* $\theta, p \in \mathrm{H}^s(\Omega)$. *Then, there exists a positive constant* C*, independent of* h*, such that*

$$\inf_{(\boldsymbol{\xi}_h, \mathbf{v}_h) \in \mathbb{K}_h} \|(\boldsymbol{\eta}, \mathbf{u}) - (\boldsymbol{\xi}_h, \mathbf{v}_h)\|_{\mathbb{H}}$$
$$\leq C\, h^s \left(\left(1 + \frac{\|\mathcal{B}\|}{\beta_{\mathtt{d}}}\right) \left(\|\boldsymbol{\eta}\|_{\mathbf{H}^{1+s}(\Omega)} + \|\mathbf{u}\|_{\mathbf{H}^{1+s}(\Omega)}\right) + \frac{\|\mathcal{C}\|}{\beta_{\mathtt{d}}} \left(\|\theta\|_{\mathrm{H}^s(\Omega)} + \|p\|_{\mathrm{H}^s(\Omega)}\right) \right). \tag{A.1}$$

Proof. Let $(\boldsymbol{\zeta}_h, \mathbf{w}_h) \in \mathbb{H}_h$ be arbitrary and define

$$\mathbf{N}_h := \mathcal{C}(\widehat{\theta}_h, \widehat{p}_h) - \mathbf{G} - \mathcal{B}(\boldsymbol{\zeta}_h, \mathbf{w}_h) \quad \text{in} \quad \mathbb{Q}_h' \,. \tag{A.2}$$

The discrete inf-sup condition (4.1) implies that the operator induced by $\mathcal{B}$ from $\mathbb{H}_h$ onto $\mathbb{Q}_h'$ is surjective. Hence, there exists $(\mathbf{r}_h, \mathbf{s}_h) \in \mathbb{H}_h$ such that

$$\mathcal{B}(\mathbf{r}_h, \mathbf{s}_h) = \mathbf{N}_h \quad \text{in} \quad \mathbb{Q}_h' \tag{A.3}$$

and

$$\|(\mathbf{r}_h, \mathbf{s}_h)\|_{\mathbb{H}} \le \frac{1}{\beta_{\mathtt{d}}} \|\mathbf{N}_h\|_{\mathbb{Q}_h'} \,. \tag{A.4}$$

On the other hand, the second equation of (2.12), restricted to $\mathbb{Q}_h$, gives

$$\mathbf{G} = \mathcal{C}(\theta, p) - \mathcal{B}(\boldsymbol{\eta}, \mathbf{u}) \quad \text{in} \quad \mathbb{Q}_h' \,.$$

Using this identity in (A.2), we obtain

$$\mathbf{N}_h = \mathcal{C}(\widehat{\theta}_h, \widehat{p}_h) - \mathcal{C}(\theta, p) + \mathcal{B}(\boldsymbol{\eta}, \mathbf{u}) - \mathcal{B}(\boldsymbol{\zeta}_h, \mathbf{w}_h) = \mathcal{C}(\widehat{\theta}_h - \theta, \widehat{p}_h - p) + \mathcal{B}(\boldsymbol{\eta} - \boldsymbol{\zeta}_h, \mathbf{u} - \mathbf{w}_h) \,.$$

The boundedness of $\mathcal{B}$ and $\mathcal{C}$ then yields

$$\|\mathbf{N}_h\|_{\mathbb{Q}_h'} \le \|\mathcal{C}\| \|(\theta, p) - (\widehat{\theta}_h, \widehat{p}_h)\|_{\mathbb{Q}} + \|\mathcal{B}\| \|(\boldsymbol{\eta}, \mathbf{u}) - (\boldsymbol{\zeta}_h, \mathbf{w}_h)\|_{\mathbb{H}} \,. \tag{A.5}$$

Combining (A.4) and (A.5), we deduce

$$\|(\mathbf{r}_h, \mathbf{s}_h)\|_{\mathbb{H}} \le \frac{\|\mathcal{C}\|}{\beta_{\mathtt{d}}} \|(\theta, p) - (\widehat{\theta}_h, \widehat{p}_h)\|_{\mathbb{Q}} + \frac{\|\mathcal{B}\|}{\beta_{\mathtt{d}}} \|(\boldsymbol{\eta}, \mathbf{u}) - (\boldsymbol{\zeta}_h, \mathbf{w}_h)\|_{\mathbb{H}} \,. \tag{A.6}$$

We now define the corrected element $(\widehat{\boldsymbol{\zeta}}_h, \widehat{\mathbf{w}}_h) := (\boldsymbol{\zeta}_h + \mathbf{r}_h, \mathbf{w}_h + \mathbf{s}_h)$. It follows from (A.2) and (A.3) that

$$\mathcal{B}(\widehat{\boldsymbol{\zeta}}_h, \widehat{\mathbf{w}}_h) = \mathcal{B}(\boldsymbol{\zeta}_h, \mathbf{w}_h) + \mathcal{B}(\mathbf{r}_h, \mathbf{s}_h) = \mathcal{B}(\boldsymbol{\zeta}_h, \mathbf{w}_h) + \mathbf{N}_h = \mathcal{C}(\widehat{\theta}_h, \widehat{p}_h) - \mathbf{G} \,,$$

and hence $(\widehat{\boldsymbol{\zeta}}_h, \widehat{\mathbf{w}}_h) \in \mathbb{K}_h$ (cf. (4.6)). Moreover, the triangle inequality and (A.6) imply

$$\|(\boldsymbol{\eta}, \mathbf{u}) - (\widehat{\boldsymbol{\zeta}}_h, \widehat{\mathbf{w}}_h)\|_{\mathbb{H}} \le \left(1 + \frac{\|\mathcal{B}\|}{\beta_{\mathtt{d}}}\right) \|(\boldsymbol{\eta}, \mathbf{u}) - (\boldsymbol{\zeta}_h, \mathbf{w}_h)\|_{\mathbb{H}} + \frac{\|\mathcal{C}\|}{\beta_{\mathtt{d}}} \|(\theta, p) - (\widehat{\theta}_h, \widehat{p}_h)\|_{\mathbb{Q}} \,.$$

Finally, since the constructed element $(\widehat{\boldsymbol{\zeta}}_h, \widehat{\mathbf{w}}_h)$ belongs to $\mathbb{K}_h$, we first bound the infimum over $\mathbb{K}_h$ by the error associated with this particular element. Then, by the arbitrariness of $(\boldsymbol{\zeta}_h, \mathbf{w}_h) \in \mathbb{H}_h$, taking the infimum over $\mathbb{H}_h$ and using $(\mathbf{AP}_h^{\boldsymbol{\zeta}})$, together with the best-approximation properties of the $\mathrm{L}^2(\Omega)$-orthogonal projections $(\widehat{\theta}_h, \widehat{p}_h)$ and $(\mathbf{AP}_h^{\psi})$, yields (A.1) and concludes the proof. □

B Preliminaries for reliability

Let $\mathcal{E}_h$ denote the set of edges when $d = 2$ and faces when $d = 3$ of the triangulation $\mathcal{T}_h$, with corresponding diameters denoted by h_e. We introduce the sets of boundary and interior facets

$$\mathcal{E}_h(\Gamma) := \big\{ e \in \mathcal{E}_h : \; e \subset \Gamma \big\} \quad \text{and} \quad \mathcal{E}_h(\Omega) := \mathcal{E}_h \setminus \mathcal{E}_h(\Gamma).$$

For each $T \in \mathcal{T}_h$, we also define

$$\mathcal{E}_{h,T} := \big\{ e \in \mathcal{E}_h : \ e \subset \partial T \big\}, \qquad \mathcal{E}_{h,T}(\Omega) := \mathcal{E}_{h,T} \cap \mathcal{E}_h(\Omega), \qquad \mathcal{E}_{h,T}(\Gamma) := \mathcal{E}_{h,T} \cap \mathcal{E}_h(\Gamma).$$

Given an interior facet $e = \partial T_+ \cap \partial T_-$, we denote by $\mathbf{n}_+$ and $\mathbf{n}_-$ the unit normal vectors on e pointing outward from T_+ and T_-, respectively. For a piecewise continuous tensor-valued function $\boldsymbol{\tau}$, its normal jump across e is defined by

$$[\![\boldsymbol{\tau}\mathbf{n}]\!] := \boldsymbol{\tau}|_{T_+}\mathbf{n}_+ + \boldsymbol{\tau}|_{T_-}\mathbf{n}_- . \tag{B.1}$$

Let us now recall the main properties of the Clément interpolation operators (cf. [21], [18]). Defining $X_h := \big\{ v_h \in C(\overline{\Omega}) : \quad v_h|_T \in \mathrm{P}_1(T) \quad \forall\, T \in \mathcal{T}_h \big\}$ and denoting by $\mathbf{X}_h$ its tensor version, we let $\mathcal{I}_h : \mathrm{H}^1(\Omega) \to X_h$ and $\boldsymbol{\mathcal{I}}_h : \mathbf{H}^1(\Omega) \to \mathbf{X}_h$ be the usual Clément interpolation operator and its vector version, respectively. Some local properties of $\mathcal{I}_h$, and hence of $\boldsymbol{\mathcal{I}}_h$, are established in the following lemma (cf. [18]):

Lemma B.1 *There exist positive constants $C_{1,\mathcal{I}}$ and $C_{2,\mathcal{I}}$, such that*

$$\|v - \mathcal{I}_h(v)\|_{\mathrm{L}^2(T)} \,\le\, C_{1,\mathcal{I}}\, h_T \,\|v\|_{\mathrm{H}^1(\Delta(T))} \quad \forall\, T \in \mathcal{T}_h \,, \tag{B.2}$$

and

$$\|v - \mathcal{I}_h(v)\|_{\mathrm{L}^2(e)} \,\le\, C_{2,\mathcal{I}}\, h_e^{1/2} \,\|v\|_{\mathrm{H}^1(\Delta(e))} \quad \forall\, e \in \mathcal{E}_h \,, \tag{B.3}$$

where $\Delta(T) := \cup\big\{ T' \in \mathcal{T}_h : \quad T' \cap T \neq \emptyset \big\}$ and $\Delta(e) := \cup\big\{ T' \in \mathcal{T}_h : \quad T' \cap e \neq \emptyset \big\}$.

We also recall that, when homogeneous Dirichlet boundary conditions are imposed, one may use the homogeneous Clément operator $\mathcal{I}_{h,0} : \mathrm{H}^1_0(\Omega) \to X_h \cap \mathrm{H}^1_0(\Omega)$, obtained by setting to zero the degrees of freedom associated with boundary nodes. The local estimates (B.2) and (B.3) remain valid for $\mathcal{I}_{h,0}$, with the same type of constants, independent of h. In particular, its vector version $\boldsymbol{\mathcal{I}}_{h,0} : \mathbf{H}^1_0(\Omega) \to \mathbf{X}_h \cap \mathbf{H}^1_0(\Omega)$ satisfies the corresponding componentwise estimates. In what follows, for simplicity of notation, we denote these homogeneous operators again by $\mathcal{I}_h$ and $\boldsymbol{\mathcal{I}}_h$.

C Preliminaries for efficiency

For the efficiency analysis of $\boldsymbol{\Xi}$ (cf. (5.1)), we proceed as in [26, 15, 12, 25] and employ a localization technique based on element- and facet-bubble functions, together with inverse and discrete trace inequalities. More precisely, given $T \in \mathcal{T}_h$ and a facet $e \in \mathcal{E}_{h,T}$, we denote by ϕ_T and ϕ_e the usual element- and facet-bubble functions, respectively (cf. [42, eqs. (1.5) and (1.6)]), satisfying

$$\phi_T \in \mathrm{P}_{d+1}(T), \qquad \mathrm{supp}(\phi_T) \subseteq T, \qquad \phi_T = 0 \quad \text{on} \quad \partial T, \qquad 0 \le \phi_T \le 1 \quad \text{in} \quad T, \tag{C.1}$$

and

$$\phi_e|_T \in \mathrm{P}_d(T), \qquad \mathrm{supp}(\phi_e) \subseteq \omega_e, \qquad \phi_e = 0 \quad \text{on} \quad \partial\omega_e, \qquad 0 \le \phi_e \le 1 \quad \text{in} \quad \omega_e, \tag{C.2}$$

where $\omega_e := \bigcup \big\{ T' \in \mathcal{T}_h : \ e \in \mathcal{E}_{h,T'} \big\}$.

We also recall from [42] that, for each $k \in \mathbb{N} \cup \{0\}$, there exists an extension operator $L : C(e) \to C(\omega_e)$ such that

$$L(p)|_T \in \mathrm{P}_k(T) \quad \text{and} \quad L(p)|_e = p \qquad \forall\, p \in \mathrm{P}_k(e)\,. \tag{C.3}$$

The corresponding vector-valued extension, obtained by applying L componentwise, is denoted by $\mathbf{L}$. The specific properties of ϕ_T, ϕ_e, and L are collected in the following lemma, for whose proof we refer to [42, Lemma 3.3].

Lemma C.1 *Given $k \in \mathbb{N} \cup \{0\}$, there exist positive constants c_1, c_2, c_3, and c_4, depending only on k and the shape-regularity constant of the family $\{\mathcal{T}_h\}_{h>0}$, such that, for each $T \in \mathcal{T}_h$ and each facet $e \in \mathcal{E}_{h,T}$, there hold*

$$\|\phi_T q\|^2_{\mathrm{L}^2(T)} \leq \|q\|^2_{\mathrm{L}^2(T)} \leq c_1 \|\phi_T^{1/2} q\|^2_{\mathrm{L}^2(T)} \qquad \forall\, q \in P_k(T)\,, \tag{C.4}$$

$$\|\phi_e L(p)\|^2_{\mathrm{L}^2(e)} \leq \|p\|^2_{\mathrm{L}^2(e)} \leq c_2 \|\phi_e^{1/2} p\|^2_{\mathrm{L}^2(e)} \qquad \forall\, p \in P_k(e)\,, \tag{C.5}$$

and

$$c_3 h_e^{1/2} \|p\|_{\mathrm{L}^2(e)} \leq \|\phi_e^{1/2} L(p)\|_{\mathrm{L}^2(T)} \leq c_4 h_e^{1/2} \|p\|_{\mathrm{L}^2(e)} \qquad \forall\, p \in P_k(e)\,. \tag{C.6}$$

In turn, the aforementioned inverse inequality is stated as follows (cf. [21, Lemma 1.138]).

Lemma C.2 *Let $d \in \{2,3\}$, and let k, ℓ, and m be nonnegative integers such that $m \leq \ell$. Then, for each $T \in \mathcal{T}_h$, there exists a constant $c > 0$, independent of h and T, but depending on k, ℓ, m, d, and the shape-regularity constant of the triangulation, such that*

$$\|v\|_{\mathrm{H}^\ell(T)} \leq c\, h_T^{m-\ell} \|v\|_{\mathrm{H}^m(T)} \qquad \forall\, v \in \mathrm{P}_k(T). \tag{C.7}$$

References

[1] D. Amigo, F. Lepe, E. Otárola, and G. Rivera, *A virtual element method for a convective Brinkman–Forchheimer problem coupled with a heat equation*. Comput. Math. Appl. 191 (2025), 1–23.

[2] V. Anaya, R. Caraballo, S. Caucao, L.F. Gatica, R. Ruiz-Baier, and I. Yotov, *A vorticity-based mixed formulation for the unsteady Brinkman–Forchheimer equations*. Comput. Methods Appl. Mech. Engrg. 404 (2023), Paper No. 115829.

[3] I. Babuška and G.N. Gatica, *A residual-based a posteriori error estimator for the Stokes–Darcy coupled problem*. SIAM J. Numer. Anal. 48 (2010), no. 2, 498–523.

[4] J.W. Barrett and W.B. Liu, *Finite element approximation of the p-Laplacian*. Math. Comp. 61 (1993), no. 204, 523–537.

[5] M.A. Biot, *General theory of three-dimensional consolidation*. J. Appl. Phys. 12 (1941), no. 2, 155–164.

[6] D. Boffi, F. Brezzi, and M. Fortin, *Mixed finite element methods and applications*. Springer Series in Computational Mathematics, 44. Springer, Heidelberg, 2013.

[7] F. Brezzi and M. Fortin, *Mixed and hybrid finite element methods*. Springer Series in Computational Mathematics, 15. Springer-Verlag, New York, 1991.

[8] H.C. Brinkman, *A calculation of the viscous force exerted by a flowing fluid on a dense swarm of particles*. Appl. Sci. Res. 1 (1949), 27–34.

[9] R. Bürger, S. Kumar, D. Mora, R. Ruiz-Baier, and N. Verma, *Virtual element methods for the three-field formulation of time-dependent linear poroelasticity*. Adv. Comput. Math. 47 (2021), Paper No. 2.

[10] A.J. Bustos, S. Caucao, and G.N. Gatica, *Mixed-primal and fully-mixed formulations for the convection-diffusion-reaction system based upon Brinkman–Forchheimer equations.* Comput. Math. Appl. 207 (2026), 222–249.

[11] J. Camaño, S. Caucao, and C. Inzunza, *A five-field mixed formulation for the fully dynamic Biot–Brinkman model.* Preprint 2025-28, Centro de Investigación en Ingeniería Matemática (CI^2MA), Universidad de Concepción, 2025.

[12] J. Camaño, S. Caucao, R. Oyarzúa, and S. Villa-Fuentes, *A posteriori error analysis of a momentum conservative Banach spaces-based mixed-FEM for the Navier–Stokes problem.* Appl. Numer. Math. 176 (2022), 134–158.

[13] R. Caraballo, C.W. In, A.F. Martín, and R. Ruiz-Baier, *Robust finite element methods and solvers for the Biot–Brinkman equations in vorticity form.* Numer. Methods Partial Differential Equations 40 (2024), no. 3, Paper No. e23083.

[14] S. Caucao and J. Esparza, *An augmented mixed FEM for the convective Brinkman–Forchheimer problem: A priori and a posteriori error analysis.* J. Comput. Appl. Math. 438 (2024), Paper No. 115517.

[15] S. Caucao, G.N. Gatica, R. Oyarzúa, and F. Sandoval, *Residual-based a posteriori error analysis for the coupling of the Navier–Stokes and Darcy–Forchheimer equations.* ESAIM Math. Model. Numer. Anal. 55 (2021), no. 2, 659–687.

[16] S. Caucao, D. Mora, and R. Oyarzúa, *A priori and a posteriori error analysis of a pseudostress-based mixed formulation of the Stokes problem with varying density.* IMA J. Numer. Anal. 36 (2016), no. 2, 947–983.

[17] M.A. Christie and M.J. Blunt, *Tenth SPE comparative solution project: A comparison of upscaling techniques.* SPE Reserv. Eval. Eng. 4 (2001), no. 4, 308–317.

[18] P. Clément, *Approximation by finite element functions using local regularization.* RAIRO Anal. Numér. 9 (1975), no. R-2, 77–84.

[19] E. Colmenares, G.N. Gatica, and R. Oyarzúa, *A posteriori error analysis of an augmented mixed-primal formulation for the stationary Boussinesq model.* Calcolo 54 (2017), no. 3, 1055–1095.

[20] W. Ehlers, *Darcy, Forchheimer, Brinkman and Richards: classical hydromechanical equations and their significance in the light of the TPM.* Arch. Appl. Mech. 92 (2022), 619–639.

[21] A. Ern and J.-L. Guermond, *Theory and practice of finite elements.* Applied Mathematical Sciences, 159. Springer-Verlag, New York, 2004.

[22] P. Forchheimer, *Wasserbewegung durch Boden.* Z. Ver. Dtsch. Ing. 45 (1901), 1782–1788.

[23] G.N. Gatica, *A simple introduction to the mixed finite element method. Theory and applications.* SpringerBriefs in Mathematics. Springer, Cham, 2014.

[24] G.N. Gatica, L.F. Gatica, and F.A. Sequeira, *Analysis of an augmented pseudostress-based mixed formulation for a nonlinear Brinkman model of porous media flow.* Comput. Methods Appl. Mech. Engrg. 289 (2015), 104–130.

[25] G.N. Gatica, C. Inzunza, R. Ruiz-Baier, and F. Sandoval, *A posteriori error analysis of Banach spaces-based fully-mixed finite element methods for Boussinesq-type models.* J. Numer. Math. 30 (2022), no. 4, 325–356.

[26] G.N. Gatica, A. Márquez, and M.A. Sánchez, *Analysis of a velocity-pressure-pseudostress formulation for the stationary Stokes equations.* Comput. Methods Appl. Mech. Engrg. 199 (2010), no. 17–20, 1064–1079.

[27] G.N. Gatica, M. Munar, and F.A. Sequeira, *A mixed virtual element method for a nonlinear Brinkman model of porous media flow.* Calcolo 55 (2018), Paper No. 21.

[28] R. Glowinski and A. Marroco, *Sur l'approximation, par éléments finis d'ordre un, et la résolution, par pénalisation-dualité, d'une classe de problèmes de Dirichlet non linéaires.* Rev. Française Automat. Informat. Recherche Opérationnelle Sér. Rouge Anal. Numér. 9 (1975), no. R-2, 41–76.

[29] F. Hecht, *New development in FreeFem++.* J. Numer. Math. 20 (2012), no. 3-4, 251–265.

[30] F. Hecht, *FreeFem++*, Version 3.58-1, third edition. Laboratoire Jacques-Louis Lions, Université Pierre et Marie Curie, Paris, 2018.

[31] Q. Hong, J. Kraus, M. Kuchta, M. Lymbery, K.-A. Mardal, and M.E. Rognes, *Robust approximation of generalized Biot–Brinkman problems.* J. Sci. Comput. 93 (2022), Paper No. 77.

[32] M. Jayadharan and I. Yotov, *Multiscale mortar mixed finite element methods for the Biot system of poroelasticity.* Comput. Methods Appl. Mech. Engrg. 435 (2025), 117597.

[33] G. Ju, M. Cai, J. Li, and J. Tian, *Parameter-robust multiphysics algorithms for Biot model with application in brain edema simulation.* Math. Comput. Simulation 177 (2020), 385–403.

[34] K.-A. Lie, *An Introduction to Reservoir Simulation Using MATLAB/GNU Octave: User Guide for the MATLAB Reservoir Simulation Toolbox (MRST).* Cambridge University Press, Cambridge, 2019.

[35] S. Kumar, R. Oyarzúa, R. Ruiz-Baier, and R. Sandilya, *Conservative discontinuous finite volume and mixed schemes for a new four-field formulation in poroelasticity.* ESAIM Math. Model. Numer. Anal. 54 (2020), no. 1, 273–299.

[36] D. Mora, J. Vellojin, and N. Verma, *A virtual element method for the Biot–Brinkman equations using Nitsche's technique.* Comput. Methods Appl. Mech. Engrg. 448 (2026), Paper No. 118447.

[37] R. Oyarzúa and R. Ruiz-Baier, *Locking-free finite element methods for poroelasticity.* SIAM J. Numer. Anal. 54 (2016), no. 5, 2951–2973.

[38] M. Renardy and R.C. Rogers, *An introduction to partial differential equations*, 2nd ed. Texts in Applied Mathematics, 13. Springer, New York, 2004.

[39] H. Steeb and J. Renner, *Mechanics of poro-elastic media: A review with emphasis on foundational state variables.* Transp. Porous Media 130 (2019), 437–461.

[40] C. Taylor and P. Hood, *A numerical solution of the Navier–Stokes equations using the finite element technique.* Comput. & Fluids 1 (1973), no. 1, 73–100.

[41] P.S. Vassilevski and U. Villa, *A mixed formulation for the Brinkman problem*. SIAM J. Numer. Anal. 52 (2014), no. 1, 258–281.

[42] R. Verfürth, *A review of a posteriori error estimation and adaptive mesh-refinement techniques*. Wiley-Teubner, Chichester, 1996.

[43] L. Zhao, E.T. Chung, and E.-J. Park, *A locking-free staggered DG method for the Biot system of poroelasticity on general polygonal meshes*. IMA J. Numer. Anal. 43 (2023), no. 5, 2777–2816.